# Nd Model Age Mapping in the Grenville Province

**Nd Model Age Mapping of the**

**Central Gneiss Belt**

**In the western Grenville Province**

**Of Ontario, Canada**

By

Robert B. North, B. Sc.

A Thesis

Submitted to the School of Graduate Studies

In partial fulfillment of the requirements

For the Degree

Master of Science

McMaster University

April 2001

Master of Science | McMaster University

(Geology) | Hamilton, Ontario

Title: Nd Model Age Mapping of the Central Gneiss Belt

In the western Grenville Province of Ontario, Canada.

Author: Robert B. North

Honours B. Sc. (McMaster University)

Supervisor: Dr. A.P. Dickin

Number of Pages: xiv, 104

# Abstract

Nd isotope analysis is well suited for mapping major tectonic boundaries in highly metamorphosed orogenic belts. In this study, approximately 80 samples have been analyzed to map 2 such boundaries in the Central Gneiss Belt of the Grenville Province of Ontario. In Central Ontario, lithotectonic terranes with mapped outcrops of gneisses intruded by eclogites and/or coronitic metagabbro have Nd model ages less than 1.8 Ga are interpreted as components of the allochthonous polycylic belt. More northerly terranes are comprised of similar gneissic materials, but have different types of mafic intrusives and have model ages greater than 1.8 Ga. These terranes are interpreted as fragments of the parautochthonous belt. These two belts are divided by a major thrust, termed the Allochthon Boundary Thrust (ABT) (Rivers, et. al., 1989). Continuing to the north, another step in the Nd model ages has been used to identify and map a cryptic suture between Archean and early Proterozoic crustal materials (Dickin & McNutt, 1989).

Along the Georgian Bay coastline, between Pointe Au Baril and Parry Sound, the Shawanaga Shear Zone has been interpreted as the location of the ABT (Culshaw, et. al., 1994). Analysis of over 50 samples are used to map the crustal formation ages in this region and have confirmed this interpretation. Orthogneisses of the Britt Domain have Nd model ages in the range 1.8 – 1.9 Ga. Reworking of the original crust has given these rocks U-Pb crystallization ages of ~1.45 Ga, which means that these rocks have been metamorphosed prior to the Grenvillian event. Crossing the ABT, the orthogneisses of the Shawanaga Domain have a younger range of crustal formation ages, 1.4 – 1.7 Ga. The U-Pb crystallization ages of these rocks are ~1.36 Ga, and they lack signs pre-Grenvillian metamorphism. To the south of Franklin Island, the location of the ABT is difficult to map, as outcrop lies beneath the waters of Georgian Bay. Results of the Nd isotope analyses suggest that the ABT passes through the western edge of the Snake Islands, rather than to their east, as previously interpreted (Culshaw, et. al., 1994).

Approximately 15 Nd isotope analyses were used to investigate a recently proposed location of the ABT (Ketchum & Davidson, 2000) in the vicinity of the Powassan Batholith. Results from near Arnstein, Restoule and Magnetewan agreed with the existing location of the ABT. To the east of the Powassan Batholith, 3 Nd model ages coupled with a lack of mappable eclogites and/or coronitic metagabbros suggest that earlier interpretations of the position of the ABT may be correct and that further studies in this region are necessary.

A cryptic suture identified by crustal formation ages has been the focus of several previous studies (Dickin & McNutt, 1989, 1990; Holmden & Dickin, 1995; Dickin, 1998; Guo & Dickin, 1996). This suture has been mapped from the Georgian Bay coast through Lake Nipissing to the Ontario-Quebec border. New Nd isotope analyses and studies of the regional magnetics have identified a thrust slice between the Grenville Front tectonic zone (GFTZ) and the parautochthonous belt. The cryptic suture appears to coincide with a previously undescribed tectonic boundary west of the Key River. To the west of this boundary, straight orthogneisses within the thrust slice have Nd model ages greater than 2.2 Ga. These differ from the orthogneisses and metaplutonic tonalites to the east of this boundary, which exhibit kilometer-scale isoclinal folds and crustal formation ages between 1.8 – 2.0 Ga, the previously identified range for the Britt Domain.

Major steps in the depleted mantle model ages are observed in all three regions, allowing mapping of the ABT and the Penokean Suture. It is concluded that, in metamorphic orogenic belts, such as the Grenville Province, detailed mapping of major tectonic boundaries is greatly enhanced by the use of Nd isotope analysis.

# Acknowledgements

I wish to thank my supervisor Dr. Alan P. Dickin for suggesting this research project. I would also like to thank Catharina Jaeger for her support, guidance and humour in the clean lab. Further thanks go out to all those who have shared time with me in both the clean lab and geochronology lab.

I would like to thank Dr. Bill Morris for his guidance with the satellite imagery and the magnetic data analysis. Kristi Markham, Matt Pozza and Dr. Joe Boyce also deserve recognition for their constructive criticism with this part of the project.

I would like to thank all of the graduate students of the McMaster School of Geography and Geology for the various suggestions, conversations and distractions they have provided over the last two-and-a-half years.

And finally, I'd like to extend a very special thank you to my innumerable friends and family. Without your support and encouragement, I may not have been able to do so much with a few rocks from around the cottage!!

This work is dedicated with love to my Grandparents,

Martin and Elsie Johns.

# Table of Contents

**Chapter 3:**
**The ABT in the Shawanaga region**



**Nd Model age results**



**Chapter 4:**
**The ABT in the Powassan Region**



**Nd Model Age Results**



**Chapter 5:**
**The Suture at Key Harbour**

## List of Figures

## List of Tables

# Chapter 1

## Introduction:

### 1.1.0. The Grenville Province

The Grenville Province is a Mid-Proterozoic orogenic belt forming the southeasternmost structural province in the Canadian Shield. It extends from the eastern coast of Labrador, across southern Quebec and central Ontario, to Georgian Bay (Fig. 1.1). It consists primarily of gneissic rocks in the upper amphibolite- and granulite-facies. Once interpreted as a metamorphic terrane, the Grenville Province is now described as an exhumed segment from the middle to deep levels of an extensive collisional orogen. U-Pb dating (zircons, monazites & titanites) has given the orogenic event an age range of 1160 to 970 Ma. The orogen resulted from a collision between Laurentia and a combination of magmatic arcs and continental terranes that lay to the southeast (Rivers et al. 1989). This event created the supercontinent Rodinia (Hoffman, 1989).

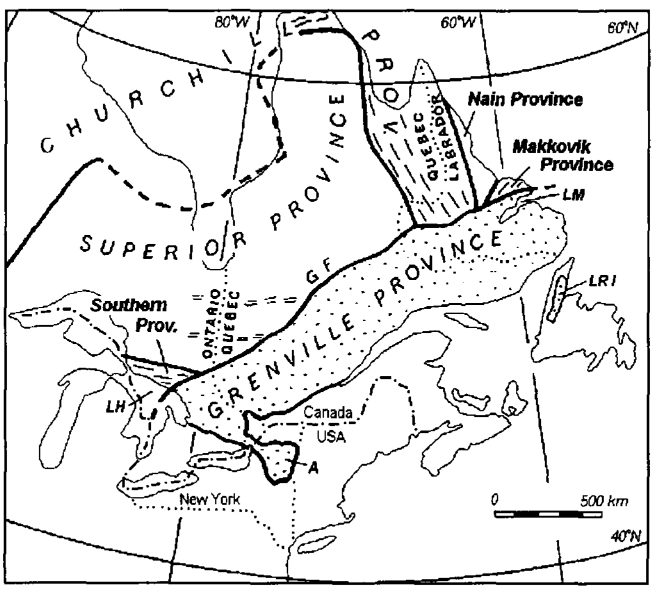


**Fig. 1.1:** Geographic location of the Grenville Province and its relation to surrounding provinces (Rivers et al., 1989)

The structurally complex package of rocks which make up the Grenville Province is divided into groups that have undergone metamorphism during previous orogenic events and rocks that were only subjected to the Grenville orogeny. The former are termed polycyclic, while the latter are named monocyclic. The differences between these rock packages are not always evident in the field. Therefore, it is only after geochronologic studies that these terms can be applied.

Numerous studies have been undertaken to subdivide and define terranes within the Grenville Province, but all modern studies rely on the tectonic divisions provided by Rivers et al. (1989). Their work is based on the separation of distinctly different tectonic units (Fig. 1.2). First-order boundaries between the differing tectonic units were identified, but could not always be mapped throughout the orogen. Features that extend to the crust-mantle boundary are included in the category of first-order boundaries. The areas that are divided by these boundaries form subparallel and continuous belts along the entire length of the orogen. Second-order boundaries are used to define the subdivisions of the belts into terranes. These terranes are recognized as areas that have common lithotectonic characteristics. In general, the second-order boundaries are large-scale shear zones. Within a terrane, smaller scale shear zones are used to define the boundaries between domains, which can be identified by recognizable gneiss associations and/or other lithologic structures, (i.e. dykes, gabbroic pods, etc.,).

### 1.1.1. The Belts and Their Boundaries

The Central Gneiss Belt (CGB) stretches across Ontario from Georgian Bay to Quebec. It includes the Grenville Front Tectonic Zone (GFTZ), the Parautochthonous Belt (PB) and parts of the Allochthonous Polycyclic Belt (APB). This means that it is bounded by the Huronian metasediments of the Superior Province to the north, and the Grenville Supergroup of the Central Metasedimentary Belt to the south. The CGB is made up of a number of mid-crustal, northwest thrusted slices displaced during the Grenville orogeny (Culshaw, Davidson & Nadeau, 1983). Isotopic studies of Nd model age dating have shown that the CGB is a region of accreted island arc terranes (Dickin & McNutt, 1989). These terranes were accreted through a series of orogenies and collisions, which occurred during the Proterozoic.

The Grenville Front Tectonic Zone (GFTZ) is a major crustal discontinuity with a northeast trend that extends for 2000 km. It is composed of several terranes, including the Beaverstone (BST in Fig. 1.2.) and Timiskaming (TT in Fig. 1.2) in Ontario and Western Quebec. It truncates structural trends in the adjacent provinces to the northwest. It is an area that has experienced major uplift, change in metamorphic grade, faulting and mylonitization (Rivers et al., 1989). The GFTZ represents the northwest limit of the Grenville Province. Seismic studies have shown that its bounding shear zones have a moderate eastward dip of about 30°, and may extend down to the lower crust (Green et al., 1988; Milkerit et. al., 1992).

The Parautochthonous Belt (PB) is found sandwiched between the GFTZ and the Allochthon Boundary Thrust. Its reaches 150 km in width and seems to have a lithologic continuity with the foreland rocks north of the GFTZ in some places (Rivers et al., 1989). Isoclinal folds and northeast trending shear zones dominate much of its length in the northwest. The metamorphic grade increases southeastward from the GFTZ. The parautochthon has been subdivided into a number of second-order terranes. Each of these terranes has a distinct pre-Grenvillian tectonometamorphic history.

The Allochthon Boundary Thrust (ABT) is a first-order boundary. It separates the parautochthon from the allochthonous terranes to the south. It has been mapped in Labrador using a mix of structural, metamorphic, geochronologic and mapping studies. The application of aeromagnetics has allowed an extrapolation of the structure into eastern Quebec. It is less distinct in Ontario, thus it remains a subject of ongoing research. In Labrador, it is identified by the presence of subhorizontal mylonites and southeast plunging lineations. It often seems to coincide with a break in isotopic ages.

The Allochthonous Polycyclic Belt (APB) lies to the southeast of the ABT. It is composed of terranes that are younger than those in the parautochthon. It is called polycyclic because many of its rocks show evidence of having experienced one or more major orogenic events that predate the Grenville orogeny. There are monocyclic intrusive rocks located in some of the terranes. Though it has not been extensively mapped, the allochthon is recognized as a region of high-grade orthogneisses and paragneisses. It has been intruded by Mesoproterozoic granites, gabbros and

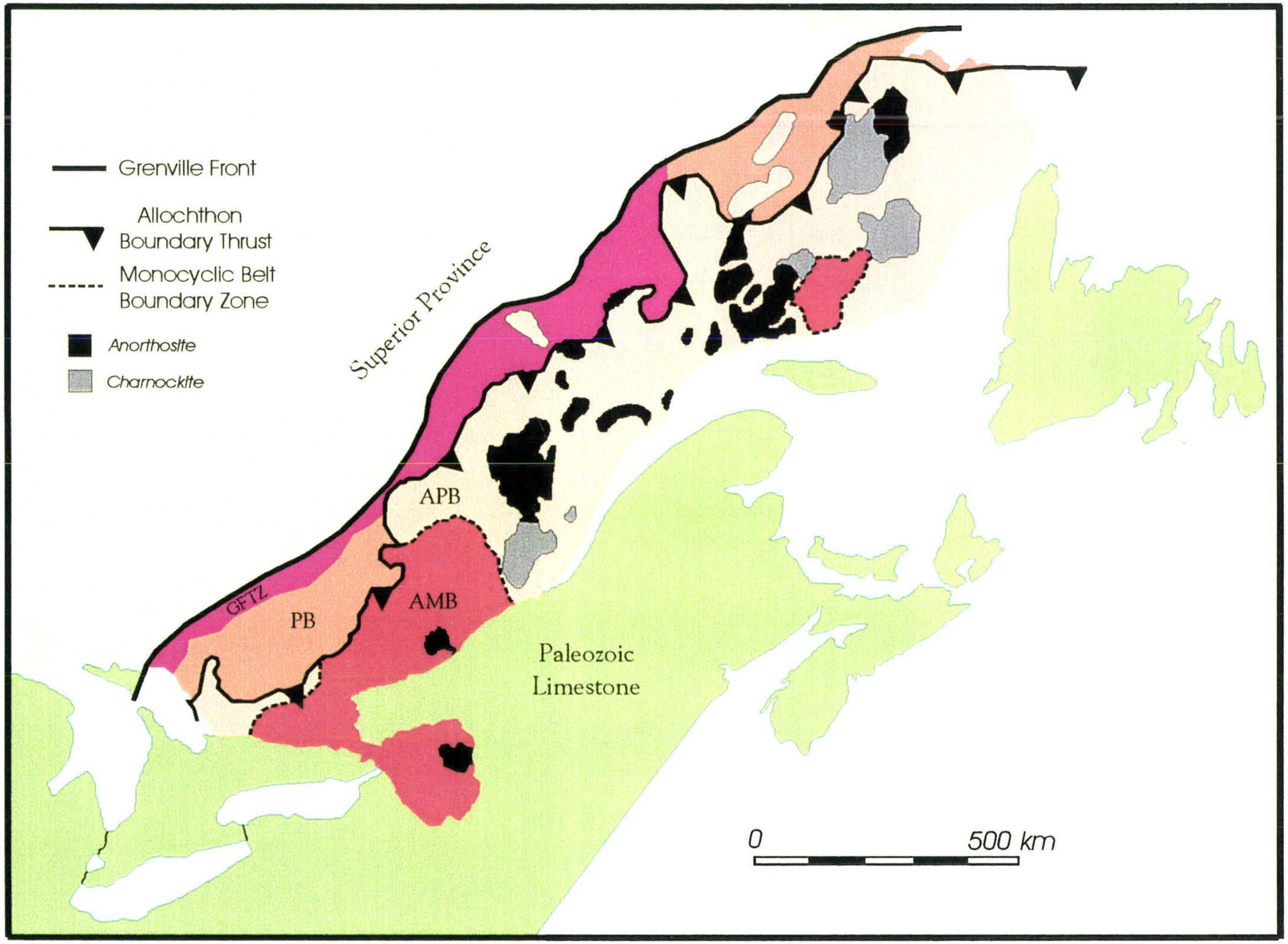


Fig. 1.2. Tectonic divisions of the Grenville Province, modified from Rivers, et. Al. (1989). The Central Gneiss Belt (CGB) consists of the PB and the APB. The southeastern exposure of the AMB is often referred to as the Central Metasedimentary Belt (CMB).

PB = Parautochthonous Belt
APB = Allochthonous Polycyclic Belt
AMB = Allochthonous Monocyclic Belt
GFTZ = Grenville Front Tectonic Zone

The Monocyclic Belt Boundary Zone (MBBZ) separates the APB from a suite of rocks that only experienced the Grenvillian orogeny, the Allochthonous Monocyclic Belt (AMB). This is not continuous along the length of the orogen. In eastern Quebec, it is identified by southeast extension of mylonites. In the west, it is recognized by extensional faulting, which followed northwest-directed ductile thrusting (Rivers et al., 1989).

The Allochthonous Monocyclic Belt (AMB) appears in the Wakeham Terrane in eastern Quebec and in the southwest of the exposed Grenville Province. The latter area is known as the Central Metasedimentary Belt (CMB). The rocks of the monocyclic belt are believed to include marine platform and/or continental margin deposits. They may also include fragments of island arcs, overlain by continental and shallow marine sediments. Both of these successions have ages of approximately 1200 - 1400 Ma and experienced metamorphism during the Grenville orogeny. The metamorphic grade of the rocks ranges from greenschist to granulite facies. Both regions have been intruded by syntectonic granitoids. The full extent of these rocks is not known.

## Identification of the ABT:

### 1.2.0. Importance of the Allochthon Boundary Thrust

Rivers et. al, (1989) cautioned that the location and extent of the first-order belts described above might be altered by more in-depth studies. This has proven true in Central Ontario, where detailed work (Culshaw et. al., 1988, 1989, 1994, 1997; Jamieson et. al., 1992; Ketchum, 1994) has shown that the ABT lies within the Shawanaga Shear Zone (SSZ in Fig. 1.3.), rather than in the Parry Sound Shear Zone (PSSZ in Fig. 1.3.), as originally proposed. Modifications to the Rivers et. al. (1989) model give rise to reinterpretations of the crustal architecture for the parautochthon and allochthon, which in turn, have significant implications for Grenvillian tectonic models. Contrasting ideas about the tectonothermal evolution of the CGB (i.e. break-back thrusting vs. forward-propogated piggy-back thrusting), are discussed in greater detail in Ketchum and Davidson (2000). Our understanding of the Grenvillian orogenic history in the western

CGB would be significantly improved if the position of this boundary could be more accurately located.

### 1.2.1. Position of the Allochthon Boundary Thrust

The position of the ABT is well established between Georgian Bay and Burk's Falls. Here it follows the Shawanaga shear zone (SSZ in Fig. 1.3.), which separates the Britt and Shawanaga Domains. The shear zone extends northeast towards Lake Nipissing, but turns southward near Lake Restoule, seeming to follow the edge of the Powassan Batholith. In Quebec, Kellet et. al. (1994), used aeromagnetics to distinguish a boundary between regionally extensive quartzofeldspathic gneiss and overlying paragneiss in the Northern Grenville Province. These authors proposed that this boundary was the ABT in this region. Later studies (Davidson, 1995, 1996; Indares and Dunning, 1997) suggest the Lac Watson shear zone (LWSZ in Fig. 1.3.) as a more appropriate position for the ABT in this region. Between these distant regions, the location of the ABT was placed along the southern and eastern edges of the Algonquin Domain (Rivers et. al., 1989). This has since been disputed, as Ketchum (1994), Davidson (1995) and Culshaw et. al. (1997) have suggested more northerly locations, passing through either Algonquin Park or North Bay.

Ketchum (1994) suggested that the ABT could be mapped by observing the distribution of mafic rocks which form three distinctive suites:

- *(i)* olivine metadiabase derived from the 1.24 Ga Sudbury dyke swarm
- *(ii)* regionally extensive, 1.17 – 1.15 Ga coronitic olivine metagabbro
- *(iii)* retrogressed eclogite associated with metamorphosed anorthositic and ultramafic rocks

In the Shawanaga region, type (*i*) is restricted to the shear zone footwall, while the other two mafic suites are found in the hanging wall. Ketchum and Davidson (2000) conducted field studies to test whether their spatial distribution conforms to the pattern described at the Shawanaga shear zone, and therefore identified zones which may represent the position of the ABT. Applying the known distribution of 1.17 – 1.15 Ga coronitic metagabbro bodies in the Algonquin domain (Fig. 1.3), suggests that the ABT

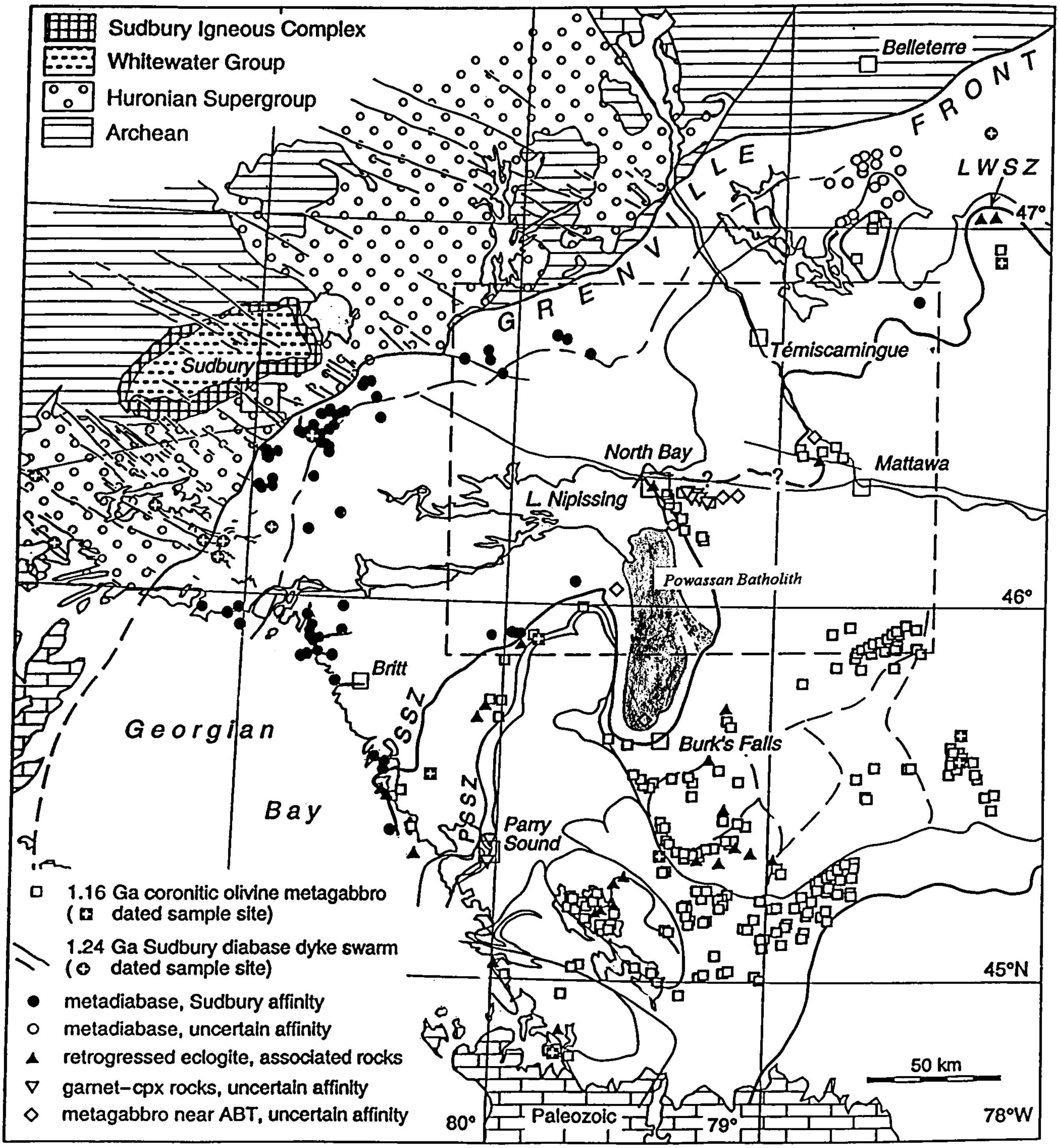


Fig. 1.3. Distribution of three mafic rock suites throughout the western Central Gneiss Belt, Ontario and westernmost Quebec. The broken line near the Grenville Front represents the southeastern margin of the Grenville Front tectonic zone. The SSZ shown in this figure coincides with the ABT, (from Ketchum & Davidson, 2000).

lies north and west of the suggested placement (southeast of Burk's Falls in Fig. 1.3.) of Rivers et. al. (1989), and also implies that the Algonquin Domain may be primarily allochthonous.

1.2.2. Petrology of the Three Mafic Rock Suites

Sudbury diabasic and metadiabasic rocks are noted for their alkaline chemistry, characterized by enrichment in Fe, K, P, Zr, Ba and LREE, and impoverishment in Mg, Ni, Cr relative to many other dyke swarms in the Canadian Shield (Fahrig et. al., 1965; Condie et. al., 1987). These dykes were intruded during a relatively short period at ~1.24 Ga (Krogh et. al., 1987). Folded olivine metadiabase dykes near the Grenville Front have been correlated with the Sudbury swarm based on chemistry and age (Bethune and Davidson, 1997; Dudas et. al., 1994). Examples of these pods and discontinuous dykes can be found along the coast of Georgian Bay, as far south as the Shawanaga shear zone. As stated above, they have been identified in the footwall, but not in the hanging wall.

Corinitic olivine metagabbros occur in equant masses, ranging in size from several meters to one kilometer. Relative to the Sudbury metadiabase, these rocks tend to have higher Mg/(Mg + Fe), higher contents of Ca, Al, Cr and Ni, lower contents of Fe, alkalis, LREE, Ba and Zr. Whole-rock chemistry, grain size, and presence or absence of plagioclase xenocrysts are used to distinguish these metagabbros from the 1.24 Ga Sudbury metadiabases. This mafic rock suite is common south and east of the Shawanaga shear zone, and can be found in the immediate hanging wall of the shear zone (Ketchum & Davidson, 2000).

The last mafic suite occurs as isolated pods and lenses, or as a component of larger deformed complexes, which may include ultramafic and anothorsitic rocks. These occurrences are most often found within highly strained quartzofeldspathic host rocks marking the structural boundaries between lithotectonic domains (Ketchum & Davidson, 2000). Unlike the Sudbury metadiabases or the coronitic metagabbros, it is rare to find relict primary plagioclase in the eclogite-like rocks. These pods of retrogressed eclogite can be found throughout the CGB, southeast of the Shawanaga shear zone. They have been documented in the hanging wall of the shear zone (Needham, 1992), but have not been located structurally beneath it.

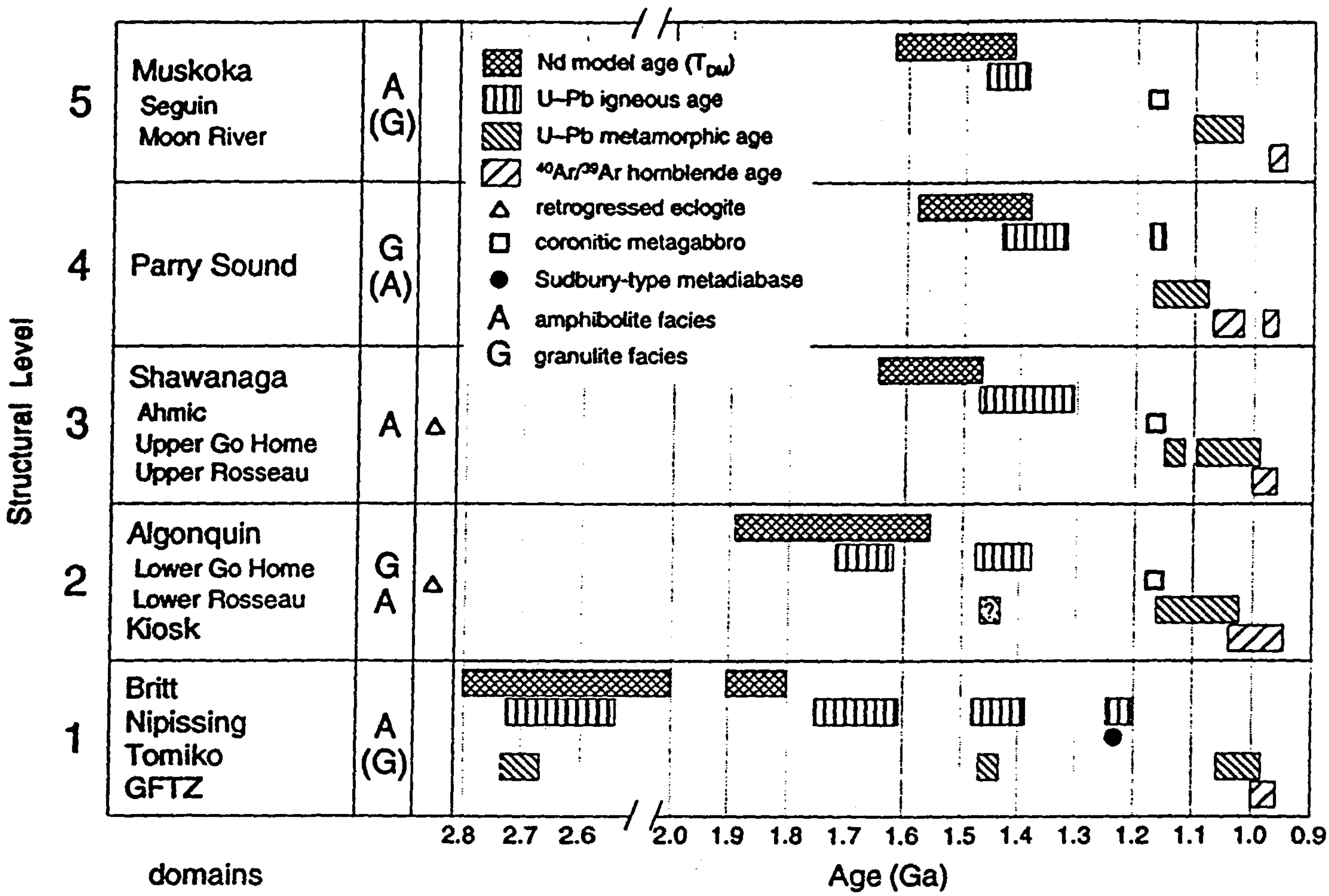


Fig. 1.4. Schematic representation of chronologic, metamorphic and mafic rock Characteristics of the five structural levels of the Central Gneiss Belt, defined by Ketchum & Davidson (2000).

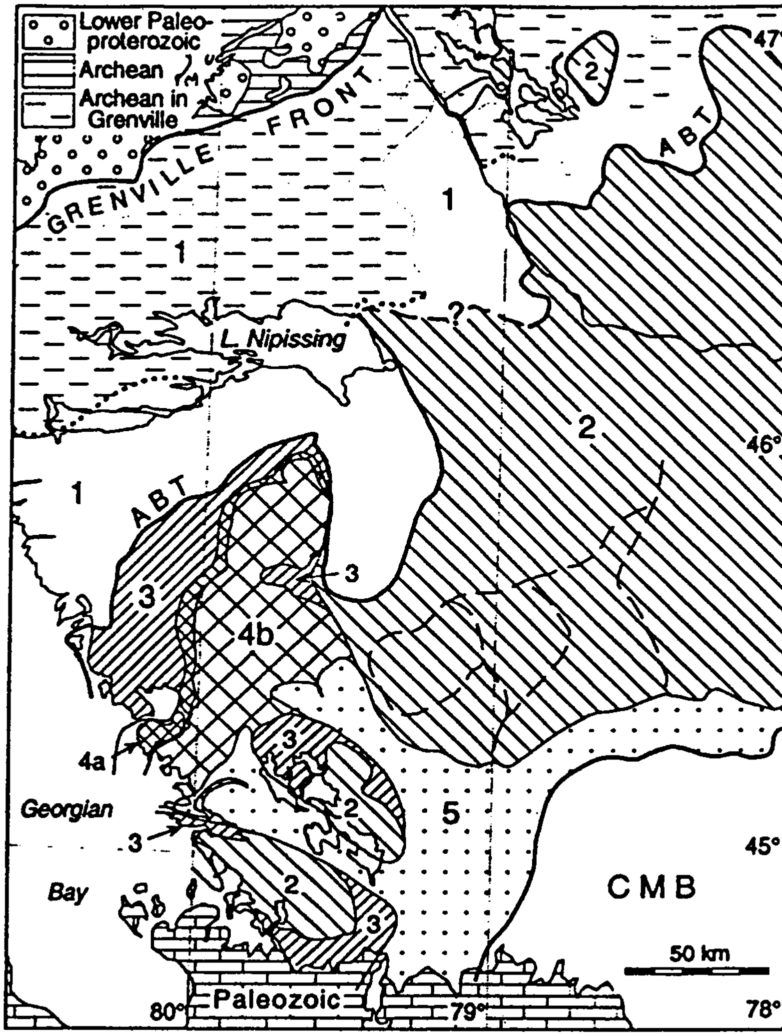


Fig. 1.5. Summary map of the structural divisions proposed by Ketchum & Davidson (2000). Numbers on the map coincide with the structural levels shown in Fig. 1.4.

1.2.3. Structural Model of the Grenville Province

Arguing that the spatial distribution of these mafic rock suites observed across the Shawanaga shear zone should be the same all along the ABT, Ketchum and Davidson (2000) proposed a change in position of the ABT (Fig. 1.3). These authors have placed it running north-south along the eastern edge of the Powassan batholith, turning eastward at North Bay. This new position of the ABT requires changes to the structural model of the CGB. In their model, the CGB is divided into five structural levels based on the distinct combinations of Grenvillian and pre-Grenvillian characteristics (Fig 1.4 & Fig. 1.5):

*Structural Level 1* - This unit is equivalent to the parautochthonous belt and comprises both Archean and Proterozoic crust. This unit has been subject to several Nd isotope studies (described below), investigating these differing crustal components. As described above, this unit is host to Sudbury swarm metadiabases.

*Structural Level 2* - This is the lowest allochthonous unit and forms the hanging wall of the ABT southeast of Burk's Falls (Fig. 1.3). The Algonquin, lower Go Home, and lower Rosseau domains were previously described as part of structural level 1 (Culshaw et. al., 1997). They have been placed in structural level 2 because of the mafic rock suites which they host, (i.e. retrogressed eclogite and coronitic metagabbro). According to Nd model age mapping, this unit lacks Archean crustal material. It should be noted that Fig. 7. From Ketchum and Davidson (2000) shows an overlap in the Nd model ages reported in structural level 1 and structural level 2. Some of the Nd model ages included in the data for structural level 2 are paragneisses and the ages represent sedimentary provenance ages. Removing these model ages eliminates the apparent overlap.

*Structural Level 3* - This level includes the Shawanaga, Ahmic, upper Go Home and upper Rosseau domains. The differences between these domains and the domains of structural level 2 are (*i*) U-Pb crystallizations ages that are entirely MesoProterozoic, (*ii*) amphibolite-facies migmatites are dominant (Culshaw et. al., 1997), and (*iii*) the range of the Nd model ages of these units have a younger lower limit, at ~ 1.4 Ga. The retrogressed eclogites and coronitic metagabbros are found near the base of this unit, which makes up the hanging wall of the ABT in the Shawanaga domain.

*Structural Level 4* - This level consists of the Parry Sound domain, which has been described as an allochthonous slice originally from the Central Metasedimentary Belt or the Adirondack Highlands (Wodicka et. al., 1996). This unit lacks all three of the mafic rock suites found throughout the other structural levels of the CGB, which supports the hypothesis that this domain experienced part of its Grenvillian history at a location south and east of its current position.

*Structural Level 5* - This level includes the Muskoka domain and the Seguin and Moon River subdomains. Nd Model ages for these domains are similar to those in structural level 3. This unit is host to coronitic metagabbro, but no documentation of the retrogressed eclogite exists. Absence of high-pressure metamorphism in this unit is a result of out-of-sequence thrust emplacement (Culshaw et. al., 1997).

Nd model age mapping of the ABT is possible because it separates terranes with Archean to PaleoProterozoic ages (*structural level 1*) from terranes with MesoProterozoic ages (*structural levels 2 – 5*).

## Identification of the Penokean Suture:

### 1.3.0. Identification of the Penokean Suture

Approximately 60 km south of the Grenville Front, there is a geologic boundary over which there exists a step in Nd model ages (Fig. 1.6). This boundary lies within the Britt Domain and lacks a zone of regional high strain associated with Grenvillian terrane boundaries. It was interpreted as a pre-Grenvillian terrane boundary (Dickin and McNutt, 1989), marking the southeastern margin of the Archean craton. This boundary separates the Archean or re-worked Archean foreland from accreted Proterozoic crustal material. The age of this boundary has been correlated with the Penokean Orogeny, which will be discussed in Chapter 5 of this text. Studies of paragneisses and plutons near this boundary (Dickin & McNutt, 1989, 1990; Dickin et. al., 1990; Holmden and Dickin, 1995; Dickin, 1998) have shown that Nd model ages of >2.2 Ga are found north of the suture, while Nd model ages of ≤ 2.0 Ga lie south of the suture. It was suggested that this boundary represented a collisional suture, which formed at the termination of southerly-dipping subduction under a 1.9 Ga island arc (Dickin et. al., 1990).

## Objectives of this Research:

1.4.0. Overall Objectives

Evolution of the pattern of early Proterozoic orogens has proven difficult to define as a result of the intensive overprinting of the Grenvillian orogeny. Older structural features and relationships have been obscured by this overprinting. Cooling ages and plutonic crystallization ages are used to determine the geological evolution of a gneiss terrane, but the crustal extraction age of its protolith is a more fundamental characteristic. Use of the Sm-Nd model age method is recommended for dating this event (McCulloch and Wasserburg, 1978). Sm and Nd experience appreciable fractionation during crustal extraction processes, but relatively little fractionation during erosional, sedimentary and metamorphic processes. Differences in crustal extraction ages can then be used to map and define terrane boundaries.

In this study, the two most fundamental boundaries within the Grenville Province are investigated. The ABT marks the geologic boundary between parautochthonous and allochthonous crust. Its location is relatively well established in the Shawanaga shear zone, north of Parry Sound, and in the Lac Watson shear zone, in western Quebec, but it is not so confidently positioned outside of these locations. One of the major focuses of this study is to enhance the knowledge of the Nd isotope signature on either side of this boundary in the Shawanaga Inlet region. Mapping the ABT accurately in this region is difficult, as it lies beneath waters of Georgian Bay. This should create a guide for future studies in regions where the ABT is not well defined.

The Penokean Suture marks the southernmost extent of Archean crust in the Grenville Province. Continuation of previous Nd isotope studies, combined with studies of aeromagnetic and remotely sensed data have been undertaken to produce a more detailed map in the Key Harbour region. This part of the study also investigates the possibly of applying geophysical techniques to study the trend of the suture where isotopic sampling is not feasible. As in the Shawanaga region, the ability to accurately map the geologic features is limited by the presence of Georgian Bay.

The following pages contain an introduction to the individual field areas, shown in Fig. 1.6., and the objectives specific to the those regions.

### 1.4.1. The Shawanaga Area

The primary field area lies between Pointe Au Baril and Parry Sound on Georgian Bay (Fig. 1.6, Field Area 1). Several samples were collected from the outcrops along Highway 69, but the majority of the sampling was done on Georgian Bay. The objectives of the study here are:

1. To locate the ABT as precisely as possible by isotopic mapping of the boundary between terranes with different formation ages.

### 1.4.2. Around the Powassan Batholith

This part of the study is a reconnaissance of the areas surrounding the Powassan Batholith, (Fig 1.6, Field Area 2). This includes the Britt Domain, Shawanaga Domain and the Ahmic Domain on the western edge of the batholith, and the Kiosk Domain to its east. The objectives of the study in this area are:

1. Using the model age constraints determined from the Shawanaga Area, to determine the approximate location of the ABT as it passes through this region.

2. To determine the direction of future studies in this region.

### 1.4.3. Key Harbour to the Gull Rocks

The third field area lies on the Northeastern corner of Georgian Bay, from the mouth of the Key River out to the Gull Rocks, (Fig. 1.6, Field Area 3). The Penokean Suture passes through this region. The objectives of the study in this area are:

1. To utilize magnetic data in order to map lineaments which represent tectonic structures and boundaries.

2. To determine the usefulness of geophysical methods for mapping the suture where it is not possible to collect samples, such as its location as it crosses underneath Georgian Bay.

3. To locate the discontinuity in the isotopic signature as precisely as possible, providing a local-scale map of the trend of the suture.

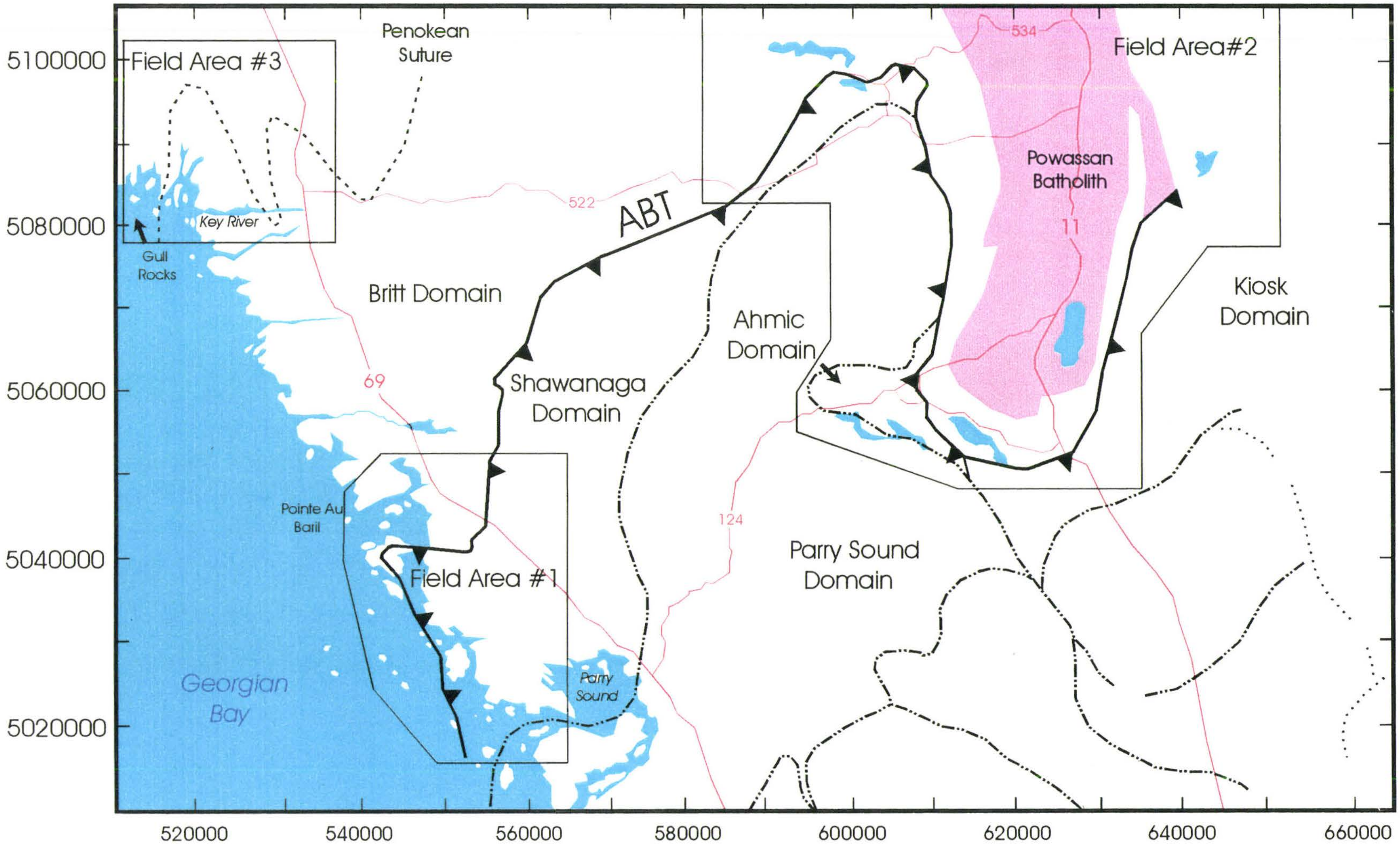


Fig. 1.6. Overview map of the western Central Gneiss Belt, showing locations of the field studies conducted during this research.

# Chapter 2

## Radiogenic Isotope Chemistry:

### 2.1.0. Isotope Systematics

There are seven naturally occurring Sm isotopes: $^{144}Sm$, $^{147}Sm$, $^{148}Sm$, $^{149}Sm$, $^{150}Sm$, $^{152}Sm$ & $^{154}Sm$. Amongst these, $^{147}Sm$, $^{148}Sm$, and $^{149}Sm$ are radiogenic. The decay of $^{148}Sm$ to $^{144}Nd$ and $^{149}Sm$ to $^{145}Nd$ (DePaolo, 1988) do not produce measurable differences in the abundance of the daughter isotopes, because they have half-lives of approximately $1 \times 10^{16}$ years. The decay of $^{147}Sm$ to $^{143}Nd$ has a half-life of 106 Ga. Over periods of several millions of years, this decay system produces small, yet measurable differences in the abundance of $^{143}Nd$, and is therefore the basis for Sm-Nd dating.

Nd also has seven naturally occurring isotopes: $^{142}Nd$, $^{143}Nd$, $^{144}Nd$, $^{145}Nd$, $^{146}Nd$, $^{148}Nd$ & $^{150}Nd$. As stated above, $^{143}Nd$, $^{144}Nd$ and $^{145}Nd$ are the products of the radioactive decay of $^{147}Sm$, $^{148}Sm$ and $^{149}Sm$. $^{142}Nd$ must be ignored, because it can be generated by the decay of the $^{146}Sm$, an extinct radionuclide. The second most abundant isotope is $^{144}Nd$, which decays to $^{140}Ce$. However, this system has a half-life greater than $1 \times 10^{14}$ years and has resulted in a 0.00015% decrease of $^{144}Nd$ (DePaolo, 1988), during the 4.5 Ga history of the Earth. Due to its abundance and half-life, $^{144}Nd$ is treated as a stable isotope and used as the normalizing isotope in the Sm-Nd decay system.

In the case of a given system, such as an igneous rock or mineral, the following equation describes the decay of $^{147}Sm$:

$$\frac{^{143}Nd}{^{144}Nd} = \frac{^{143}Nd_I}{^{144}Nd_I} + \frac{^{147}Sm}{^{144}Nd}(e^{\lambda t}-1)$$

in which, I represents the initial abundance, $\lambda$ is the decay constant and t is the age of the system. The equation is normalized by dividing all three radionuclides by the stable nuclide $^{144}Nd$. This also gives the equation the same form as that used for the Rb-Sr dating technique. The equation can be plotted as an isochron diagram, but the similar chemistry of Sm and Nd make wide ranges of Sm/Nd ratios difficult to obtain. U-Pb and Sm-Nd dating techniques are employed in the study of metamorphic rocks, where the simpler Rb-Sr method is unsuitable. U-Pb dating is now used to measure crystallization ages, but can not be used to determine the crustal residence ages. The Sm-Nd method "sees through" the effects of metamorphism, allowing study of the original crustal formation age of a given rock.

### 2.1.1. Nd Model Age Concept

The objective of a Nd model age study is to calculate the time at which the rocks were segregated from the depleted mantle reservoir and began to form the continental crust. Through the ages, the Earth's crust has grown by selectively removing the lighter elements from the mantle. A result of this "melting off" is the evolution of buoyant "islands" of "Sial", often referred to as microcontinents. These microcontinents resist subduction because their density is less than that of the mantle. Tectonic activity caused these microcontinents to collide with one another and with the larger tectonic cratons. This resulted in the microcontinents amalgamating with each other and the larger cratons to from the large continents of today. The record of these past geological events can only be revealed by studying continental rocks.

The Earth was formed 4.6 Ga ago. Sm and Nd are believed to have condensed when the solar nebula was cooling (Grossman & Larimar, 1974). Nd model ages were originally based on the isotopic ratios of chondritic meteorites. These meteorites are thought to be representative of the "original" nebular isotopic compositions, because they contain both refractory and volatile elements, which have experienced minimal fractionation. According to the CHUR (<u>Ch</u>ondritic <u>U</u>niform <u>R</u>eservoir) model, the Nd evolution line defines the initial ratios of continental igneous rock through time. Measurement of the Sm/Nd ratio in any crustal rock yields its age of its formation, or the age of formation of its precursor. This requires sufficient fractionation to occur during the process of crustal extraction from the mantle.

The afore-mentioned chemical similarities of Sm and Nd cause them to experience only slight fractionation during the crystal-liquid processes. When dealing with terrestial rocks, the departure of $^{143}Nd/^{144}Nd$ from the CHUR evolution line are minute. The ε Nd notation was developed to provide a way to express these small departures. The initial $^{143}Nd/^{144}Nd$ ratios are represented in parts per $10^4$ deviation from the CHUR evolution line. The mathematical equation takes the form:

$$\varepsilon\,\mathrm{Nd}(t) = \frac{(^{143}\mathrm{Nd}/^{144}\mathrm{Nd})_{\mathrm{sample}}(t) - (^{143}\mathrm{Nd}/^{144}\mathrm{Nd})_{\mathrm{CHUR}}(t)}{(^{143}\mathrm{Nd}/^{144}\mathrm{Nd})_{\mathrm{CHUR}}(t)} \times 10^4$$

where $t$ is the time at which ε Nd is calculated. The units are termed epsilon units. Normalizing all data to CHUR in the ε Nd notation also produces the advantage of removing the effects of different fractionation corrections used in Nd analysis as the metal or the oxide species.

While the CHUR Nd evolution line worked well for Archean plutons, studies of the mid-ocean ridge basalts and the metamorphosed Proterozoic basement in the Colorado Front Range soon produced ε Nd values that were well above the CHUR evolution line. This led to the time dependent Depleted Mantle Model ($T_{DM}$) (DePaolo, 1981). The $T_{DM}$ model was developed by fitting a quadratic curve to 1.8 Ma Colorado Front Range gneisses (ε Nd = +3.7), modern island arc data sets (ε Nd = +8.5), and a zero point at 4.5 Ga. This curve represents the Nd evolution of a progressively depleted reservoir, which provided the materials necessary for calc-alkaline magamatism. In the early Archean, this evolution line is similar to the CHUR evolution line. From the late Archean (~2.7 Ga) to the present day, there is a progressive divergence from the CHUR evolution line (Fig. 2.1). The composition of the depleted mantle, relative to CHUR, at time $T$, is described by the equation:

$$\varepsilon\,\mathrm{Nd}(T) = 0.25T^2 - 3T + 8.5$$

where $T$ is in Ga. A plot of ε Nd vs. time shows the difference between $T_{DM}$ and $T_{CHUR}$ (Fig. 2.2). This difference reflects the fact that the $T_{DM}$ incorporates a greater removal of Nd than Sm as crustal materials were repeatedly extracted from the mantle reservoir.

Intra-crustal events such as erosion, sedimentation and metamorphism have a minimal effect on Sm/Nd ratios. The only significant fractionation that they experience is that incurred during crustal extraction from the mantle. When the magma separates from the mantle, it becomes enriched in Nd over Sm. The $^{143}Nd/^{144}Nd$ ratio of the sample is measured along with Sm and Nd concentrations. This information is used to

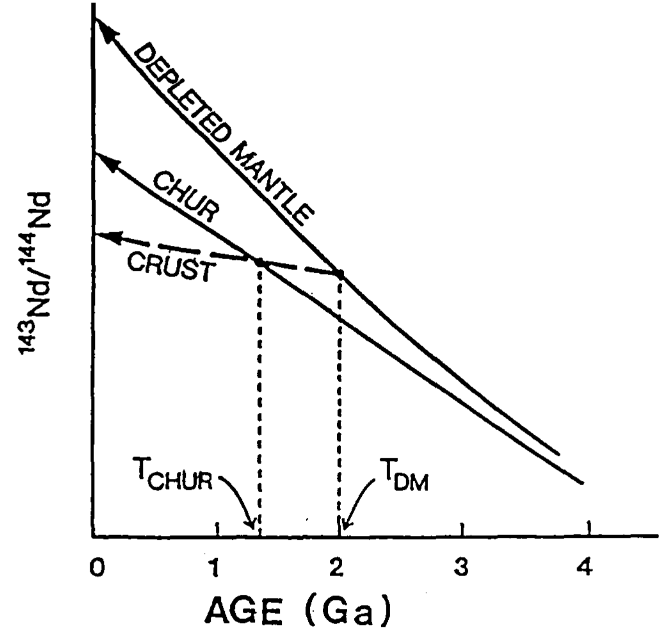


**Fig. 2.1.** Model ages calculated with the $T_{CHUR}$ model tend to be underestimated, relative to $T_{DM}$ model ages, for rocks that are derived from a deplete mantle source (DePaolo, 1981).

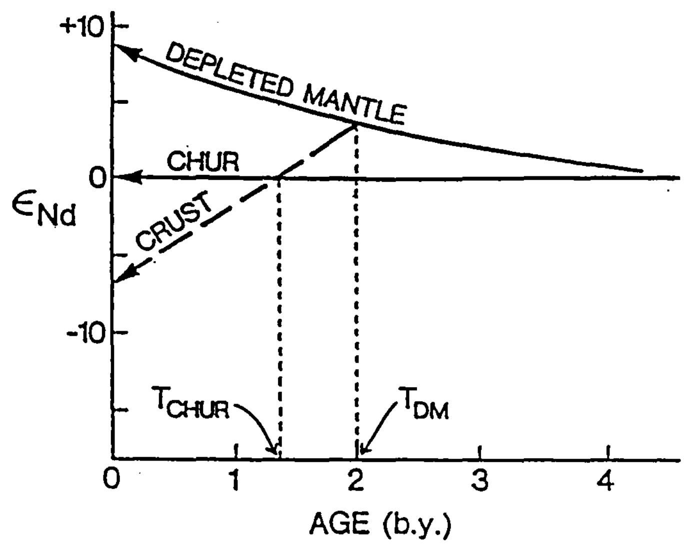


Fig. 2.2. Changes in ε Nd through time. ε Nd is measured relative to $T_{CHUR}$, which does not change over time. There is a positive increase in the ε Nd signature of the mantle, as Sm and Nd are repeatedly extracted from it over time. The inverse is true for the crust, which acquires Nd when a new magmatic body is formed.

extrapolate the Nd evolution line back to the $T_{DM}$ curve, where the intersection defines the crustal formation age of the crust-forming magma (Fig. 2.1 & Fig. 2.2).

Previous studies in the Grenville Province, (Dickin & McNutt, 1989; Dickin, 1998), have employed the $T_{DM}$ model, arguing that it is more suitable for Proterozoic subduction-related magmas than the CHUR model, because they are derived from magmas which are less depleted than the magmas which form the MORB (e.g. Patchett & Bridgewater, 1984). The $T_{DM}$ model has been used for other North American studies (DePaolo, 1981; Nelson & DePaolo, 1985; Bennett & DePaolo, 1987), which means that direct comparisons are easier if it is used.

The interpretation of Nd model ages as crustal formation ages is based on two major assumptions (Arndt & Goldstein, 1987):

1. A short time was involved for the sample between the mantle extraction and the crustal emplacement.
2. All material of the sample came from a single extraction event and the Sm/Nd ratio of the sample has not been modified by subsequent events.

The second assumption is especially significant, as several intracrustal events can modify the Nd isotopic ratios. These events include sedimentary mixing of detritus from different sources, crustal assimilation of a magma and crustal anatexis.

Granitoids, which are common in the Grenville Province, can formed from mantle-derived magmas subjected to crustal assimilation or from crustal materials through anatexis. As a juvenile mantle-derived magma ascends, it might experience crustal assimilation from more ancient wall rocks. This is a likely event in tectonic environments, where continental crust is thick, such as active continental margins and continental rifts. Crustal assimilation results in lower $\varepsilon$ Nd values and older Nd model ages (Fig. 2.3).

Nd model ages have also been used to study the petrogenesis and crustal age structure at depth of granitoids formed by crustal anatexis. Since these granitoids are derived by melting of older crust, the model ages are generally younger than those of the source rocks. This is caused by the fractionation of the Sm and Nd during the remelting of the existant crust. Discrepancies in the model ages are dependent on the time gap between the original crustal formation and the new granitoid formation. Nd isotopic

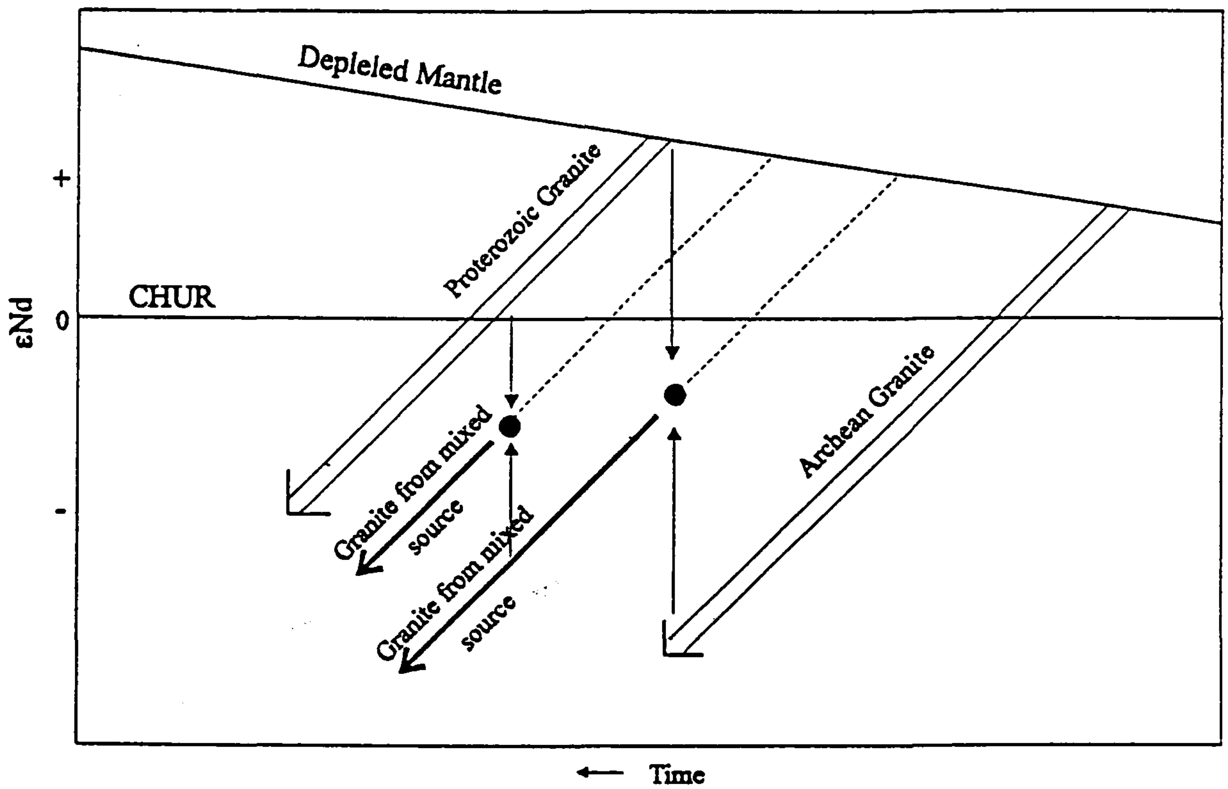


Fig. 2.3. Rocks derived from mixed sources do not give model ages representative of crust-forming events (from Arndt & Goldstein, 1987).

studies of crust-derived granitoids have been performed by Farmer & DePaolo (1983), Nelson & DePaolo (1985), and Bennett & DePaolo (1987) in the western USA, and by Dickin & McNutt (1989), Dickin, et. al. (1990) in the Grenville Province in Ontario. These studies have revealed the existence of older basement beneath granitoid plutons.

# Chapter 3:

## The ABT in the Shawanaga Region:

### 3.1.0. Introduction

The focus of this part of the study is to map the Allochthon Boundary Thrust in the Shawanaga region and out into Georgian Bay. The ABT is a first-order tectonic boundary, dividing the monocyclic and polycyclic belts of the Grenville Province. In the Shawanaga region, the ABT is a large shear zone which divides the Britt Domain from the Shawanaga Domain (Culshaw, et. al., 1997). This study involves the use of Nd isotopes to map the ABT, based on a measurable discontinuity in the model ages. The Britt Domain, to the north & west of the shear zone, is characterized by Nd model ages between 1.8 Ga and 2.0 Ga (Dickin & McNutt, 1989), while the Shawanaga Domain is characterized by Nd model ages between 1.3 and 1.7 Ga. Using these constraints, sampling was performed in order to map the boundary between these two domains. With large-scale intense shearing, it is conceivable that pressures and temperatures could attain high enough levels to cause a mixing of the Britt and Shawanaga materials. This mixing will produce a transition zone where the Nd model age results lie in the 1.7 Ga to 1.8 Ga gap. Sampling transects across the shear zone can be used to approximate the width of this transition zone.

### 3.1.1. The Field Area

The study area (Fig. 3.1) extends from Pointe Au Baril, southwards to Bateau Island, (Ontario Topographic Maps 41 H/7, 41 H/8 & 41 H/9). The Shawanaga shear zone crosses Highway 69 with a north-south trend, at the bridge over the Shawanaga River. Just south of this location, it turns westward, crossing the Shawanaga Inlet, where a sharp fold turns it south again. The shear zone runs parallel to the coastline, comes into contact with the outer coast of Franklin Island and continues southwards. A majority of the sampling was conducted in areas near the location of the shear zone determined by previous mapping (Davidson, et. al., 1982; Culshaw, et. al., 1983, 1990, 1994, 1997, 2000). Further sampling was conducted around the Snake Islands, which had produced

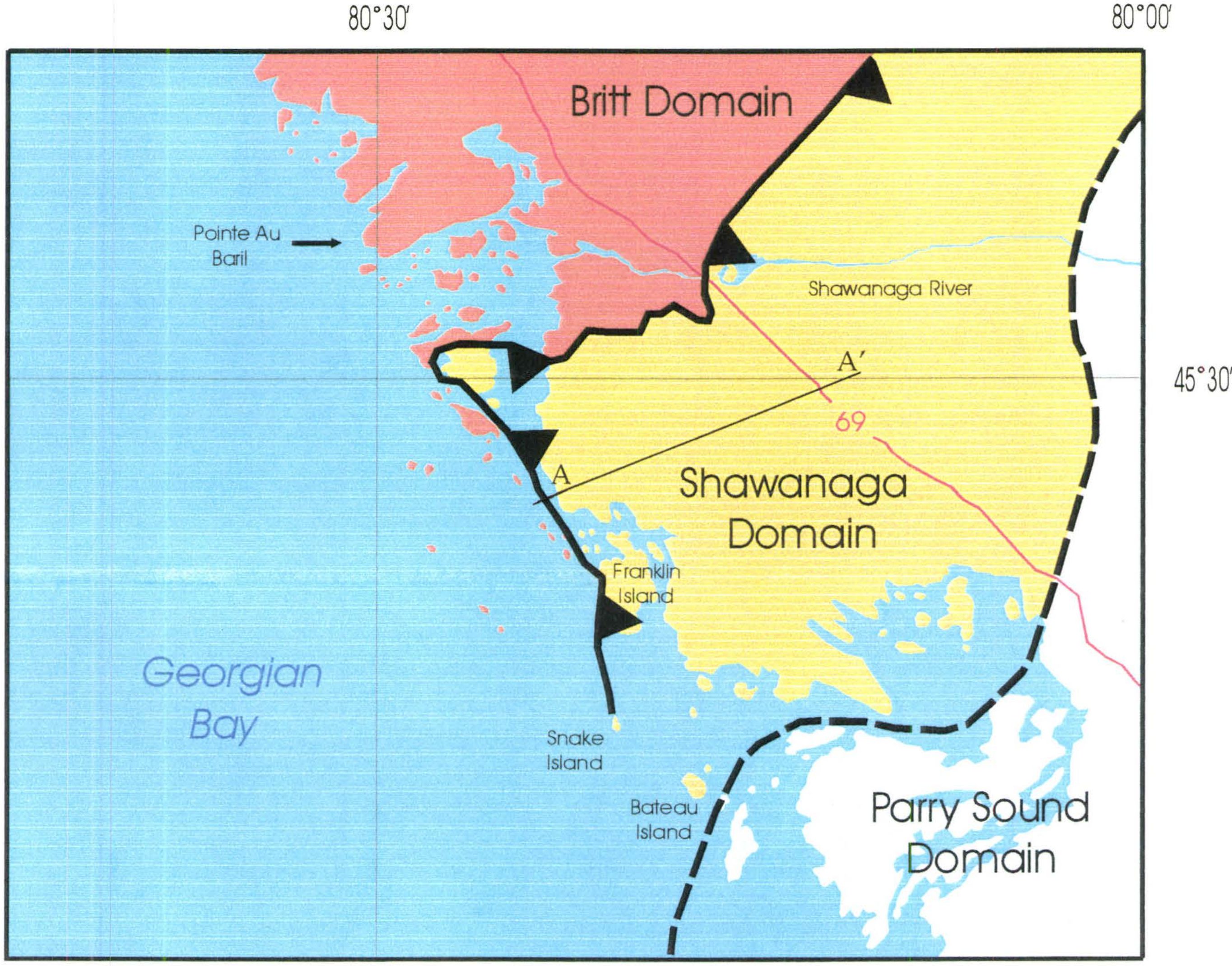


Fig. 3.1. Overview map of the Shawanaga Region, where 57 samples were collected for Nd Model Age determinations.

unexpected results in the early stages of the study. Several samples were collected from roadside outcrops along Highway 69 as well.

3.1.2. Geologic Setting

The field area covers the Britt and Shawanaga Domains of the Central Gneiss Belt. These domains are separated by the Shawanaga shear zone, which marks the allochthon boundary thrust in the western Grenville Province. Evidence for a polyphase history of the shear zone is provided by tectonstratigraphic data and kinematic indicators. It is believed that the shear zone originated as a thrust, because of the tectonostratigraphic contrasts between the Britt and Shawanaga Domains (Culshaw et. al., 1994). Although the timing of the thrusting is not known, U-Pb data (Krogh et. al., 1993) suggest that it occurred at ~1080 Ma. Further studies (Ketchum et. al., 1998), suggest that extensional reactivation occurred at ~1020 Ma. There is no constraint on the amount of displacement during thrusting or extension, although the juxtaposition of totally different rock suites suggests it must have been considerable.

**Britt Domain**

The Britt Domain extends from the Grenville Front Tectonic Zone to the Shawanaga shear zone. It is composed of granitic to tonalitic orthogneisses with subordinate paragneisses. A significant portion of the domain has been intruded by 1740 – 1600 Ma granitoid plutons (Krogh, et. al., 1993; Corrigan, et. al., 1994). There is also a large volume of 1460 – 1430 Ma megacrystic granitoid plutons (Corrigan, et. al., 1994). Along with the paragneisses, these rocks were metamorphosed and deformed to amphibolite-facies during the Grenville orgeny, although there are several granulite-facies assemblages preserved in the southernmost Britt Domain (Ketchum et. al., 1994). As previously stated, Nd model ages in the Britt Domain range from 2.0 Ga to 1.8 Ga. The Britt Domain is divided into two major gneiss associations, the Bayfield Association and the Nadeau Island Association.

*Bayfield Gneiss Association*

This grouping lies north of Pointe Au Baril and is composed of four lithologies that have been described as the Bayfield Gneiss Association. These are:

1) pink leucogneiss
2) grey leucocratic migmatic orthogneiss
3) grey leuco- to mesocratic garnet-biotite paragneiss
4) calc-silicate and amphibolite gneiss.

*Nadeau Island Gneiss Association*

This grouping is found in the region between Pointe Au Baril and the Shawanaga shear zone. Much of the region is intruded by granites and quartz monzonites with megacrystic k-feldspar. The five lithologies that make up Nadeau Island Association are:

1) grey migmatitic leucocratic orhtogneiss
2) grey leucocratic migmatitic garnet-bearing orthogneiss
3) unclassified paragneiss
4) pink layered leucocratic paragneiss
5) rusty weathered graphitic paragneiss

**Shawanaga Domain**

The lowest allochthonous domain, forming the hanging wall of the Shawanaga shear zone, is the Shawanaga Domain. In the south, the contact with the Parry Sound Domain is a narrow zone of extensional reactivation (Culshaw, et. al., 1997). The Nd model age results in the Shawanaga Domain fall in the range 1.3 Ga to 1.7 Ga. There are four lithologic units described in the Shawanaga Domain.

*Shawanaga Pluton*

The Shawanaga Pluton is a ~1460 Ma (T. Krogh, unpublished data), migmatitic granite sheet that is found at the base, or northern section of the domain.

*Ojibway Gneiss Association*

Overlying the Shawanaga Pluton is the Ojibway Association. This is exposed in the Shawanaga Inlet and further south on Franklin Island. It is composed of three lithologies:

1) grey metatexite with hornblende-epidote bearing leucosomes
2) grey migmatitic tonalitic to granodioritic gneiss with variable pink leucosomes
3) grey hornblende-epidote-biotite tonalitic orthogneiss

*Sand Bay Gneiss Association*

This rock package is also readily identified in the Shawanaga Inlet, on Franklin Island, and in Sand Bay. Fig. 3.2 shows a lithologic cross-section of the Sand Bay Association, as studied along the mainland coast of the Shawanaga Inlet (Culshaw & Dostal, 1997) .The four lithologies of which it is comprised are:

1) grey tonalitic orthogneiss
2) grey quartz-feldspar-biotite paragneiss with pink leucosomes
3) medium to dark grey biotite-rich quartz-plagioclas pargneiss & schist
4) para-amphibolite

*Lighthouse Assemblage*

Formerly described as part of the Parry Sound Domain, this group of rocks is now considered to be the uppermost part of the Shawanaga Domain. It is composed of migmatitic pelitic and psammitic gneiss, amphibolite, calc-silicate gneiss and quartzofeldspathic gneiss. This assemblage is rich in garnet.

**Mafic Intrusives**

One of the interesting differences between the Britt and Shawanaga Domains is the types of mafic intrusive rocks that are found within these domains. The Britt Domain hosts suites of metamorphosed and deformed mafic dykes, while the Shawanaga Domain contains pods of coronitic metagabbro and rare garnet-clinopyroxene metabasite. The metagabbro bodies are found throughout allochthonous domains in the Central Gneiss Belt, with the Parry Sound Domain as the one exception. The garnet-clinopyroxene metabasites are also restricted to allochthonous domains, and are often described as retrogressed eclogites (Ketchum, et. al., 1998).

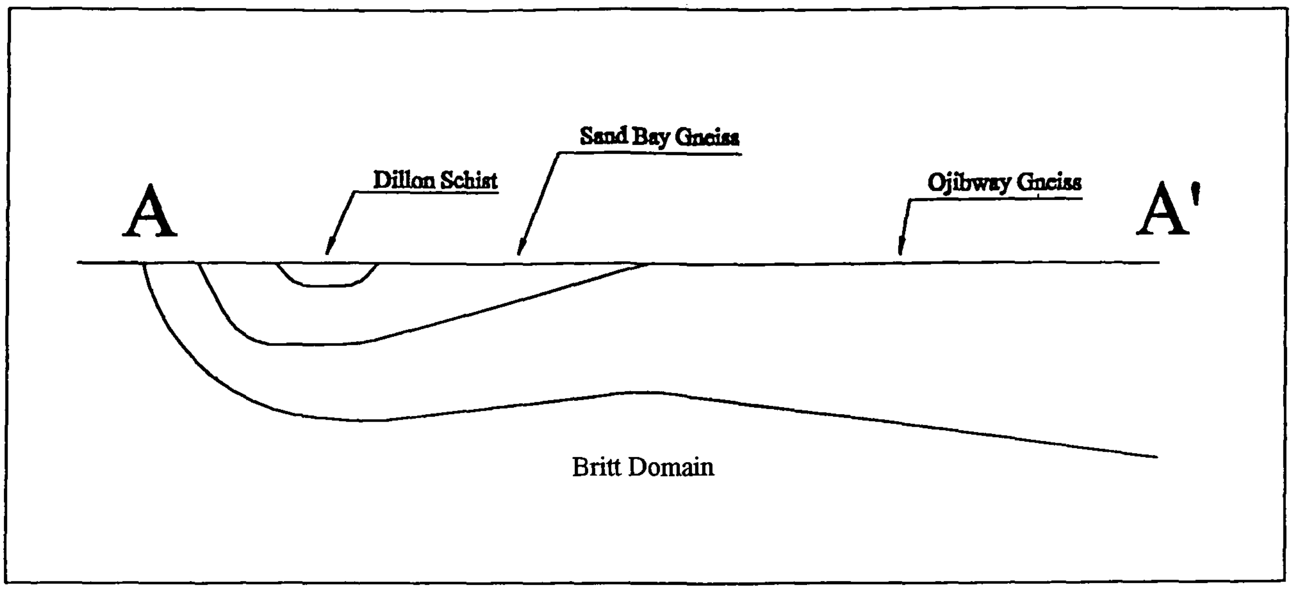


Fig. 3.2. A sketch profile of the simplified fold structure in the Shawanaga Domain. The location of A – A' is shown in Fig. 3.1.

**Structural Geology**

In the study area, there is a large-scale syncline with a northwest-southeast trending axis. As illustrated in Fig. 3.2, the western limb of the syncline is much steeper than the eastern limb, making the western limb more useful for describing the afore-mentioned stratigraphy of the Shawanaga Domain.

## Nd Model Age Results:

3.2.0. Objectives

In the Shawanaga Inlet region, sampling was conducted to provide Nd model age constraints on the location of the ABT. The aim of this study is to test the mapped position of the ABT by sampling the gneiss associations on either side of it and confirm the previously established Nd model age ranges for these gneisses. In areas where the position of the ABT is loosely constrained (i.e. southwest of Franklin Island), Nd model age mapping can be used to locate the ABT. Another aspect of the ABT which will be investigated is the apparent width of the transition zone in which Nd model ages represent a mixing of the younger and older gneisses. As in the Shawanaga region, these samples would either indicate a more precise position for the ABT, or identify a zone of ductile shear in which mixing of younger and older rocks occurred.

3.2.1. Nd Model Age Results

A total of 57 samples were collected and studied in this field area. In the Pointe Au Baril region (Fig. 3.3b.), 15 samples were studied to evaluate the changes in the Nd model ages along the ABT, which is represent here by the boundary between the Shawanaga pluton and the Britt Domain. Another 43 samples were collected on Georgian Bay between Hertzberg Island and Bateau Island (Fig. 3.3c. & Fig. 3.3d.), to study and confirm the mapped location of the ABT, identified as the boundary between the Objiway and Nadeau Island gneiss associations. Along Highway 69, 2 samples were collected and studied, to add to previously known data (GF103, GF107 in Table 3.1a.).

The Nd model age results present in Table 3.1. have been divided into 4 groups. There are gneissic rocks with Britt Domain ages, gneissic rocks with Shawanaga Domain ages, gneissic rocks with intermediate ages and plutons with intermediate ages. This is

# Fig. 3.3a. Legend For Shawanaga Region Maps

## MesoProterozoic Plutons

Associated grey granodiorite & monzodiorite

Associated granite & quartz monzonite

Shawanaga Pluton: grey hornblende-biotite granodiorite/
associated pink granite & grey granodiorite

## Britt Domain (1.8 - 2.0 Ga)

Bayfield Gneiss Association

Nadeau Island Gneiss Association

ABT

## Shawanaga Domain (1.4 - 1.7 Ga)

Ojibway Gneiss Association

Sand Bay Gneiss Association

Dillon Schist (Sand Bay Gneiss Association)

## Snake Island Area

Tonalitic Granodiorite

Unclassified Gneiss

Anorthosite

Coronitic Metagabbro and Retrogressed Eclogites
(shown in Fig. 3.7.)

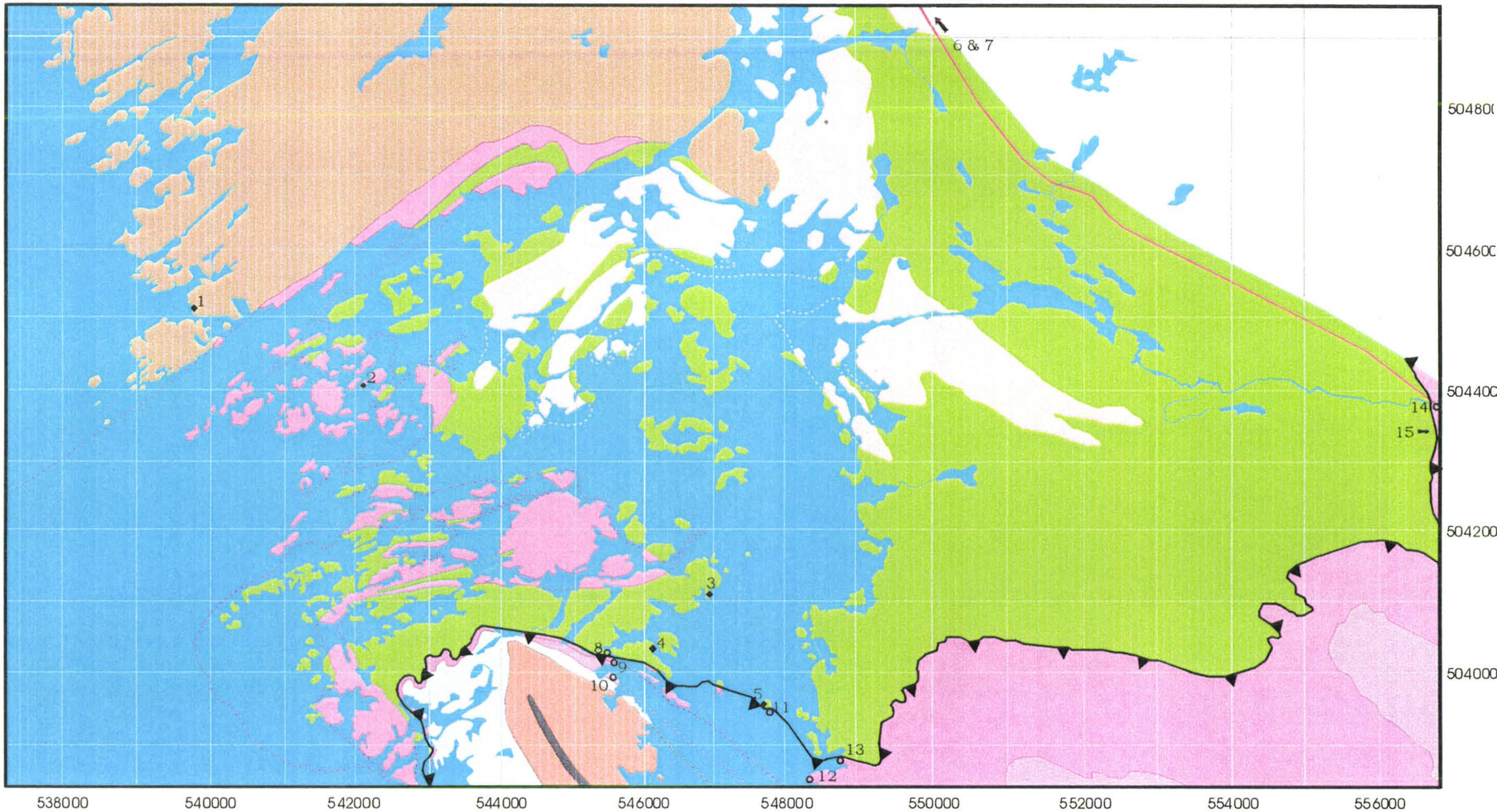


Fig. 3.3b. Geologic map: Pointe Au Baril area, modified from Culshaw, et. Al. (2000)

- ◆ Paleoproterozoic Nd model age
- ▲ Mesoproterozoic Nd model age
- ○ Granitic Pluton

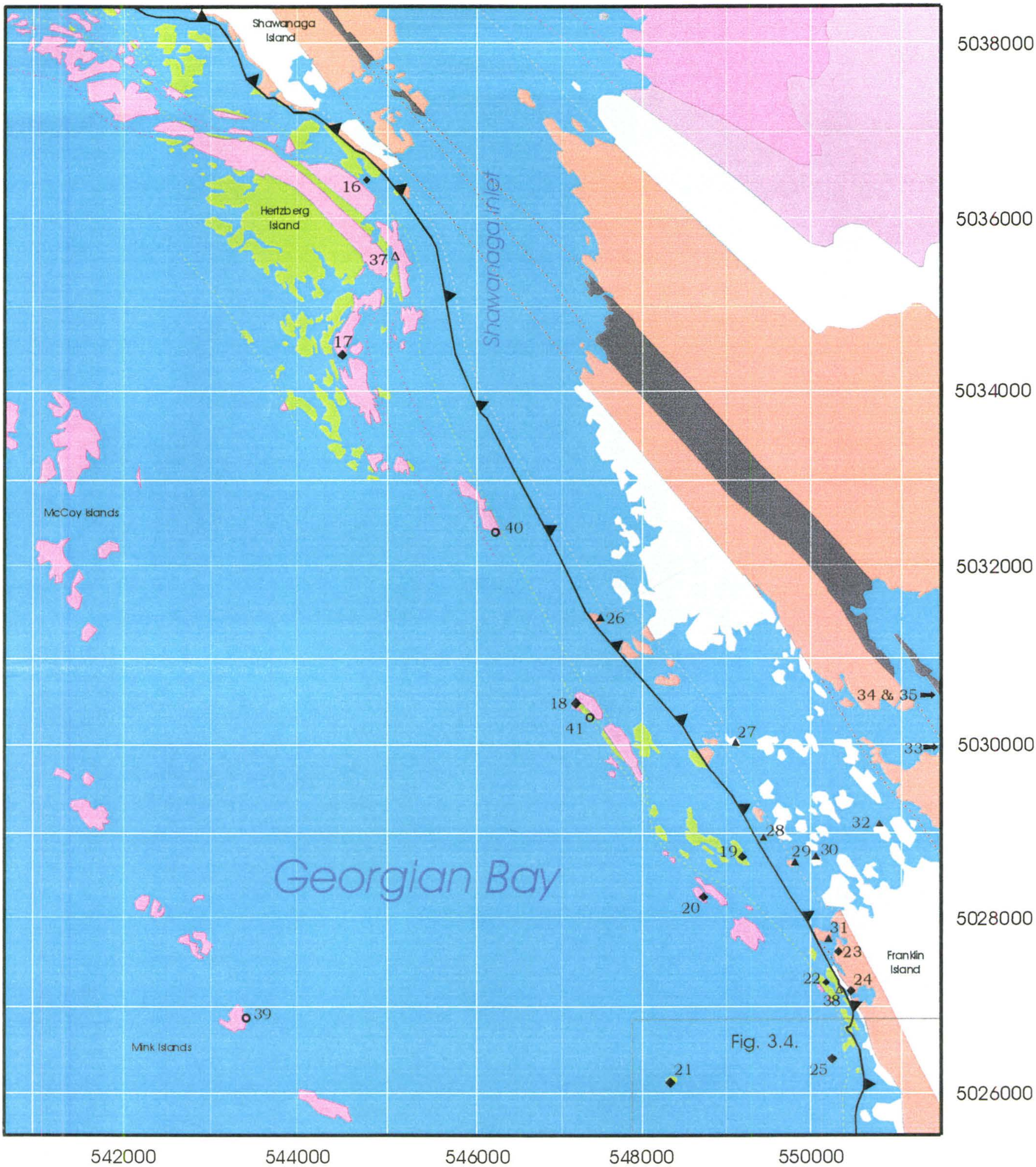


Fig. 3.3c. Geologic map: Hertzberg Island to Franklin Island,, modified from Culshaw, et. Al. (2000)

- ◆ Paleoproterozoic Nd model age
- ▲ Mesoproterozoic Nd model age
- △ Mixed Nd model age
- o Granitic Pluton

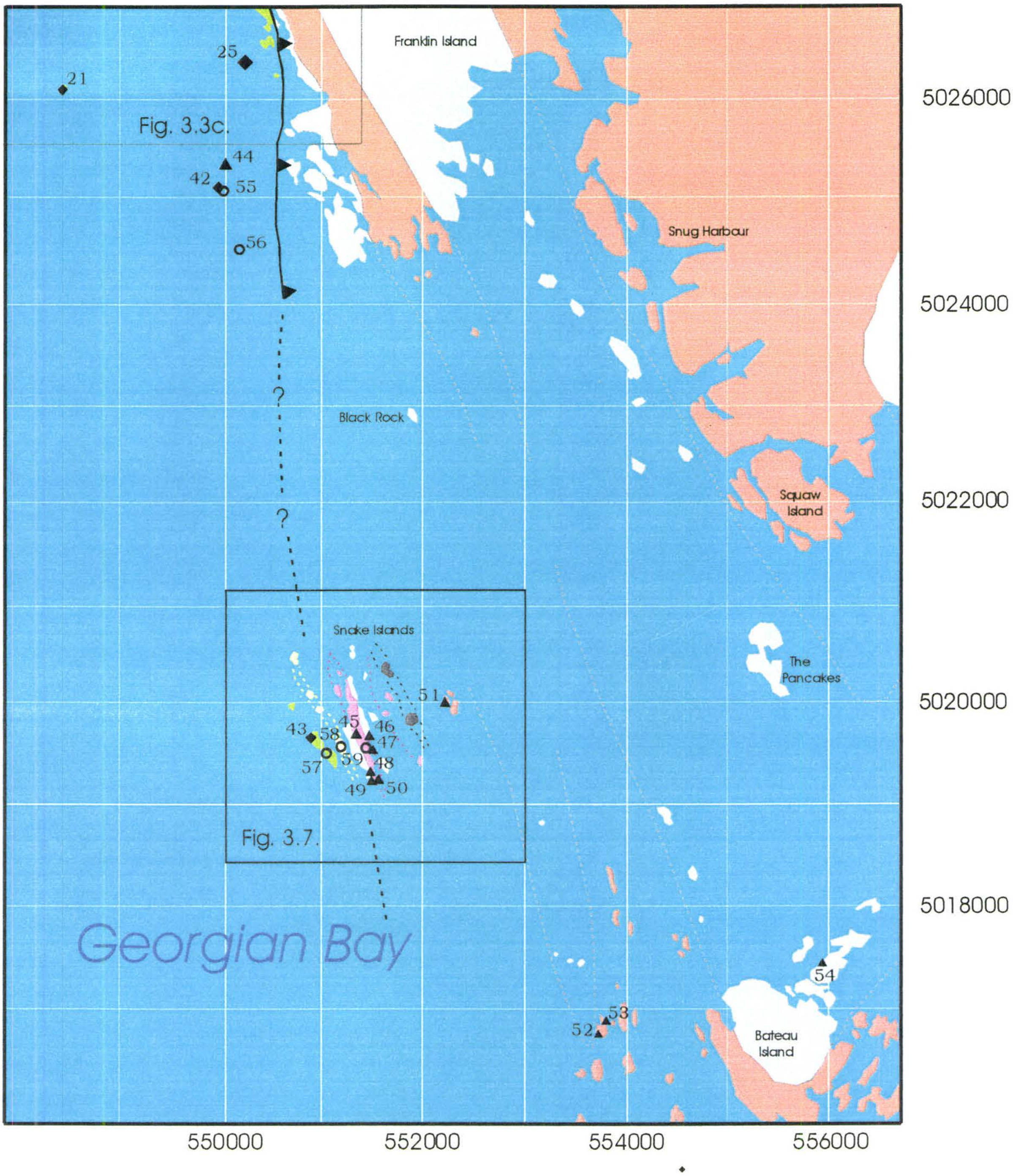


Fig. 3.3d. Geologic map: Franklin Island to Bateau Island, modified from Culshaw, et. Al. (2000)

◆ Paleoproterozoic Nd model age
▲ Mesoproterozoic Nd model age
o Granitic Plutons

Table 3.1. Nd Results from Map 1: Pointe Au Baril Region

| Sample Numbers | | Grid Reference | SM (ppm) | ND (ppm) | $Sm^{147}/Nd^{144}$ | $Nd^{143}/Nd^{144}$ | E($t$)* | TDM (Ga) |
|---|---|---|---|---|---|---|---|---|
| **Britt Domain** | | | | | | | | |
| 1 | PB1 | 387-450 | 5.828 | 33.79 | 0.1043 | 0.511692 | -1.3 | 1.88 |
| 2 | PB2 | 409-438 | 4.458 | 25.13 | 0.1072 | 0.511785 | 0.0 | 1.80 |
| 3 | PB5# | 459-412 | 5.506 | 33.48 | 0.0994 | 0.511632 | -1.5 | 1.88 |
| 4 | SH24R | 452-403 | 4.740 | 24.40 | 0.1174 | 0.511879 | -0.1 | 1.84 |
| 5 | SH21R | 467-396 | 5.885 | 26.01 | 0.1367 | 0.512130 | 1.2 | 1.80 |
| 6 | GF103## | 467-548 | 9.097 | 53.30 | 0.1032 | 0.511679 | ? | 1.88 |
| 7 | GF107## | 482-509 | 8.497 | 46.62 | 0.1101 | 0.511780 | ? | 1.86 |
| **Shawanaga Pluton** | | | | | | | | |
| 8 | SH30 | 445-404 | 10.335 | 54.81 | 0.1140 | 0.511946 | 1.9 | 1.67 |
| 9 | SH31 | 446-402 | 14.121 | 66.19 | 0.1290 | 0.512096 | 2.0 | 1.70 |
| 10 | SH32 | 446-399 | 9.954 | 49.9 | 0.1206 | 0.511997 | 1.6 | 1.71 |
| 11 | SH22R | 468-396 | 8.788 | 43.26 | 0.1228 | 0.511981 | 0.9 | 1.78 |
| 12 | SH1 | 475-386 | 15.270 | 74.70 | 0.1236 | 0.512053 | 2.2 | 1.67 |
| 13 | SH23 | 478-389 | 8.110 | 62.28 | 0.0787 | 0.511486 | -0.6 | 1.76 |
| 14 | GF117.5 | 559-439 | 8.033 | 72.76 | 0.0667 | 0.511313 | -1.7 | 1.79 |
| 15 | GF118.5 | 566-434 | 7.830 | 38.72 | 0.1223 | 0.511994 | 1.3 | 1.75 |

*$t$ = 1450 Ma

# U-Pb age of 1.6 Ga (Ketchum, 1998)

## data from Dickin & McNutt (1989)

Table 3.2. Nd Results from Map 2: Hertzberg Island to Franklin Island

| Sample Numbers | | Grid Reference | SM (ppm) | ND (ppm) | $Sm^{147}/Nd^{144}$ | $Nd^{143}/Nd^{144}$ | E(*t*)* | TDM (Ga) |
|---|---|---|---|---|---|---|---|---|
| **Britt Domain** | | | | | | | | |
| 16 | SH35 | 448-364 | 10.339 | 56.72 | 0.1102 | 0.511749 | -1.3 | 1.90 |
| 17 | SH4 | 445-345 | 6.234 | 34.53 | 0.1091 | 0.511745 | -1.2 | 1.89 |
| 18 | SH2 | 473-304 | 7.347 | 37.69 | 0.1178 | 0.511850 | -0.7 | 1.90 |
| 19 | SH43 | 493-288 | 9.218 | 49.14 | 0.1134 | 0.511842 | -0.1 | 1.82 |
| 20 | SH12 | 487-282 | 7.933 | 45.35 | 0.1057 | 0.511672 | -2.0 | 1.93 |
| 21 | SH14 | 484-262 | 0.323 | 1.92 | 0.1019 | 0.511654 | -1.6 | 1.89 |
| 22 | SH47 | 502-273 | 4.661 | 31.32 | 0.0899 | 0.511545 | -1.5 | 1.84 |
| 23 | SH46 | 504-276 | 7.570 | 42.87 | 0.1067 | 0.511760 | -0.4 | 1.83 |
| 24 | SH48 | 503-273 | 6.205 | 34.71 | 0.1080 | 0.511747 | -0.9 | 1.87 |
| 25 | SH11 | 501-265 | 9.378 | 52.33 | 0.1083 | 0.511711 | -1.7 | 1.93 |
| **Shawanaga Domain** | | | | | | | | |
| 26 | SH34 | 475-315 | 12.461 | 63.33 | 0.1189 | 0.512034 | 2.7 | 1.62 |
| 27 | SH40 | 492-300 | 2.228 | 11.15 | 0.1206 | [0.512178] | 5.2 | 1.41 |
| 28 | SH44 | 495-288 | 7.041 | 38.07 | 0.1118 | 0.511967 | 2.7 | 1.61 |
| 29 | SH45 | 498-286 | 11.361 | 57.11 | 0.1202 | 0.512068 | 3.1 | 1.59 |
| 30 | FI7R | 501-287 | 1.778 | 9.06 | 0.1186 | 0.512108 | 4.2 | 1.49 |
| 31 | FI8 | 502-277 | 7.565 | 39.56 | 0.1156 | 0.511962 | 1.9 | 1.68 |
| 32 | FI4 | 507-291 | 8.057 | 43.53 | 0.1119 | 0.511950 | 2.3 | 1.63 |
| 33 | FI1 | 515-299 | 5.944 | 33.48 | 0.1073 | 0.511951 | 3.2 | 1.56 |
| 34 | DI1 | 514-307 | 4.338 | 21.14 | 0.1240 | 0.512211 | 5.2 | 1.40 |
| 35 | DI2 | 524-309 | 4.103 | 23.69 | 0.1047 | 0.511964 | 4.0 | 1.50 |
| **Mixed Ages** | | | | | | | | |
| 37 | SH5 | 451-353 | 0.333 | 1.81 | 0.1115 | 0.511858 | 0.6 | 1.77 |
| 38 | SH49 | 505-273 | 7.884 | 38.84 | 0.1227 | 0.512000 | 1.3 | 1.74 |
| **Plutons** | | | | | | | | |
| 39 | GI2 | 435-268 | 11.597 | 55.77 | 0.1257 | 0.511994 | 0.6 | 1.81 |
| 40 | SH3 | 474-303 | 15.823 | 79.22 | 0.1207 | 0.511951 | 0.7 | 1.79 |
| 41 | SH7 | 463-324 | 13.492 | 71.10 | 0.1147 | 0.511944 | 1.7 | 1.69 |

**t* = 1450 Ma

**Table 3.3. Nd Results from Map 3: Franklin Island to Bateau Island**

| Sample Numbers | | Grid Reference | SM (ppm) | ND (ppm) | $Sm^{147}/Nd^{144}$ | $Nd^{143}/Nd^{144}$ | E(*t*)* | TDM (Ga) |
|---|---|---|---|---|---|---|---|---|
| **Britt Domain** | | | | | | | | |
| 42 | SH9A | 499-251 | 2.349 | 12.79 | 0.1110 | 0.511786 | -0.7 | 1.87 |
| 43 | SI5 | 510-196 | 10.535 | 49.37 | 0.1290 | 0.512017 | 0.5 | 1.84 |
| **Shawanaga Domain** | | | | | | | | |
| 44 | SH10 | 499-254 | 0.662 | 2.72 | 0.1489 | 0.512420 | 4.6 | 1.46 |
| 45 | SI3 | 514-197 | 8.482 | 46.46 | 0.1104 | 0.511942 | 2.5 | 1.62 |
| 46 | SI2 | 515-198 | 7.736 | 39.38 | 0.1188 | 0.512036 | 2.7 | 1.61 |
| 47 | SH18 | 516-197 | 6.202 | 35.18 | 0.1065 | 0.511974 | 3.8 | 1.52 |
| 48 | SI8 | 514-194 | 7.469 | 38.74 | 0.1165 | 0.512088 | 4.2 | 1.49 |
| 49 | SI9 | 514-194 | 7.466 | 38.29 | 0.1179 | 0.511987 | 1.9 | 1.68 |
| 50 | SH20 | 516-194 | 7.752 | 44.08 | 0.1063 | 0.511941 | 3.2 | 1.56 |
| 51 | SI7 | 522-201 | 6.964 | 51.89 | 0.0811 | 0.511698 | 3.1 | 1.54 |
| 52 | OB3 | 537-165 | 8.129 | 43.46 | 0.1131 | 0.512033 | 3.7 | 1.53 |
| 53 | OB1 | 536-163 | 9.408 | 52.85 | 0.1076 | 0.512011 | 4.3 | 1.48 |
| 54 | BI1 | 559-174 | 14.150 | 71.64 | 0.1194 | 0.512038 | 2.7 | 1.62 |
| **Pluton** | | | | | | | | |
| 55 | SH9B | 499-252 | 12.545 | 63.52 | 0.1194 | 0.511994 | 1.8 | 1.69 |
| 56 | SH13 | 502-245 | 15.508 | 75.49 | 0.1242 | 0.511993 | 0.9 | 1.78 |
| 57 | SI6 | 511-195 | 13.219 | 62.44 | 0.1280 | 0.512110 | 2.5 | 1.66 |
| 58 | SI4 | 513-196 | 10.830 | 69.68 | 0.0939 | 0.511668 | 0.2 | 1.75 |
| 59 | SH19R | 515-198 | 12.737 | 84.75 | 0.0908 | 0.511684 | 1.1 | 1.68 |

**t* = 1450 Ma

summarized in a histogram (Fig. 3.4.), where the distribution of the sample results is clear. It shows a peak with a broad distribution between 1.4 Ga and 1.7 Ga for the MesoProterozoic rocks of the Shawanaga Domain and a sharp distinct peak at 1.8 – 1.9 Ga for the PaleoProterozoic rocks of the Britt Domain. Several samples also lie within zones of mixed model ages. The plutons in this region produce Nd model ages ranging between 1.6 Ga and 1.8 Ga.

Further evaluation of the model is done by looking at plots of epsilon Nd against Nd concentration of the rocks (Fig. 3.5.). This graph shows that the isotope signatures have clusters which appear to match the distribution seen in the model age histogram. The MesoProterozoic gneisses (filled triangles in Fig. 3.5.) form an elgongate field ranging between $\varepsilon(t)$ values of +2 and +6. The PaleoProterozoic samples (filled diamonds in Fig. 3.5.) form a more compact distribution, plotting primarily beneath an $\varepsilon(t)$ of 0. As expected, the plutonic samples (open circles in Fig. 3.5.) have higher Nd concentrations than the host gneisses. These samples form an elongate field, which seems to fill the gap between the MesoProterozoic and PaleoProterozoic gneisses.

### 3.2.2. Whole-Rock Elemental Analysis

The major element data for each sample are shown in Appendix B as well as the Na/K ratio, the Q and P values. The Q and P values are plotted on the geochemical-petrological grid of Debon and LeFort (1983), generating a Streckheisen-type classification of the gneisses from either side of the ABT. These values are calculated using the following equations:

$$Q = \frac{SiO_2}{3} - (K_2O + Na_2O + \frac{2}{3}(CaO))$$

$$P = K_2O - (Na_2O + CaO)$$

The Q values have been plotted against the P values in Fig. 3.6., allowing classification of the samples, based on the elemental analysis. The plutonic samples plot primarily as granites and adamellites, while the gneisses have a wider distribution. The overall distribution is common to that observed in ensialic arcs.

**Fig. 3.4. Histogram of the Nd Model Age Results**

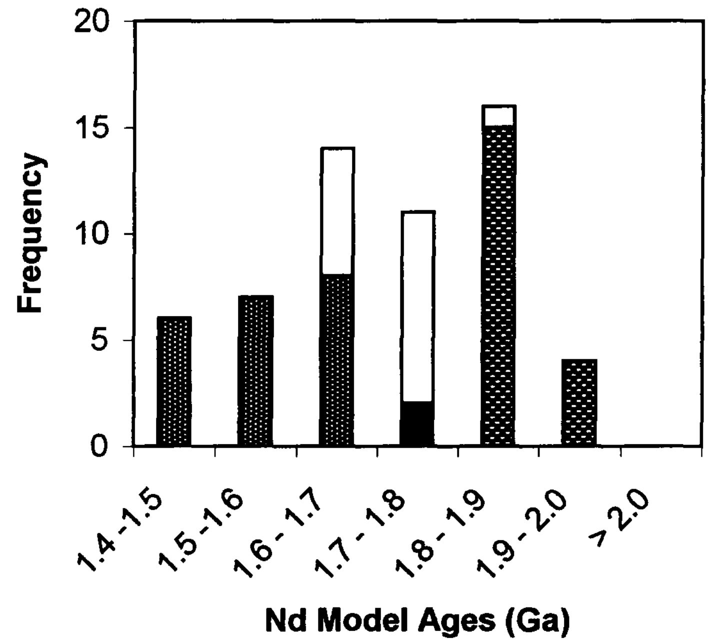

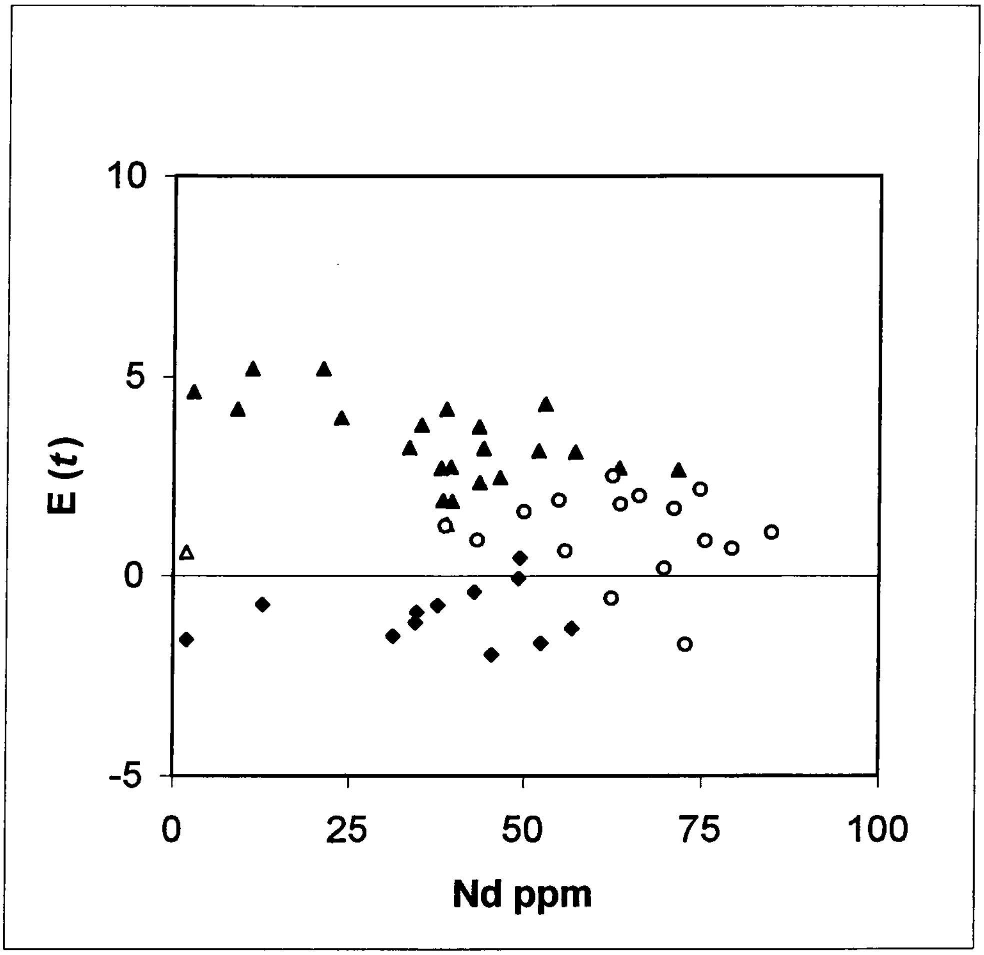


Fig. 3.5. Plot of ε Nd (1.45 Ga) against Nd concentration, showing the separation into 3 distinct groups.

- ♦ PaleoProterozoic crust
- ▲ MesoProterozoic crust
- Δ Intermediate and/or mixed-aged crustal material
- o Plutonic samples

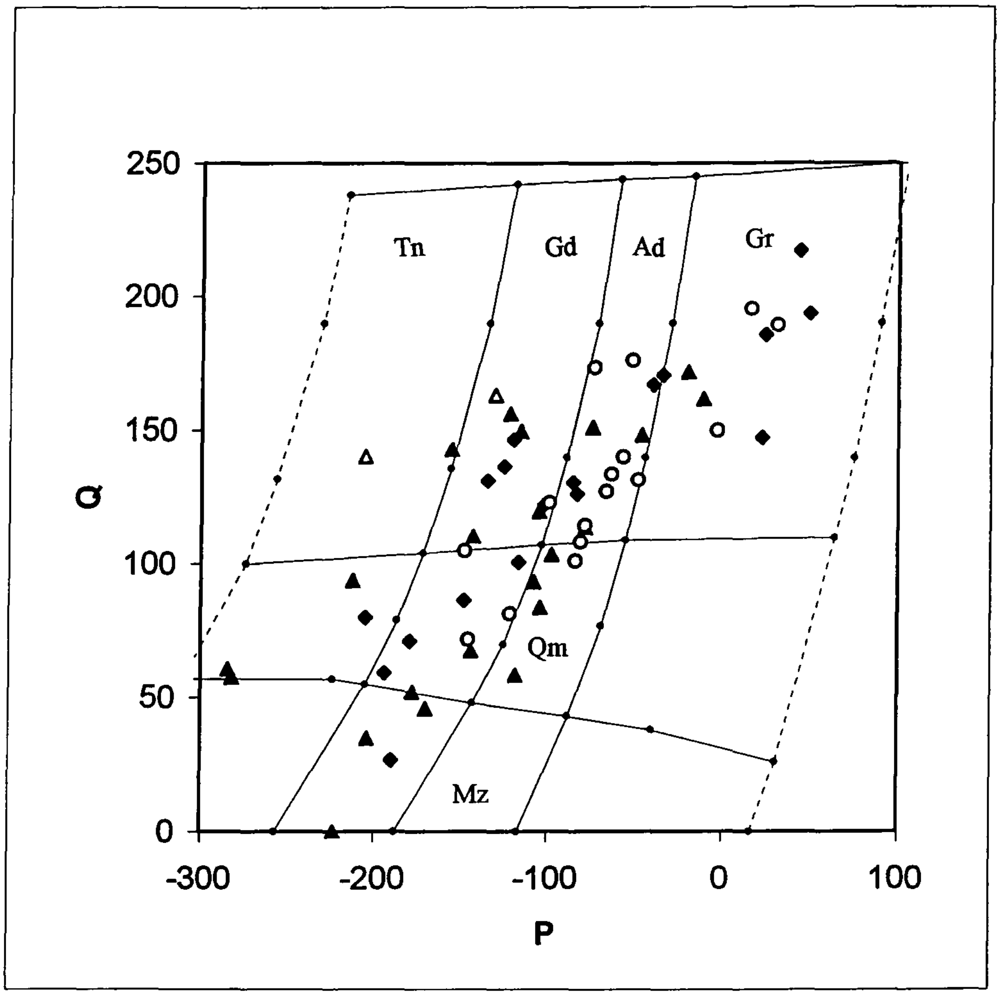


Fig. 3.6. Petrological classification of analysed samples from the Shawanaga region on the chemical-mineralogical grid of Debon and LeFort (1983) for granitoid classification.

- ♦ PaleoProterozoic crust
- ▲ MesoProterozoic crust
- Δ Intermediate and/or mixed-aged crustal material
- o Plutonic samples

### 3.2.3. Normative Calculations

The results of calculating the CIPW Norm are shown in Appendix B. The most significant numbers are the values for Normative Corundum and Normative Diopside. Samples with both a high Nd ppm and a normative diopside > 3% sample might represent plutons consisting of "reworked" crustal material, rather than new mantle material. The samples from the Britt Domain that fall into this category are Sh2 and Sh21. In the Shawanaga Domain, the samples with high Nd concentration and normative diopside values are FI7, FI8, Sh8, Sh40, SI2 and SI3. Of the plutonic samples, Sh7 and Sh32 show clear evidence of being comprised "reworked" crustal material.

### 3.2.4. Discussion

The Nd model ages results for the Shawanaga region are very clear. There is a definite step in the Nd model ages across the ABT. The Britt Domain gneisses have crustal provenance ages in the 1.8 – 2.0 Ga range, while the rocks of the Shawanaga Domain produce MesoProterozoic ages, in the range 1.4 - 1.7 Ga. Sampling conducted in proximity to the mapped ABT (Culshaw, et. al., 2000), proved that there is a sharp contact in the Nd isotope signature, which matches the sharp contact in the geology. In other words, there is no transition zone in which mixing of the Nd content of the two domains occurs.

As shown in the model age histogram (Fig. 3.4), a large number of samples did produce intermediate ages. These samples have been classifed as emplaced granitic plutons, on the basis of field evidence and whole-rock chemistry. During emplacement of these granitoids, mixing of juvenile mantle material and existing crustal material occurred, which explains the resultant intermediate Nd model ages.

Sampling in the Shawanaga Inlet (Fig. 3.3b.) showed that rocks in the Shawanaga Pluton have intermediate Nd model ages, while the gneisses of the Britt Domain have PaleoProterozoic ages. The northern edge of the Shawanaga Pluton, and hence the ABT, have been slightly modified from Culshaw, et. al. (2000). Here it is shown passing through Young Island (location of Samples 5 & 11 in Fig. 3.3b.), north of its previous location.

The samples between Hertzberg Island and Franklin Island (Fig. 3.3c.) are consistent with the mapped geology (Culshaw, et. al., 2000). The ABT is marked by the boundary between the Nadeau Island and Objibway gneiss associations. Several samples within the Britt Domain have intermediate Nd model ages. These samples represent emplacement granitoid plutons, as mentioned above. There are two anomalous results found on the northwest corner of Franklin Island (Sample 23 & 24 in Fig. 3.3c.), showing PaleoProterozoic ages in rocks mapped as part of the Shawanaga Domain. This suggests that the geology here may be more complex that originally thought.

To the south of Franklin Island, both the Nd model ages and field evidence suggest that the position of the ABT passes through the Snake Islands, as opposed to passing east of these islands as depicted in Culshaw, et. al. (2000). Along the western shoreline of Snake Island (Fig. 3.7.), several pods of retrogressed eclogites and several pods of coronitic metagabbro can be found. These mafic rock bodies are believed to be located only in the allochthonous belt, commonly found in the hanging wall of the ABT (Ketchum & Davidson, 2000). In addition to the presence of these mafic rock bodies, the Nd model age results show that Snake Island is composed of MesoProterozoic gneisses and granitic plutons with intermediate ages. Just west of Snake Island, running parallel to its western shoreline is a unit of tonalitic granodiorite, which appears to be of intermediate age. The next chain of rocks westward provided a Britt Domain PaleoProterozoic result. It therefore appears that the ABT can be mapped passing through the rocks just west of Snake Island. Further geologic study of these islands is clearly necessary.

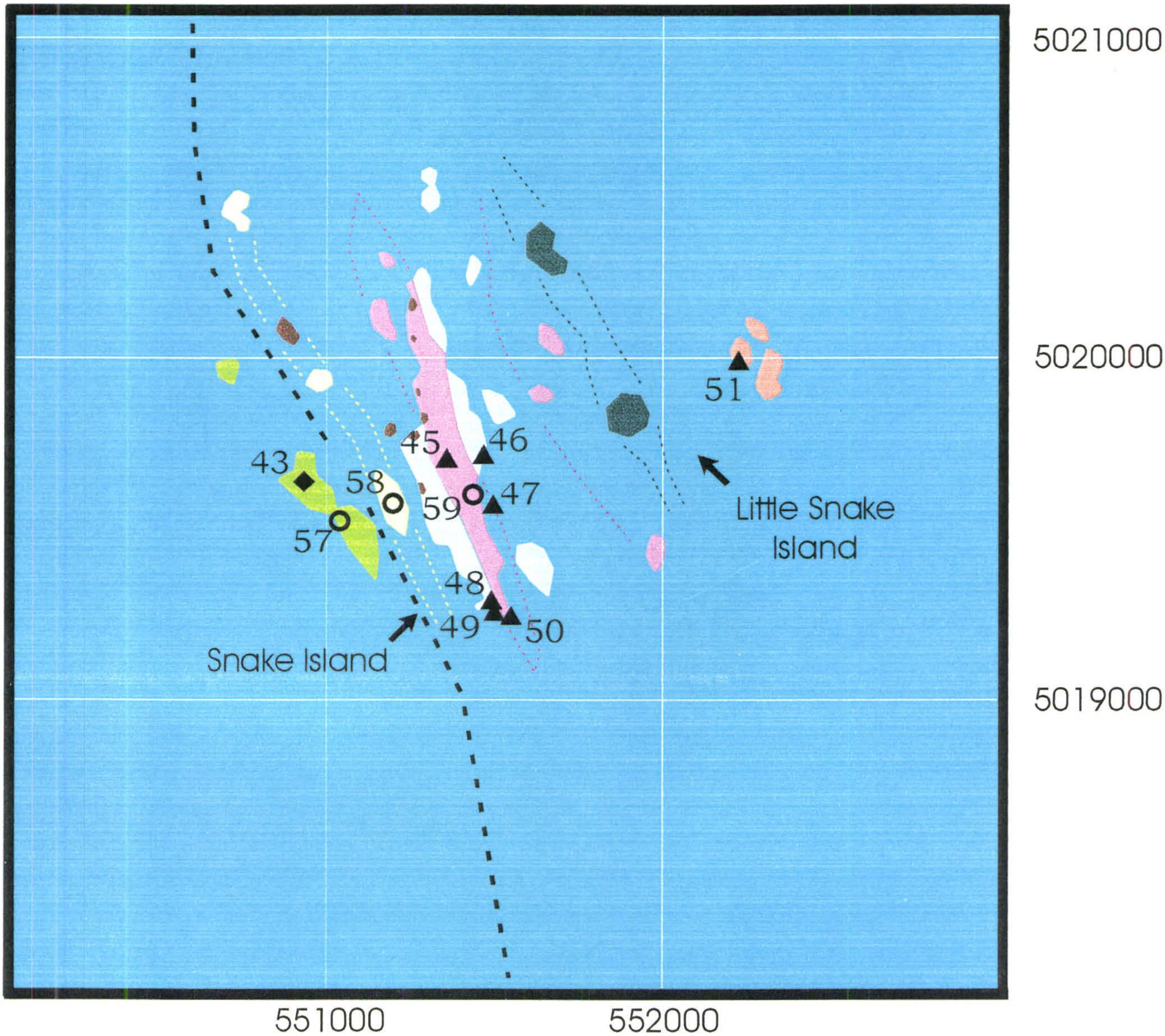


Fig. 3.7. Blow-up of the Snake Islands, with suggested location for the ABT, based on Nd model age results and mafic intrusives.

# Chapter 4:

## The ABT in the Powassan Region:

### 4.1.0. Introduction

The focus of this part of the study is to locate and map the Allochthon Boundary Thrust in the Powassan region. The ABT is a tectonic boundary, dividing the monocyclic and polycyclic belts of the Grenville Province, as described in Chapter 1. In the Shawanaga region, the ABT is a large shear zone, which divides the Britt Domain from the Shawanaga Domain. After running northwestwards from Georgian Bay to Arnstein, the ABT appears to turn south, wrapping around the southern margin of the Powassan Batholith. East of the batholith, the position of the ABT is disputed. In Fig. 4.1., *b* marks the newly proposed position of the ABT from Ketchum and Davidson (2000), and *a* marks the previously assigned location of the ABT. As described in Chapter 1, Ketchum and Davidson (2000) proposed the new position of the ABT based on the spatial distribution pattern of three mafic rock suites. As shown in Chapter 3, the ABT can be mapped using Nd model ages by separating rocks of PaleoProterozoic origin (north of the ABT) from rocks to its south of MesoProterozoic origin (south of the ABT).

### 4.1.1. The Field Area

The study area (Fig. 4.2) includes Arnstein and Restoule in the west, Callandar in the north, Burk's Falls in the south and Kawawaymog Lake in the east, (Ontario Topographic Maps 31 L/3, 31 L/4, 31 E/11, 31 E/12, 31 E/13 & 31 E/14). The northeastern extent of the Shawanaga shear zone crosses Highway 522 at the town of Arnstein, and passing in the proximity of Lake Restoule. East of Restoule, the ABT turns to the south, running approximately parallel to the margin of the Powassan Batholith. It passes in proximity to Burk's Falls, turning north to follow the eastern margin of the batholith. Its exact direction and location north of Burk's Falls have not been determined. Ketchum & Davidson (2000) have shown it going northwards to North Bay (Fig. 4.3). However, on their map, it is evident that using the distribution of the mafic rocks provides very little control for placing the ABT between North Bay and Burk's

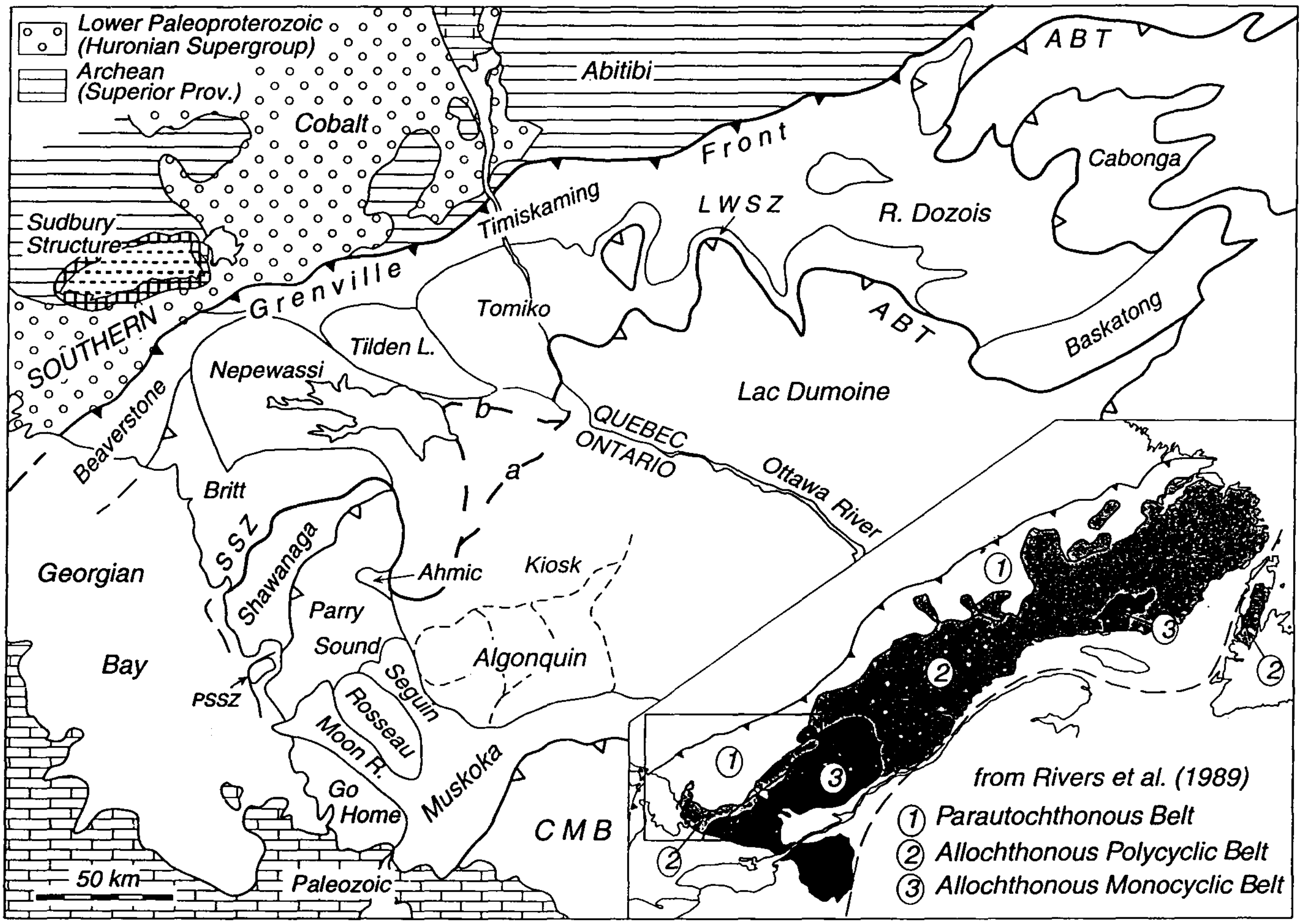


Fig. 4.1. Lithotectonic subdivisions of the Central Gneiss Belt, Grenville Province of Ontario and Western Quebec, compiled from Davidson (1986), Easton (1988), Rivers, et. al. (1989), Ketchum (1994) and Martignole and Calvert (1996). Two proposed positions for the ABT in Central Ontario are shown here. *a* corresponds to Davidson (1996), while *b* is the position proposed by Ketchum and Davidson (2000). The inset shows the major belts of the Grenville Province, as well as a more southerly position of the ABT originally assigned by Rivers, et. al. (1989).

| | |
|---|---|
| ABT | Allochthon Boundary Thrust |
| CMB | Central Metasedimentary Belt |
| LWSZ | Lac Watson Shear Zone |
| SSZ | Shawanaga Shear Zone |
| PSSZ | Parry Sound Shear Zone |

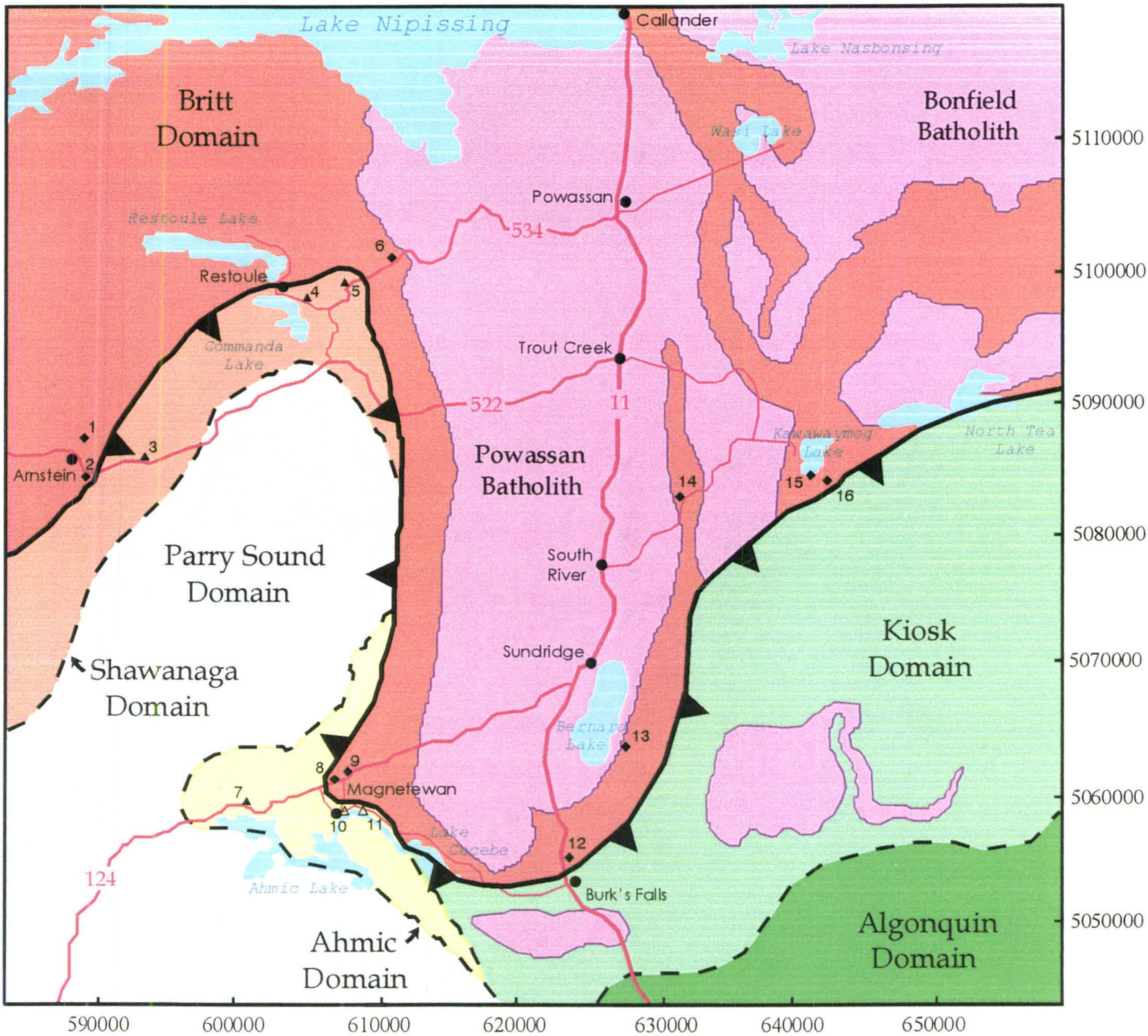


Fig. 4.2. Geologic map, compiled and modified from Davidson, et. al. (1986) and Ketchum & Davidson (2000).

- ◆ Paleoproterozoic Nd model age
- ▲ Mesoproterozoic Nd model age
- △ Mixed Nd model age

Falls. Their map allows for an alternative position of the ABT, in which it would cross through Algonquin Park, around the Bonfield Batholith, then north to the Ottawa River. The mafic rocks in the North Bay area could be assigned to a klippe of the AMB (Dickin & Guo, 2001). Nd sampling was conducted to test the newly proposed boundary and to indicate what direction future work should take.

### 4.1.2. Geologic Setting

The field area includes several Grenvillian structural domains. To the west of the Powassan Batholith lies the ABT, which bounds the Britt and Shawanaga Domains (described in the previous Chapter). The Shawanaga Domain tapers out after folding to the south around the northern edge of the Parry Sound Domain. To the southwest of the Powassan Batholith is the Ahmic Domain, which is composed of metasedimentary gneisses akin to those in the Shawanaga Domain. Bordering the southern end of the Powassan Batholith, and extending both eastward and northward along the batholith's eastern margin is the Kiosk Domain. Southeast of Burk's Falls lies the Algonquin Domain, which is underlain by metasedimentary gneisses, granulites, metaplutonic orthogneisses and mixed migmatitic and orthogneissic granulites. The Algonquin Domain is host to several clusters of coronitic olivine metagabbro bodies and a few scattered retrogressed eclogitic bodies.

Mapping units in the Algonquin and Kiosk Domains is difficult, because the rocks are of a high metamorphic grade and they have been subjected to extreme ductile deformation. Ductile attenuation has produced relatively thin rock units and original textural characteristics have been obliterated by the afore-mentioned deformation and metamorphism (Davidson & Grant, 1986). Complex structure also plays a role in minimizing the continuity of recognizable units. The Kiosk Domain is the primary focus of this study.

**Kiosk Domain**

Immediately east of the Powassan Batholithic complex, lies the Kiosk Domain. Davidson and Grant (1986) describe the southern Kiosk Domain as an east-northeast trending straight belt which swings southwest to follow the margin of the Powassan

Batholith at its southernmost extent. The southernmost lithology of the Kiosk Domain is a matrix of mafic, quartzofeldspathic and pelitic gneisses. They host several plutons with characteristics similar to the Powassan Batholith. To their immediate north lie grey quartzofeldspathic gneisses in the form of elongate plutons. These gneisses have tonalitic to granodioritic compositions and are host to a cluster of coronitic olivine metagabbro bodies. Cutting across North Tea Lake, and marking the boundary between the southern Kiosk Domain and the northern Kiosk Domain (Davidson & Grant, 1986), are a series of mylonitic tectonites. The northern Kiosk Domain consists of southerly trending plutons which terminate against the straight zone of tectonites. These plutons are described as a metasedimentary gneiss assemblage, including quartzite and pink, sillimanite-bearing, migmatitic, quartzofeldspathic leucogneiss (Davidson & Grant, 1986). The gneissosity trends are quite variable in the zone north of North Tea Lake.

## Nd Model Age Results:

4.2.0. Objectives

To the west of the Powassan Batholith, sampling was conducted to provide further Nd model age constraints on the location of the ABT. Arnstein and Restoule represent the northern extent of the ABT in this region. To the south, several samples were collected to locate the extent of the Ahmic Domain, which is bounded in the east by the ABT. As in the Shawanaga region, these samples would either indicate a more precise position for the ABT, or identify a zone of ductile shear in which mixing of younger and older rocks occurred.

To the east of the Powassan Batholith, sampling was conducted in the Kiosk domain to test the proposal of Ketchum and Davidson (2000). Location *a* of the ABT (Fig. 4.1) appears to coincide with the mylonitic tectonites found at North Tea Lake. Outcrop in this region is limited, due to thick vegetation. The results from this region should raise further questions about location of the ABT and point the direction of future geologic studies within this region.

### 4.2.1. Nd Model Age Results

A total of 14 samples were collected and studied in this field area. West of the batholith, 3 samples were collected near Arnstein and 3 more along Highway 534 east of Restoule. To the south, 3 samples were collected to add to known data for the Ahmic Domain (AH2, AH4 in Table 4.1A). To the east of the batholith, 5 samples were collected between Burk's Falls and Kawawaymog Lake.

The number of samples is limited, however, the histogram analysis produces a similar result to that shown in the previous chapter. As in the Shawanaga region, there is a cluster of results in the 1.8 – 2.0 Ga range and a second peak at 1.4 – 1.7 Ga. Several samples also lie within the 1.7 – 1.8 Ga interval of mixed model ages. The sample set is quite small, but comparison of Fig. 4.3a. and Fig. 4.3b. shows that the results for the Powassan region do have the same pattern as those of the Shawanaga region.

Further evaluation of the model is done by looking at plots of epsilon Nd against Nd concentration of the rocks (Fig. 4.4). This graph shows that the isotope signatures have clusters which appear to match the distribution seen in the model age histogram. Again, the results from the Shawanaga region have been shown, to demonstrate that the distribution patterns of the data for the two regions are similar. Sample 5 (PO6) has an excess of Nd relative to the other samples, suggesting that it is a younger intrusive rock.

### 4.2.2. Whole-Rock Elemental Analysis

The major element data for each sample are shown in Appendix B, as well as the Na/K ratio, Q and P values used to classify the rocks on the geochemical-petrological grid of Debon and LeFort (1983). These values are calculated using the following equations:

$$Q = \frac{SiO_2}{3} - \left(K_2O + Na_2O + \frac{2(CaO)}{3}\right)$$

$$P = K_2O - (Na_2O + CaO)$$

The P values have been plotted against the Q values in Fig. 4.5., allowing classification of the samples, based on the elemental analysis.

**Table 4.1. Sm-Nd Data for rocks from the Powassan Area**

| Sample Numbers | | Grid Reference | SM (ppm) | ND (ppm) | $Sm^{147}/Nd^{144}$ | $Nd^{143}/Nd^{144}$ | E(*t*) | $T_{DM}$ (Ga) |
|---|---|---|---|---|---|---|---|---|
| **A: West of the Powassan batholith** | | | | | | | | |
| *Arnstein* | | | | | | | | |
| 1 | SH28 | 865-881 | 7.585 | 28.68 | 0.1599 | 0.512388 | 2.0 | 1.85 |
| 2 | SH26 | 844-842 | 9.417 | 50.72 | 0.1122 | 0.511840 | 0.1 | 1.81 |
| 3 | SH27 | 897-850 | 5.856 | 23.18 | 0.1527 | 0.512417 | 3.9 | 1.56 |
| *Highway 534: East of Restoule* | | | | | | | | |
| 4 | R3 | 015-972 | 5.100 | 34.58 | 0.0891 | 0.511574 | -0.8 | 1.80 |
| 5 | PO6 | 047-986 | 19.110 | 100.84 | 0.1145 | 0.511885 | 0.6 | 1.78 |
| 6 | PO5 | 087-004 | 10.171 | 54.56 | 0.1127 | 0.511793 | -0.9 | 1.88 |
| *Ahmic Domain* | | | | | | | | |
| 7 | AH2 | 978-577 | 6.020 | 36.55 | 0.0995 | 0.511888 | 3.4 | 1.54 |
| 8 | AH10 | 052-604 | 6.538 | 32.14 | 0.1230 | 0.511944 | 0.2 | 1.84 |
| 9 | AH5 | 076-617 | 4.810 | 20.58 | 0.1413 | 0.512124 | 0.3 | 1.93 |
| 10 | AH4 | 060-577 | 11.584 | 71.51 | 0.118 | 0.511753 | 1.1 | 1.70 |
| 11 | AH8 | 077-582 | 9.215 | 45.82 | 0.1216 | 0.511990 | 1.3 | 1.74 |
| **B: East of the Powassan batholith** | | | | | | | | |
| *Burke's Falls to Kawawaymog Lake* | | | | | | | | |
| 12 | PO9 | 241-549 | 8.456 | 36.65 | 0.1395 | 0.512095 | 0.0 | 1.94 |
| 13 | PO7 | 279-657 | 12.027 | 63.53 | 0.1144 | 0.511784 | -1.4 | 1.93 |
| 14 | KW1 | 317-826 | 12.860 | 62.40 | 0.1246 | 0.511883 | -1.3 | 1.98 |
| 15 | KW3 | 415-847 | 9.056 | 47.70 | 0.1148 | 0.511770 | -1.7 | 1.96 |
| 16 | PO11 | 455-809 | 7.439 | 43.42 | 0.1035 | 0.511673 | -1.5 | 1.89 |

*$t$ = 1450 Ma

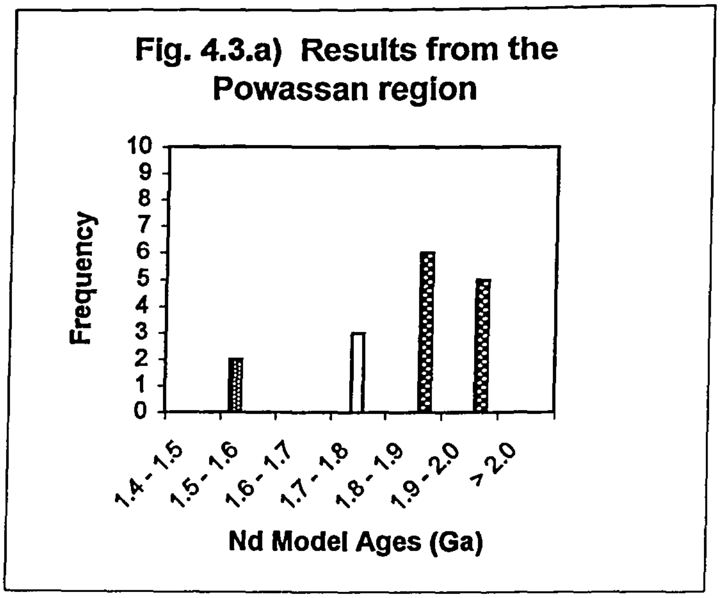


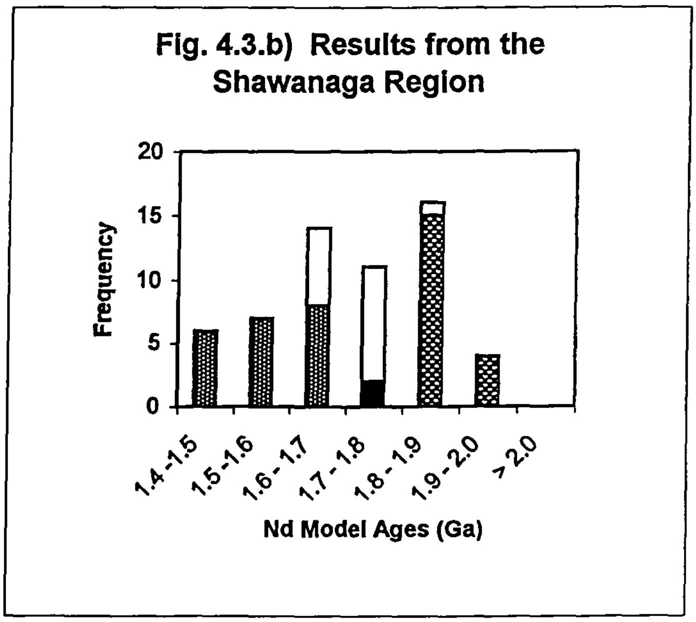


Fig. 4.3. a) Histogram of $T_{DM}$ model age results from the Powassan region. The sample set is small, but displays the same distribution of age results seen in b) the Shawanaga region results.

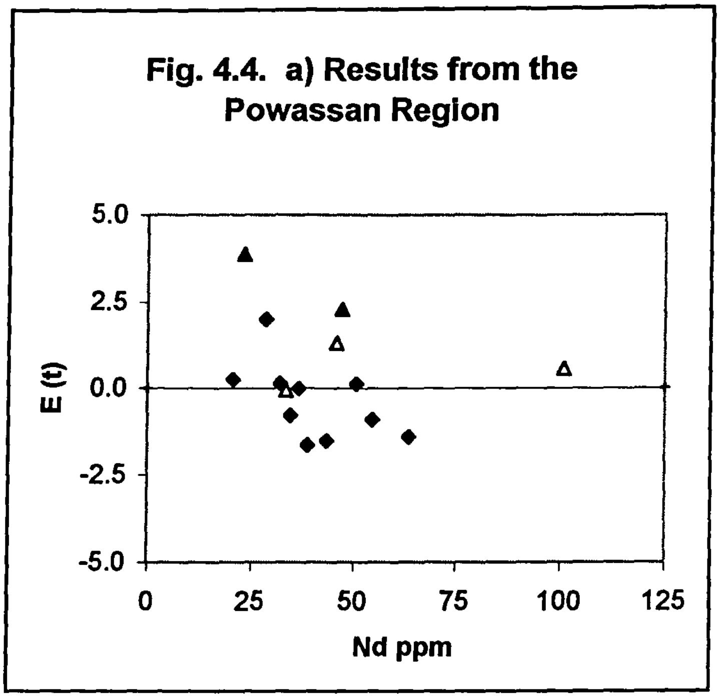


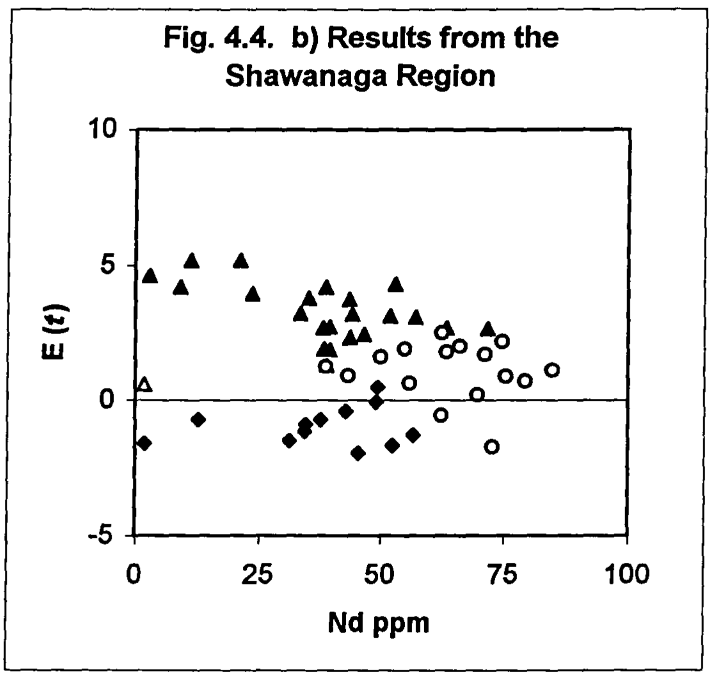


Fig. 4.4. a) Plot of ε Nd (1.45 Ga) against Nd concentration, showing the separation into 3 groups. Limited sample numbers make these group less distinct, but comparision with b) the results from the Shawanaga region show that the same relationships exist.

- ♦ PaleoProterozoic crust
- ▲ MesoProterozoic crust
- Δ Intermediate and/or mixed-aged crustal material
- o Plutonic samples

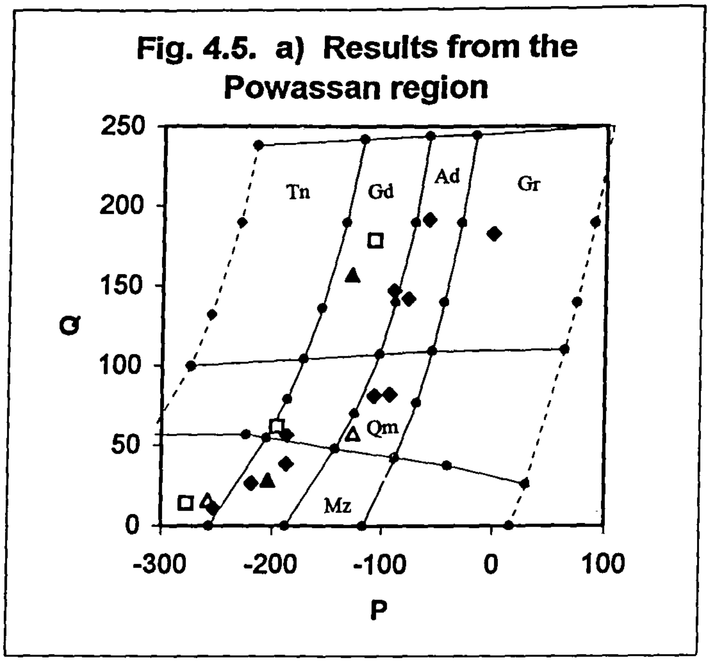


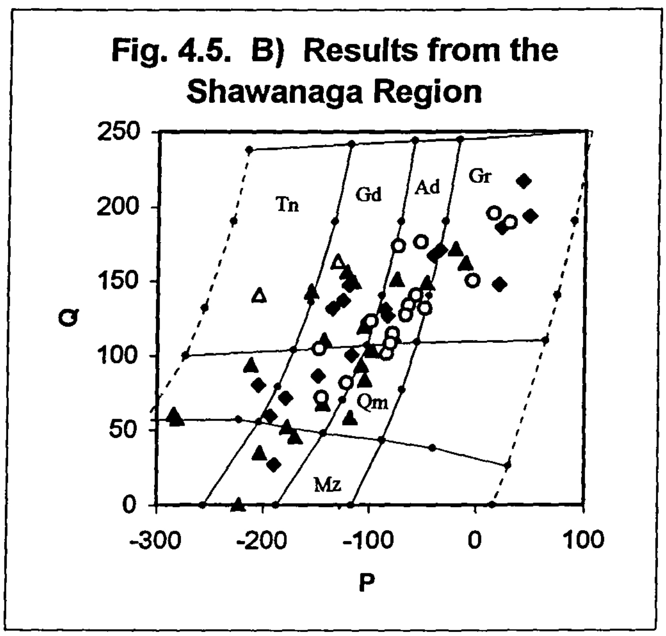


Fig. 4.5. a) Petrological classification of analysed samples from the Powassan region on the chemical-mineralogical grid of Debon and LeFort (1983) for granitoid classification. b) P vs. Q results for the Shawanaga region.

- ♦ PaleoProterozoic crust
- ▲ MesoProterozoic crust
- △ Intermediate and/or mixed-aged crustal material
- ○ Plutonic samples
- □ Undated samples

### 4.2.3. Normative Calculations

The results of calculating the CIPW Norm are shown in Appendix B. The most significant numbers are the values for Normative Corundum and Normative Diopside. For example, sample 5 (PO6) has both a high Nd ppm and a normative diopside > 3%, meaning that this sample represents a pluton consisting of "reworked" crustal material, rather than new mantle material.

### 4.2.4. Discussion

The conclusions derived for the rocks west of the Powassan Batholith are rather simple. These rocks do represent a continuation of the Shawanaga and Britt Domains studied on along the Georgian Bay coast. The Nd model ages place the ABT immediately southeast of the village of Arnstein as it crosses Highway 522 (Fig. 4.2). The position is less precise to the northeast near Restoule. Sample 4 (R3) resulted in a mixing age, and sample 5 (PO6) consists of "reworked" crustal material. The ABT has thus been placed north of these sample locations, but turns southward as indicated by the PaleoProterozoic age of sample 6 (PO5). In the Ahmic Domain, samples along Highway 124 also produce PaleoProterozoic ages. The ABT would seem to lie further west than originally placed. Directly south, in the village of Magnetewan, the model ages again show signs of crustal mixing. The ABT curves back east, then south again, cutting through the center of Lake Cecebe.

To the east of the Powassan Batholith, the results contradict the proposal of Ketchum and Davidson (2000), which has the ABT tracing northward, to the east of Sundridge and gently curves back to North Bay. A PaleoProterozoic age north of Burk's Falls confirms that the ABT lies somewhere south of that town. East of South River, 3 more samples give PaleoProterozoic Nd model ages. Sample 14 (KW1) would not contradict Ketchum and Davidson (2000) by itself. However, the other 2 samples lie south of Kawawaymog Lake. This seems to dispute the proposal of those authors and suggests that further study is required to determine the location of the ABT east of the town of Burk's Falls.

# Chapter 5:

## The Suture at Key Harbour:

### 5.1.0. Introduction

This part of the study focuses on the Penokean Suture in the Key Harbour area, (Dickin, 1998). Mapping the trend of the proposed suture through this region was performed through a combination of isotopic and geophysical mapping. The isotopic work identifies the crustal formation age signature of the terranes, revealing a large-scale age discontinuity. The magnetic mapping is used to identify tectonic structures, by tracing the regional foliation of the gneiss terrane and by identifying displacements of igneous contacts to map post-tectonic faults. Integration of the magnetic information with the isotopic data is used to help resolve the location of the Penokean Suture. It will be shown that this multi-disciplinary approach can be used to not only enhance the existing maps, but predict the trend of the suture in areas where isotopic sampling is not feasible.

### 5.1.1. The Penokean Orogeny

In addition to the previously discussed history of the Grenville Orogeny, it is also important to understand the Penokean Orogeny. Overlaying the southern margin of the Superior Province in Wisconsin, Michigan, and Minnesota, the Penokean is a 250-km wide foldbelt, (Fig 5.1). These early Proterozoic and Archean rocks have a northeast-southwest trend, and are deformed and metamorphosed (Sims & Peterman, 1983). Zircon-dating provides an age range of 1.83 – 1.89 Ga for the Penokean Orogeny, (Van Schmus, 1980). The foldbelt is divided into two major provinces, The Marquette Supergroup and The Wisconsin Magmatic Terrane. The belt of calc-alkaline volcanics and intrusives known as the Wisconsin Magmatic Terrane has been described as an allochthonous terrane that has been accreted to the passive margin clastic sediments of the Marquette Supergroup (Schulz, 1987). U-Pb zircon ages for the Hemlock Volcanics of the Menominee Group are consistent with the preferred age bracket of 1850 Ma to

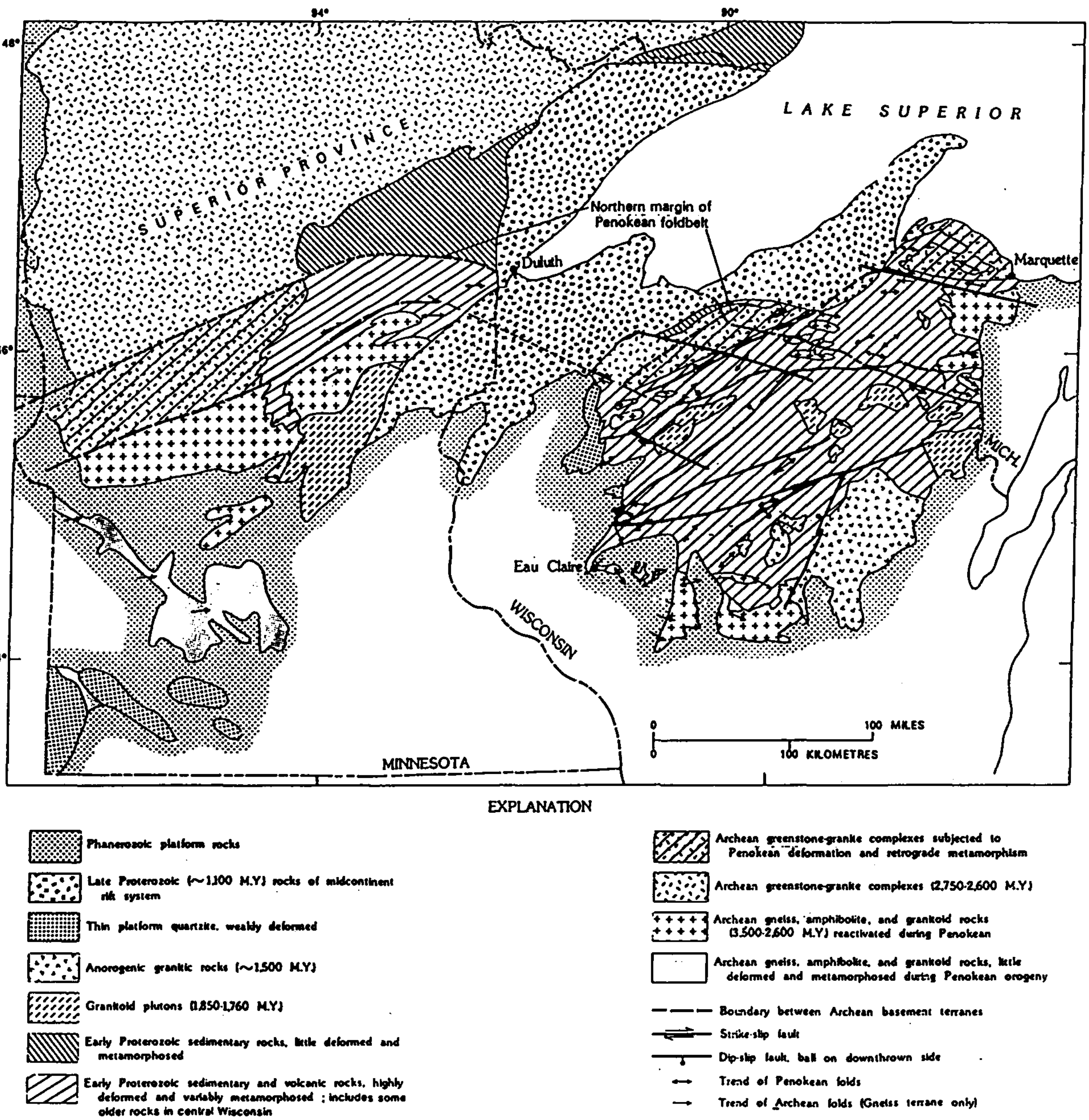


Fig. 5.1. Map of the geographical location of the Penokean Orogeny in the Great Lakes Region, (after Sims, 1981).

1950 Ma of the Marquette Supergroup, making it younger than the Huronian Supergroup, (Van Schmus and Bickford, 1981).

### 5.1.2. The Penokean Suture

The Penokean Orogeny has been linked with the collision of an allochthonous terrane which thrust over and depressed the Huronian rocks to midcrustal levels (Zolnai et al., 1984). This led to the suggestion by Dickin and McNutt (1989) that a Penokean allochthonous slice might be found south of the Manitoulin Island Discontinuity, and within the Grenville Province. The presence of an allochthonous slice would result in a crustal discontinuity. Grenvillian overprinting has made locating this boundary difficult; however, use of the Sm-Nd dating method has verified the existence of a geologic boundary across which there is a discontinuity in the Nd model ages. The location of the boundary is proposed based on the Nd model ages, where model ages of > 2.3 Ga represent Archean or reworked Archean rocks and model ages between 1.8 and 2.0 Ga mark the location of an early Proterozoic arc terrane. The boundary is believed to represent the predicted collisional suture (Zolnai et al., 1984). This suture has been mapped and described (Dickin and McNutt, 1989; Dickin, McNutt and Clifford, 1990; Holmden and Dickin, 1995; Dickin, 1998, 2000) from the northeast corner of Georgian Bay across to Lake Nipissing, and from the eastern shoreline of Lake Nipissing to the Ottawa River and into Quebec (Fig. 5.2). In the French River area, a dotted line (Fig. 5.3) shows the location of the suture. It follows the regional foliation and is therefore folded back and forth across the Key and Pickerel Rivers and then winds northeastwards across the channels of the French River, wrapping around the Pine Cove & West Bay batholiths before disappearing beneath Lake Nipissing.

### 5.1.3. Geologic Setting: French River, Main Outlet to Key River

The study area (Fig. 5.4.) is located in the parautochthon, about 40 km from the Grenville Front. The French River Main Outlet is the location of a large shear zone, marking the eastern extent of the Grenville Front Tectonic Zone. The Grenville Front separates the Southern Province from the parautochthon, which consists of high-grade gneisses and granitoids. Running down the center of the map is the Pickerel Complex

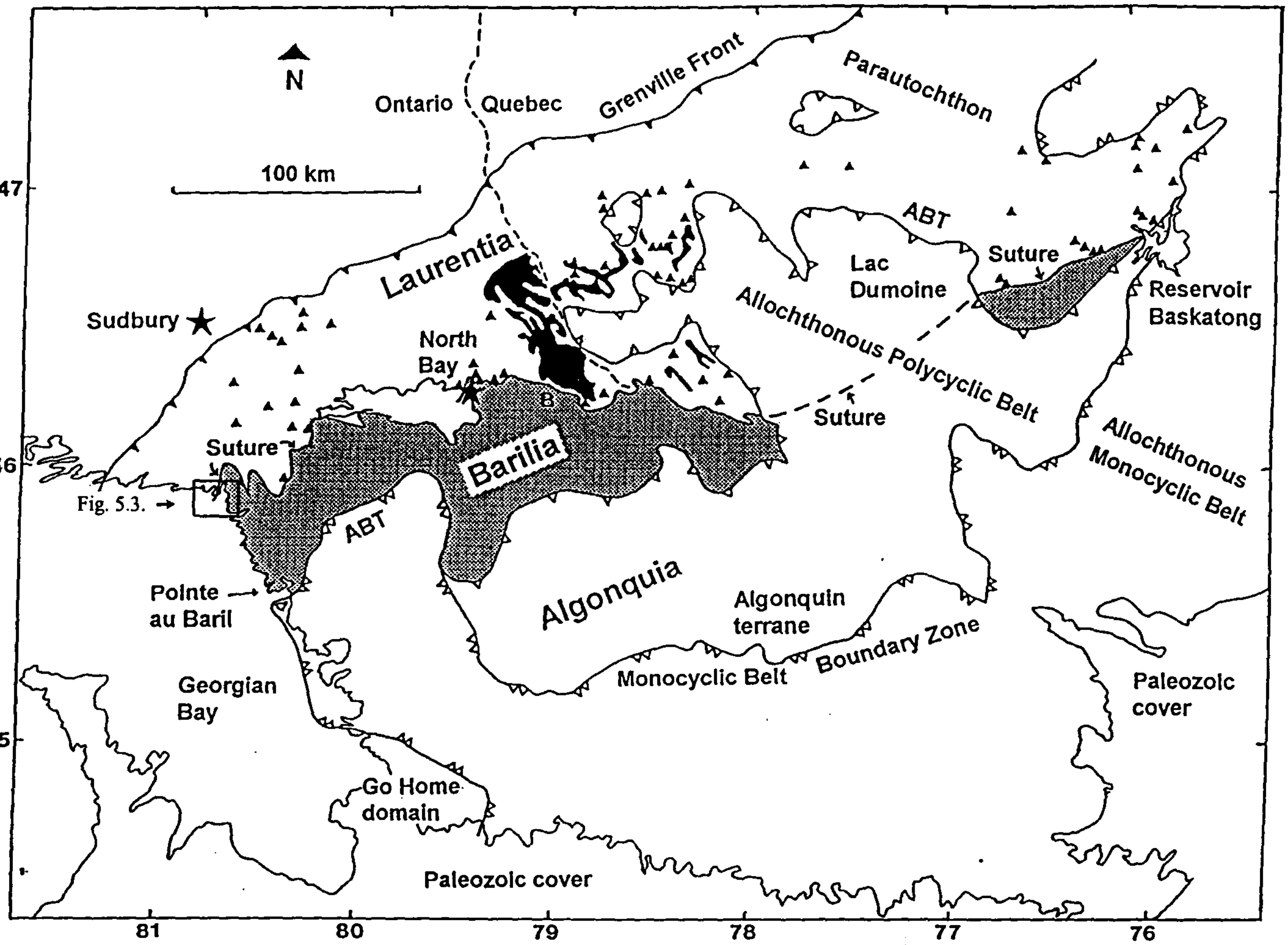


Fig. 5.2. Summary map of the Western Grenville Province, showing the extent of accreted terranes based on Nd-isotope mapping. Location of Archean $T_{DM}$ ages are indicated by triangles and B represents an Archean Pb signature within the Bonfield Batholith.

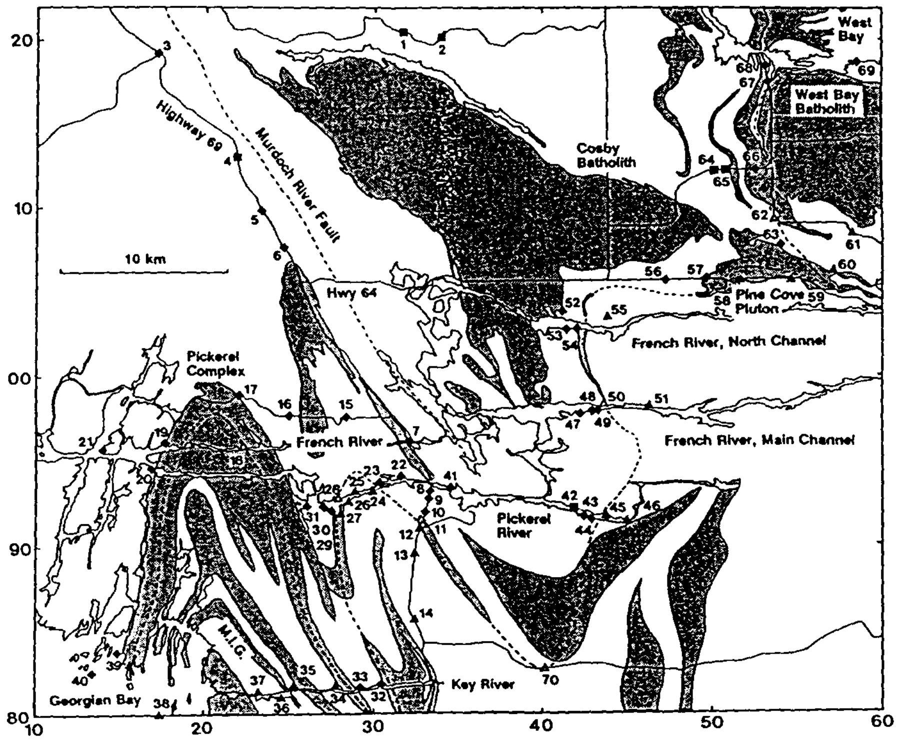


Fig. 5.3. Map of the French River Area from Dickin (1998), showing the mapped isotope discontinuity. Samples with Archean $T_{DM}$ ages are indicated by diamonds and samples with early Proterozoic $T_{DM}$ ages are indicated by triangles.

Table 5.1. Sm-Nd Data for the French River Area (Dickin, 1998).

| Sample numbers | | Grid reference | Corundum [a] diopside | 'Q' | 'P' | Nd (ppm) | Sm (ppm) | $^{147}Sm/^{144}Nd$ | $^{143}Nd/^{144}Nd$ | $\epsilon$ Nd 1.75 (Ga) | TDM (Ga) |
|---|---|---|---|---|---|---|---|---|---|---|---|
| Creighton Granite | | | | | | | | | | | |
| | CGA | 834417 | ND | ND | ND | 48.88 | 8.999 | 0.1113 | 0.511165 | −9.6 | 2.82 |
| North of Cosby Batholith | | | | | | | | | | | |
| 1 | NE3 | 317205 | −6.9 | 50 | −178 | 48.07 | 8.742 | 0.1099 | 0.511168 | −9.2 | 2.78 |
| 2 | NE4 | 341203 | 0.4 | 162 | −204 | 10.68 | 1.612 | 0.0912 | 0.510853 | −11.2 | 2.74 |
| Highway 69 section | | | | | | | | | | | |
| 3 | GF27 O | 172192 | −0.7 | 59 | −222 | 33.49 | 6.251 | 0.1128 | 0.511446 | −4.5 | 2.42 |
| 4 | GF36 | 218129 | −1.3 | 167 | −183 | 6.36 | 1.011 | 0.0962 | 0.511017 | −9.1 | 2.64 |
| 5 | GF39 P? | 232100 | 0.2 | 103 | −156 | 36.64 | 7.150 | 0.1180 | 0.511430 | −5.9 | 2.59 |
| 6 | GF42 P? | 249075 | 1.6 | 149 | −103 | 47.12 | 8.458 | 0.1087 | 0.511433 | −3.8 | 2.35 |
| 7 | GF56.1 | 321961 | −0.8 | 88 | −159 | 45.80 | 8.606 | 0.1135 | 0.511432 | −4.9 | 2.46 |
| 8 | GF59.4 | 335931 | 2.4 | 161 | −13 | 36.67 | 5.995 | 0.0988 | 0.511209 | −6.0 | 2.44 |
| 9 | GF59.8 | 334928 | 2.0 | 179 | −58 | 29.76 | 4.608 | 0.0936 | 0.511219 | −4.6 | 2.32 |
| 10 | GF60.6 | 333920 | 2.4 | 197 | −19 | 34.26 | 5.932 | 0.1047 | 0.511416 | −3.2 | 2.28 |
| 11 | GF61.3 | 330913 | 0.9 | 169 | −37 | 54.20 | 10.153 | 0.1132 | 0.511722 | +0.8 | 2.00 |
| 12 | GF61.7 | 329909 | 2.3 | 234 | 18 | 46.34 | 8.842 | 0.1154 | 0.511801 | +1.9 | 1.92 |
| 13 | GF63 P? | 326896 | 0.8 | 138 | −88 | 31.80 | 5.375 | 0.1022 | 0.511636 | +1.7 | 1.92 |
| 14 | GF67 P? | 326857 | 0.2 | 124 | −176 | 21.93 | 3.804 | 0.1048 | 0.511681 | +2.0 | 1.91 |
| West of Highway 69: Hartley Bay/French River | | | | | | | | | | | |
| 15 | HB2.7 | 283974 | −5.8 | 40 | −224 | 29.39 | 5.142 | 0.1057 | 0.511329 | −5.1 | 2.43 |
| 16 | HB6.0 | 250974 | −2.0 | 112 | −154 | 28.23 | 5.141 | 0.1100 | 0.511410 | −4.5 | 2.41 |
| 17 | HB8.8 | 222988 | 2.6 | 179 | −63 | ND | ND | 0.0943 | 0.511256 | −4.0 | 2.29 |
| 18 | FW9.9 | 224956 | 3.8 | 187 | 0 | 44.89 | 9.050 | 0.1219 | 0.511789 | +0.2 | 2.08 |
| 19 | FW14.9 | 173958 | 1.8 | 175 | −72 | ND | ND | 0.0916 | 0.511200 | −4.4 | 2.31 |
| 20 | FW15.5 | 168945 | 1.8 | 180 | −68 | ND | ND | 0.0983 | 0.511302 | −4.0 | 2.31 |
| 21 | FW18.6 | 137956 | −3.1 | 87 | −192 | 33.67 | 6.323 | 0.1136 | 0.511422 | −5.1 | 2.48 |
| West of Highway 69: Pickerel River | | | | | | | | | | | |
| 22 | PW1.9 | 316939 | −1.2 | 87 | −209 | ND | ND | 0.1049 | 0.511365 | −4.3 | 2.36 |
| 23 | PW3.1 | 305936 | 4.4 | 83 | −158 | 32.46 | 5.771 | 0.1075 | 0.511396 | −4.2 | 2.37 |
| 24 | PW3.6 | 300933 | 0.9 | 127 | −80 | 73.04 | 14.31 | 0.1185 | 0.511860 | +2.4 | 1.89 |
| 25 | PW4.6 | 290930 | −0.6 | 129 | −93 | 64.67 | 12.32 | 0.1151 | 0.511803 | +2.0 | 1.92 |
| 26 | PW5.0 | 286925 | −0.1 | 104 | −127 | 39.58 | 6.003 | 0.0917 | 0.511514 | +1.6 | 1.91 |
| 27 | PW5.6 | 280917 | 0.0 | 137 | −58 | 73.93 | 13.97 | 0.1143 | 0.511798 | +2.1 | 1.91 |
| 28 | PW5.7 | 279927 | 1.2 | 152 | −25 | 66.07 | 11.79 | 0.1078 | 0.511832 | +4.2 | 1.74 |
| 29 | PW6.0 | 276921 | −1.2 | 106 | −131 | 36.02 | 6.240 | 0.1047 | 0.511337 | −4.8 | 2.39 |
| 30 | PW6.3 | 272923 | 1.7 | 144 | −87 | 36.30 | 6.195 | 0.1031 | 0.511439 | −2.4 | 2.21 |
| 31 | PW7.4 | 262924 | 0.7 | 125 | −119 | 37.46 | 6.376 | 0.1029 | 0.511317 | −4.7 | 2.38 |
| West of Highway 69: Key River | | | | | | | | | | | |
| 32 | KR8 | 308818 | −0.2 | 132 | −153 | 31.57 | 5.227 | 0.1001 | 0.511326 | −3.9 | 2.31 |
| 33 | KR7 | 291816 | 2.6 | 192 | −54 | 43.07 | 7.049 | 0.0990 | 0.511342 | −3.4 | 2.27 |
| 34 | KR6 | 280816 | 1.8 | 172 | 3 | 56.09 | 10.599 | 0.1142 | 0.511818 | +2.5 | 1.88 |
| 35 | KR4 | 254816 | 1.9 | 117 | −123 | ND | ND | 0.1108 | 0.511752 | +2.0 | 1.91 |
| 36 | KR3 | 246812 | 0.8 | 146 | −158 | 43.03 | 6.458 | 0.0908 | 0.511540 | +2.3 | 1.86 |
| 37 | KR1 | 232813 | 3.0 | 141 | −31 | ND | ND | 0.0977 | 0.511631 | +2.6 | 1.85 |
| 38 | KR11 | 174801 | −7.0 | 182 | −190 | 17.88 | 3.434 | 0.1161 | 0.511813 | +2.0 | 1.92 |
| 39 | KR10 | 147838 | 0.7 | 126 | −91 | 33.20 | 5.282 | 0.0962 | 0.511333 | −2.9 | 2.22 |
| 40 | KR9 | 131825 | −2.2 | 158 | −102 | 24.61 | 4.284 | 0.1052 | 0.511360 | −4.4 | 2.37 |

| Sample numbers | | Grid reference | Corundum * diopside | 'Q' | 'P' | Nd (ppm) | Sm (ppm) | $^{147}Sm/^{144}Nd$ | $^{143}Nd/^{144}Nd$ | $\epsilon$ Nd 1.75 (Ga) | TDM (Ga) |
|---|---|---|---|---|---|---|---|---|---|---|---|
| East of Highway 69: Pickerel River | | | | | | | | | | | |
| 41 | PE1.0 | 346933 | −5.8 | 62 | −229 | 29.51 | 5.439 | 0.1115 | 0.511427 | −4.5 | 2.42 |
| 42 | PE8.2 | 418921 | 0.8 | 159 | −66 | 31.21 | 5.324 | 0.1031 | 0.511061 | −9.8 | 2.75 |
| 43 | PE8.8 | 423918 | −2.0 | 69 | −198 | 34.31 | 5.935 | 0.1044 | 0.511347 | −4.5 | 2.37 |
| 44 | PE9.2 | 428916 | 1.3 | 130 | −97 | 41.95 | 6.763 | 0.0974 | 0.511260 | −4.6 | 2.34 |
| 45 | PE10.2 | 437916 | −0.5 | 143 | −70 | 72.51 | 13.65 | 0.1138 | 0.511803 | +2.3 | 1.89 |
| 46 | PE11.3 | 449914 | 2.6 | 170 | −12 | 41.07 | 6.095 | 0.0897 | 0.511500 | +1.8 | 1.90 |
| East of Highway 69: French River (Main Channel) | | | | | | | | | | | |
| 47 | FE9.8 | 421977 | −6.2 | 88 | −175 | 27.06 | 5.175 | 0.1156 | 0.511511 | −3.8 | 2.39 |
| 48 | FE10.6 | 429978 | 0.3 | 140 | −76 | 29.25 | 4.633 | 0.0957 | 0.511202 | −5.4 | 2.39 |
| 49 | FE11.0 | 433979 | 1.3 | 133 | −93 | 27.16 | 4.340 | 0.0966 | 0.511215 | −5.3 | 2.39 |
| 50 | FE11.4 | 436982 | 1.7 | 158 | −92 | 56.36 | 10.407 | 0.1117 | 0.511706 | +0.9 | 2.00 |
| 51 | FE14.0 | 463980 | 1.8 | 194 | −12 | 22.94 | 3.807 | 0.1004 | 0.511648 | +2.3 | 1.88 |
| East of Highway 69: French River (North Channel) | | | | | | | | | | | |
| 52 | NC8.9 | 412037 | −15.6 | 82 | −225 | ND | ND | 0.1240 | 0.511645 | −3.1 | 2.39 |
| 53 | NC9.2 | 415027 | 1.7 | 125 | −149 | 46.91 | 8.456 | 0.1091 | 0.511315 | −6.2 | 2.54 |
| 54 | NC9.7 | 420027 | 1.6 | 68 | −148 | 44.89 | 7.347 | 0.0989 | 0.511360 | −3.0 | 2.24 |
| 55 | NC11.6 | 439035 | 1.1 | 156 | −30 | 68.45 | 10.84 | 0.0957 | 0.511571 | +1.9 | 1.90 |
| Pine Cove area | | | | | | | | | | | |
| 56 | NV9 | 474056 | 3.4 | 184 | −39 | 33.28 | 5.377 | 0.0975 | 0.511228 | −5.3 | 2.39 |
| 57 | NV15 | 497057 | −0.4 | 71 | −214 | 35.78 | 6.522 | 0.1102 | 0.511334 | −6.1 | 2.53 |
| 58 | NV11 | 516057 | 0.4 | 62 | −252 | ND | ND | 0.1173 | 0.511867 | +2.8 | 1.86 |
| 59 | N25 | 546057 | −0.5 | 143 | −86 | 51.43 | 9.490 | 0.1115 | 0.511793 | +2.6 | 1.86 |
| 60 | NV24 | 571061 | −1.8 | 118 | −88 | 75.24 | 14.046 | 0.1128 | 0.511823 | +2.9 | 1.84 |
| 61 | NV1 | 581085 | 2.3 | 171 | −41 | 73.39 | 13.60 | 0.1119 | 0.511784 | +2.4 | 1.88 |
| 62 | NV12 | 536093 | 2.1 | 107 | −108 | 62.22 | 11.239 | 0.1091 | 0.511680 | +1.0 | 2.00 |
| 63 | NV26 | 539078 | −2.6 | 61 | −207 | 29.31 | 5.236 | 0.1080 | 0.511324 | −5.8 | 2.49 |
| West Bay area | | | | | | | | | | | |
| 64 | WB42 P | 502121 | −2.7 | 132 | −136 | 33.95 | 5.592 | 0.0998 | 0.511042 | −9.4 | 2.70 |
| 65 | WB41.6 | 507121 | 0.9 | 139 | −172 | 25.06 | 4.054 | 0.0978 | 0.510939 | −11.0 | 2.79 |
| 66 | WB40 | 524122 | 0.7 | 109 | −155 | 35.46 | 6.314 | 0.1076 | 0.511355 | −5.1 | 2.44 |
| 67 | WB33.4 | 533176 | 2.8 | 168 | −88 | 44.32 | 7.219 | 0.0984 | 0.511384 | −2.4 | 2.20 |
| 68 | WB32.4 | 531186 | 3.2 | 140 | −96 | 41.68 | 6.762 | 0.0981 | 0.511252 | −4.9 | 2.37 |
| 69 | WB2 | 583187 | 1.8 | 139 | −87 | 30.07 | 4.649 | 0.0936 | 0.511197 | −5.0 | 2.35 |
| East of Highway 69: Key River | | | | | | | | | | | |
| 70 | KE6.7 | 403830 | 0.9 | 175 | 37 | 68.85 | 11.331 | 0.0995 | 0.511571 | +1.0 | 1.96 |
| Mesoproterozoic plutons | | | | | | | | | | | |
| Pickerel | | 195986 | −9.7 | 30 | −127 | 86.3 | 17.62 | 0.1235 | 0.511912 | +2.3 | 1.91 |
| Pine Cove | | 575049 | ND | ND | ND | 64.4 | 11.05 | 0.1038 | 0.511314 | −5.0 | 2.41 |
| West Bay N | | 537235 | −3.5 | 111 | −71 | 94.4 | 14.89 | 0.0952 | 0.511389 | −1.6 | 2.13 |
| West Bay S | | 535126 | −0.3 | 29 | −146 | 66.7 | 12.28 | 0.1113 | 0.511773 | +2.3 | 1.89 |

Grid references are given to the nearest 100 m.

* Positive values are % normative corundum, negative are % normative diopside.

ND = not determined.

Samples: $^{143}Nd/^{144}Nd$ average within-run precision 0.0012% (1 SDM).

Standard: $^{143}Nd/^{144}Nd$ population standard deviation 0.002% (1 SD).

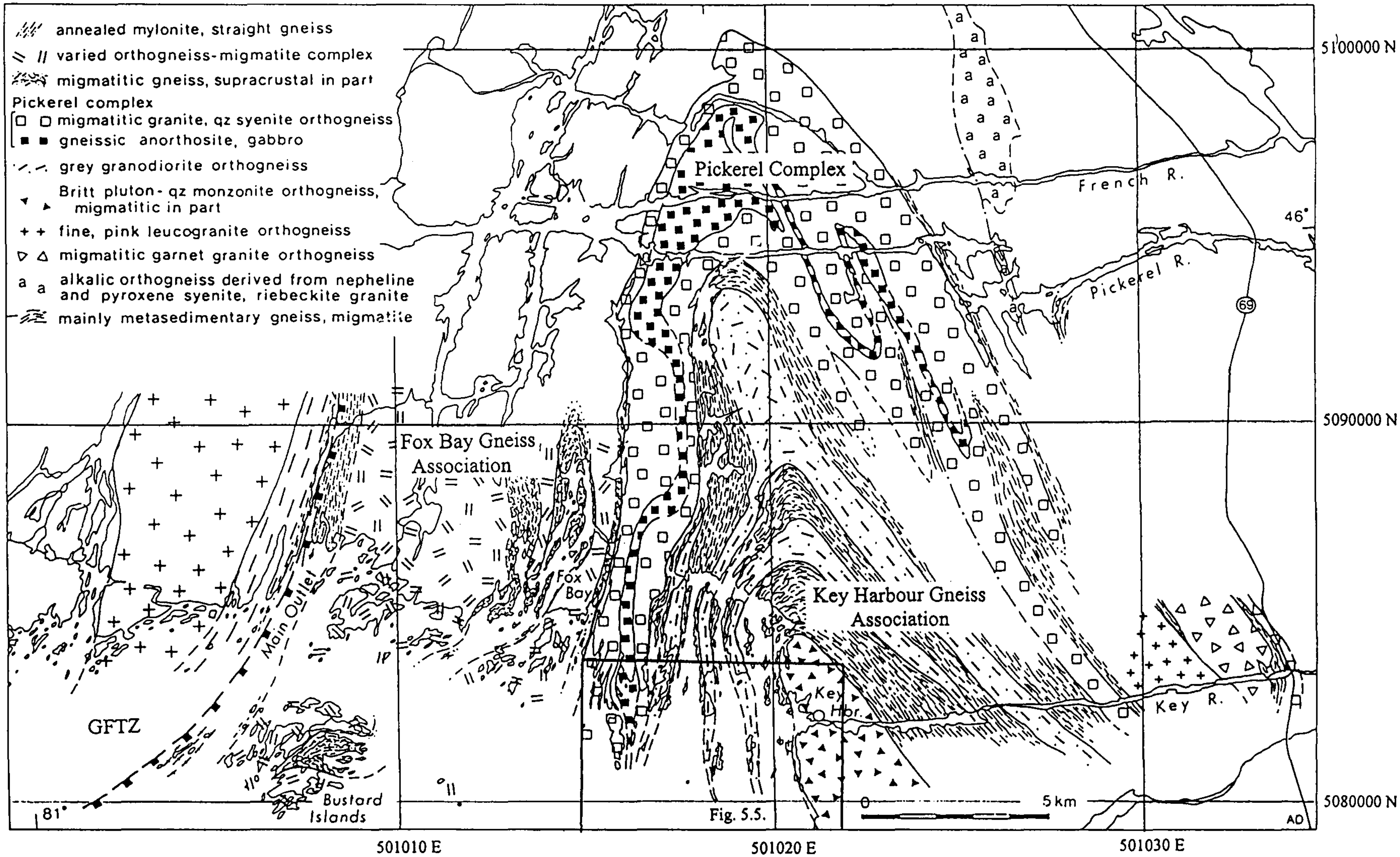


Fig. 5.4. Geologic sketch map of the French River area, extending from the main outlet of the French River to the Key River, modified from Davidson & Bethune (1988).

(Lumbers, 1975), which has been described as a granitoid intrusion emplaced into the older Key Harbour Gneiss association (Corrigan, et. al., 1994). The Nd studies previously mentioned suggest that the gneisses west of the Pickerel Complex belong to a separate tectonic package, which will be referred to as the Fox Bay Gneiss Association throughout the rest of this paper.

The area that was sampled begins on the western half of the map in Fig. 5.5. and extends westward. There are three lithologies described in this region: a) the Fox Bay gneiss association, b) the Key Harbour gneiss association (Culshaw et al., 1988) and c) a suite of intruded metaplutonic sheets and plutons.

*Fox Bay Gneiss Association*

The Fox Bay gneiss association is made up of two major units. The more prominent of these is a varied orthogneiss-migmatite complex. These dark orthogneisses range through gabbro, diorite, quartz diorite and granodiorite in composition with small, localized, lenticular plutons of pink leucogranite. The second unit underlies Fox Bay and part of the Bustard Islands, and is composed of migmatic gneisses of supracrustal origin. These migmatites are also present in the shear zone which passes through the French River Main Outlet.

*Key Harbour Gneiss Association*

The composition of the Key Harbour gneiss association is primarily leucocratic, pink to grey, granitic to tonalitic orthogneiss. There are often parallel and/or thin layers of quartzite, calc-silicate gneiss and garnet amphibolite. Of less significant abundance, but also present are, hornblende-bearing migmatites. The migmatites and gneiss were intruded by the PaleoProterozoic Key Harbour leucogranite (1694 Ma, Corrigan, et. al., 1994).

*Mid-Proterozoic granitoids and gabbro dykes*

Mid-Proterozoic metaplutonic rocks intrude into the Key Harbour gneiss assemblage. These metaplutonic bodies have granitic, monzonitic, granodioritic and dioritic compositions, mixed with small amounts of quartz syenite, monzodiorite, and anorthosite-leucogabbro. The Pickerel Complex, folded into an antiform, lies on the

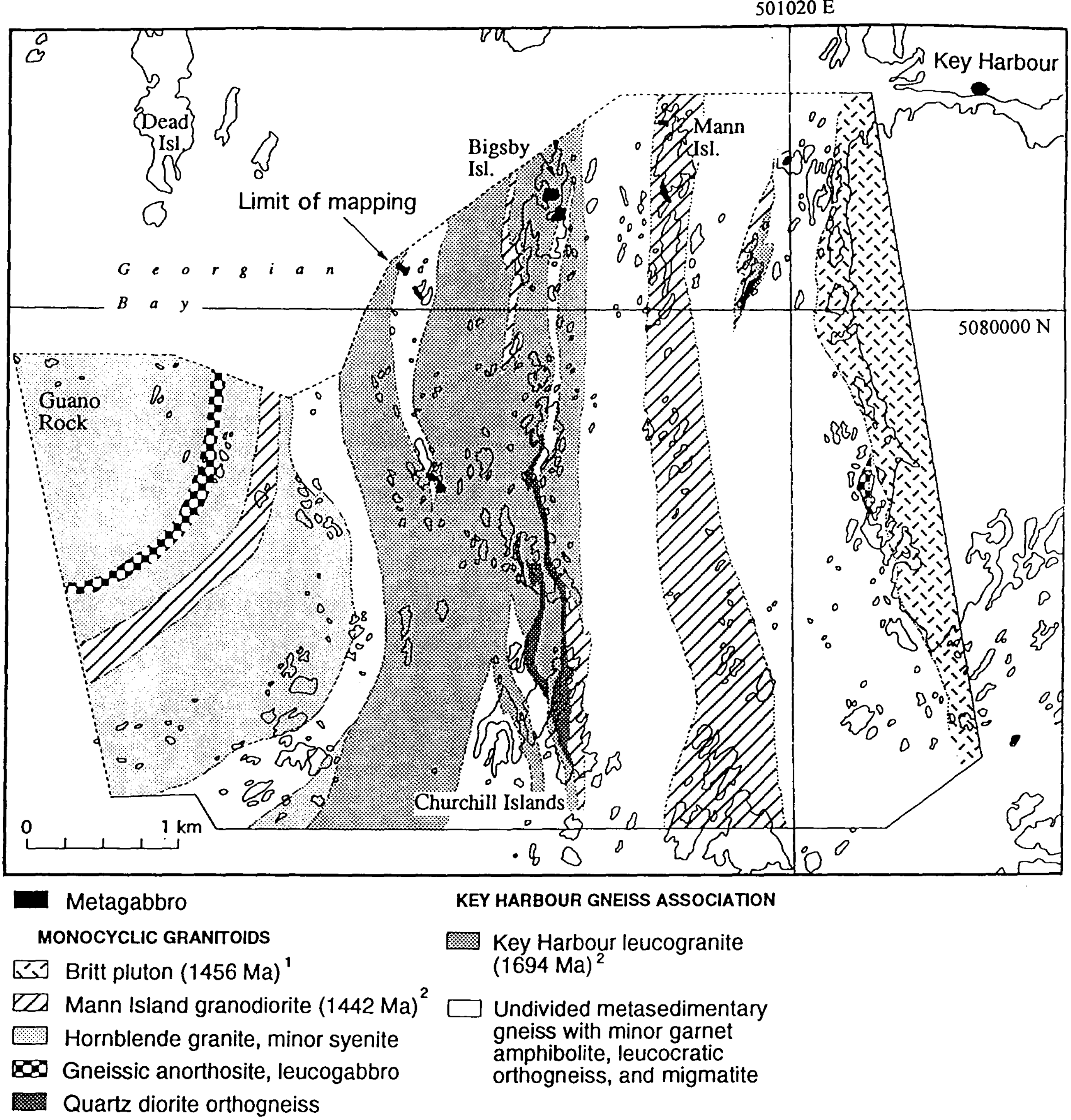


Fig. 5.5. Lithologic map of the Key Harbour area, modified from Corrigan et. al. (1994).

1. van Breeman et. al. (1986) as the source.
2. Corrigan et. al. (1994) as the source

western fringe of the map (Fig. 5.4), and is composed of hornblende-bearing granite, quartz syenite and gabbro-anorthosite (Lumbers 1975; Davidson et al., 1982) thought to be ca 1450 Ma.

The metaplutonic rocks have been intruded by pods and disrupted metagabbroic dykes, which have been suggested to be linked to the Sudbury dyke swarm, based on geochemistry and petrographics (Bethune, 1993). These dykes have coronitic textures, sharp intrusive contacts, locally chilled margins and their foliation is oriented at different angles than the country rock. Within shear zones, these have been recrystallized to garnet amphibolites.

The MesoProterozoic plutons in the study area are folded into kilometer-scale, shallow southeast-plunging folds (Schwerdtner, 1987). The most prominent of these folds is a large, open synform with a shallow south-southeast plunge. Its axial trace lies just inland from the Georgian Bay coast (Davidson et. al., 1982). The Britt Pluton makes up the core of this synform at Key Harbour. It has U-Pb of 1456 Ma (van Breeman, et. al., 1986) and is composed of variably migmatitic garnet-hornblende-biotite orthogneiss of quartz monzodiorite to granodiorite composition. Exposed higher in the synform, are two MesoProterozoic plutonic sheets, each less than 500 m thick, of grey biotite granodiorite orthogneiss with flattened augen K-feldspar. The easternmost of these is the Mann Island granodiorite, which has a U-Pb age of 1442 Ma (Corrigan, et. al., 1994). To the west of this unit is a mix of complexly deformed gneisses, including metasedimentary gneisses with minor garnet amphibolite, leucocratic orthogneisses, migmatites and the PaleoProterozoic Key Harbour leucogranite..

The outermost lithologic unit of the synform is the Pickerel Complex. On the eastern limb of the synform, there are several tight, internal folds in the Pickerel Complex. The division between the Pickerel Complex and the Fox Bay gneiss association is where the break in the Nd model ages occurs. This may mark the position of the Penokean Suture, although Dickin (1998) suggested that the Pickerel Complex was a stitching pluton relative to the suture. The age boundary is shown within the Pickerel Complex (Fig. 5.3.), rather than along its lithologic boundary with the Archean orthogneisses. Results from four localities on the age boundary (11,18, 50 and 62 in Fig.

5.3.), suggest tectonic mixing between the Archean and Proterozoic crust. Grenvillian metamorphism has obscured any evidence that this boundary may have been a zone of diffuse ductile shear (Dickin, 1998)..

5.1.4. Nd Isotope Sampling and Magnetic Field Areas

Sampling was done in a transect, between the between Key Harbour and the Bustard Islands (Ontario Topographic Map 41 H/15). Processing of the magnetic map and Landsat TM image were conducted on a scene with similar coverage to the topographic map. Further magnetic mapping was performed on a smaller scene moving to the southwest from the original scene.

## Nd Model Age Mapping:

5.2.0. Nd Model Age Results & Discussion

In addition to the 75 previously dated results (Dickin, 1998) shown in Table 5.1, six new samples were collected and studied (Table 5.2). The locations of the new samples are shown in Fig. 5.8, 5.9 and 5.10. The locations of samples 2 and 3 are important. They lie west of the proposed boundary of Dickin (1998), but east of the lithological boundary between the Pickerel Complex and the orthogneisses described earlier in this chapter. These two samples have Nd model ages < 2.0 Ga, which suggests that the suture might be marked by this lithologic boundary. However, sample 2 may be representative of the Pickerel Complex, rather than a screen of country rock (see section 5.2.3.). Samples from the Fox Bay area (39 and 40 in Fig. 5.5.) and further north, on the French River (19, 20 and 21 in Fig. 5.5) show quite clearly that the rocks immediately east of the Pickerel Complex are Archean in origin, as they all have ages > 2.2. Ga.

The previous studies had defined a gap in the Nd model ages between 2.0 and 2.3 Ga. Looking at a histogram analysis (Fig. 5.6), it can be seen that there are two distinct peaks. The first lies between 1.8 - 2.0 Ga, and the second is found around 2.2 – 2.5 Ga. A third, and much smaller peak occurs at 2.7 – 2.8 Ga. These ages could represent either

Table 5.2. Sm-Nd Data for rocks from the Key Harbour Area

| Sample Numbers | | Grid Reference | SM (ppm) | ND (ppm) | $Sm^{147}/Nd^{144}$ | $Nd^{143}/Nd^{144}$ | E(t) | $T_{DM}$ (Ga) |
|---|---|---|---|---|---|---|---|---|
| *Gull Rocks* | | | | | | | | |
| 1 | PC5A | 113-799 | 6.891 | 41.52 | 0.1003 | 0.511285 | -5.1 | 2.37 |
| *One Tree Island to Guano Rock* | | | | | | | | |
| 2 | PC6 | 148-796 | 19.249 | 114.34 | 0.1018 | 0.511768 | 2.0 | 1.90 |
| 3 | PC4 | 113-799 | 14.570 | 76.75 | 0.1147 | 0.511768 | NA | 1.96 |
| 4 | PC3 | 154-770 | 8.284 | 44.37 | 0.1128 | 0.511753 | 1.6 | 1.95 |
| 5 | PC2 | 157-769 | 11.646 | 62.36 | 0.1129 | 0.511762 | 1.7 | 1.94 |
| 6 | PC1 | 165-767 | 10.715 | 69.35 | 0.0934 | 0.511555 | 2.1 | 1.88 |

* *t* = 1750 Ma

Table 5.3. Major Element Analysis for rocks from the Key Harbour Area

| SAMPLE | PC1 | PC2 | PC3 | PC4 | PC5A | PC6 |
|---|---|---|---|---|---|---|
| $SiO_2$% | 68.06 | 76.10 | 71.37 | 78.70 | 73.75 | 69.46 |
| $Al_2O_3$% | 16.03 | 12.05 | 13.33 | 11.14 | 13.16 | 13.93 |
| $Fe_2O_3$% | 2.97 | 2.27 | 2.66 | 1.61 | 2.66 | 4.50 |
| MnO% | 0.059 | 0.024 | 0.025 | 0.023 | 0.062 | 0.084 |
| MgO% | 0.74 | 0.30 | 0.51 | 0.08 | 0.93 | 0.21 |
| CaO% | 1.17 | 0.55 | 1.26 | 0.38 | 2.28 | 1.31 |
| $Na_2O$% | 3.15 | 2.92 | 3.29 | 2.87 | 2.73 | 4.00 |
| $K_2O$% | 7.24 | 5.51 | 5.03 | 5.06 | 3.71 | 5.61 |
| $TiO_2$% | 0.433 | 0.271 | 0.457 | 0.171 | 0.310 | 0.401 |
| Total: | 99.85 | 100.00 | 97.93 | 100.03 | 99.59 | 99.51 |
| $Na_2O/K_2O$ | 0.7 | 0.8 | 1.0 | 0.9 | 1.1 | 1.1 |
| Q | 109 | 205 | 168 | 232 | 216 | 122 |
| P | 32 | 13 | -22 | 8 | -50 | -33 |

Table 5.4. Normative Calculations for rocks from the Key Harbour Area

| SAMPLE | PC1 | PC2 | PC3 | PC4 | PC5A | PC6 |
|---|---|---|---|---|---|---|
| *Q* | 16.86 | 35.08 | 28.23 | 40.72 | 35.97 | 19.95 |
| *Or* | 42.73 | 32.52 | 29.69 | 29.87 | 21.90 | 33.11 |
| *Ab* | 26.62 | 24.68 | 27.81 | 24.26 | 23.07 | 33.81 |
| *An* | 5.15 | 2.46 | 5.59 | 1.75 | 10.65 | 3.47 |
| *C* | 1.12 | 0.38 | 0.42 | 0.30 | 0.75 | 0.00 |
| *Di* | 0.00 | 0.00 | 0.00 | 0.00 | 0.00 | 2.26 |
| *Hy* | 5.89 | 3.89 | 4.72 | 2.48 | 6.07 | 5.81 |
| *Ol* | 0.00 | 0.00 | 0.00 | 0.00 | 0.00 | 0.00 |
| *Mt* | 0.43 | 0.33 | 0.39 | 0.23 | 0.39 | 0.65 |
| *Il* | 0.82 | 0.52 | 0.87 | 0.33 | 0.59 | 0.82 |
| *Ap* | 0.22 | 0.09 | 0.22 | 0.04 | 0.22 | 0.15 |
| Total: | 99.84 | 99.94 | 97.92 | 99.98 | 99.59 | 100.04 |

**Fig. 5.6. Histogram of the Nd model age results**

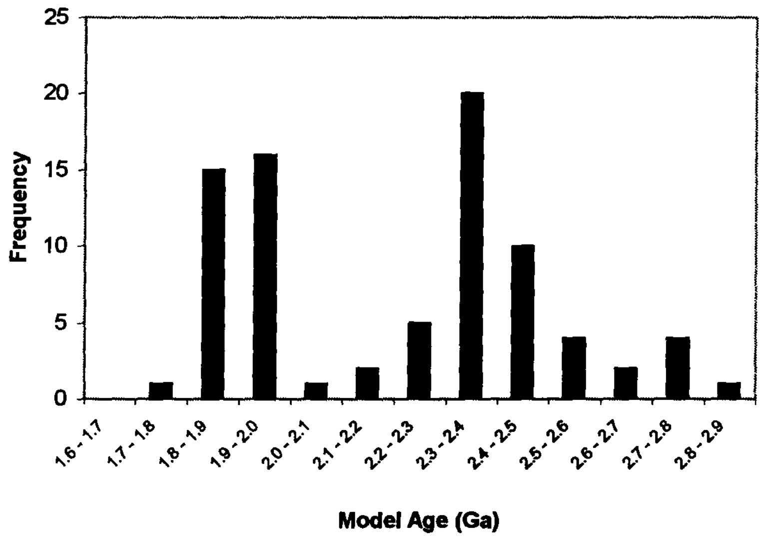

the formation age of the continental crust, or they may be representative of events which caused younger and older crustal material to become mixed. The oldest peak corresponds with the Kenoran Orogeny, from which a pluton near Hagar, north of the French River, has been dated at 2679 ± 2 Ma (Chen et. al., 1995). The Penokean Orogen has been studied in Wisconsin (500 km to the west), and is dated at 1.85 Ga, which corresponds with the youngest peak. The middle peak in the histogram does not correspond to a known orogenic event, but it has been suggested that this peak represents the emplacement of granitoid plutons by melting of mafic crustal underplating (Dickin, 1998). This underplating would have been of a Huronian Age and likely melted by a later event, such as the Killarnean magmatic event.

Further evaluation of the model is done by looking at plots of epsilon Nd against Nd concentration of the rocks (Fig. 5.7). This graph shows that the isotope signatures have tighter clusters than can be seen in the model age histogram. Dickin (1998) recognized clear gaps between the Archean crust, the intermediate group ("reworked Archean crust"), and the PaleoProterozoic arc crust. Filled triangles and a filled diamond represent the samples collected for this study. Comparing the new data with the old data, it is evident five of these six samples belong to the juvenile arc crust. The exception is sample 1 (PC5A) from the Gull Rocks, which is reworked Archean crust.

Also of interest is the distribution of data in both the model age histogram and the $\varepsilon(T)$ vs. Nd ppm. The Penokean ages form a tight distribution between 1.9 and 2.0 Ga in the model age histogram. The same samples form an elongate cluster in the $\varepsilon(T)$ vs. Nd ppm graph. The Kenoran-aged samples form similar distribution patterns in the two diagrams. The remaining data form a broad distribution in the histogram and a tighter, circular cluster in the $\varepsilon(T)$ vs. Nd ppm graph. The reasons for these different distributions are not entirely evident. The Penokean and Kenoran data represent known orogenic events, which could explain their tight distributions in the histogram. The broad distribution of the central peak could represent on-going processes, such as plutonism and under-plating, or it may be generated as a result of mixing of younger and older crustal materials. Reasons for the distribution pattern in the $\varepsilon(T)$ vs. Nd ppm graph are less evident.

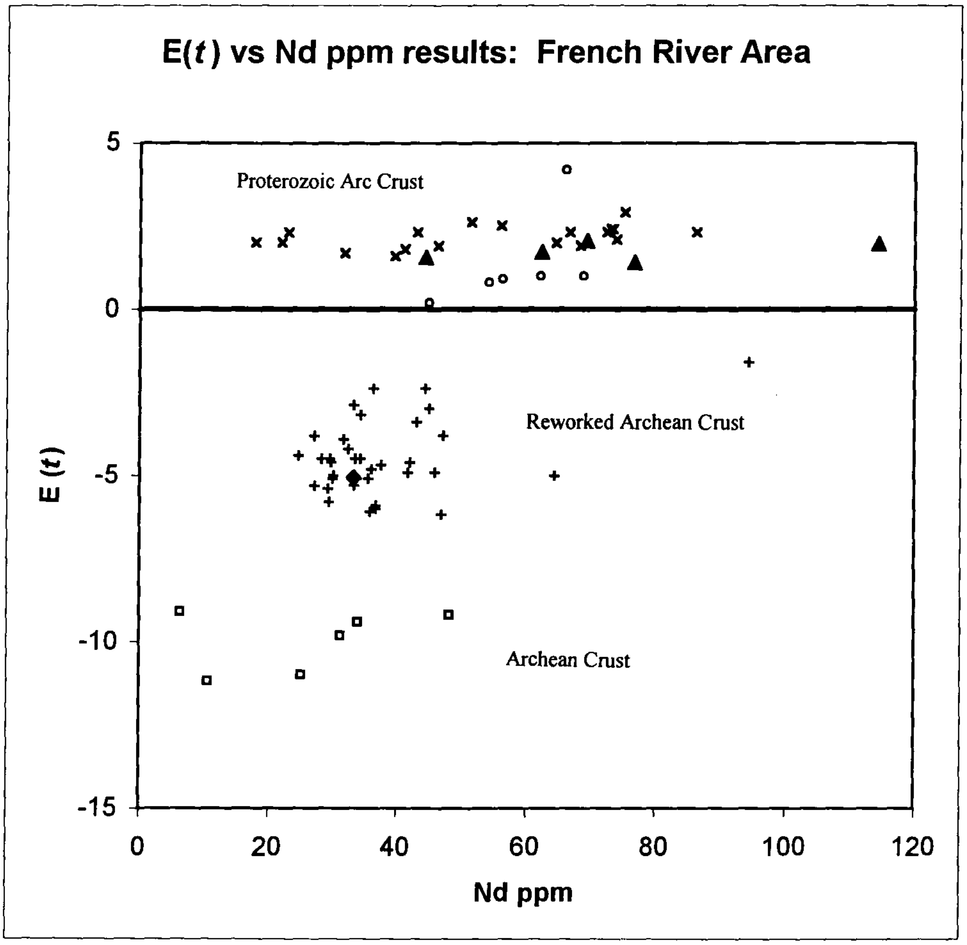


Fig. 5.7. Graph of εNd vs. Nd ppm.

- □ represent Kenoran $T_{DM}$ ages[1]
- + represents "reworked Archean" $T_{DM}$ ages[1]
- x represents early Proterozoic $T_{DM}$ ages[1]
- o represents samples near the suture with mixed $T_{DM}$ ages[1]
- ◆ represents "reworked Archean" $T_{DM}$ ages[2]
- ▲ represents early Proterozoic $T_{DM}$ ages[2]

1. From Dickin (1998)
2. From this study.

5.2.1. Whole-Rock Elemental Analysis

The major element breakdown of each sample is shown in Table 5.3, as well as the Na/K ratio, the Q and P values. With these values the gneisses can be plotted on the geochemical-petrological grid of Debon and LeFort (1983), which uses chemical data to generate a Streckheisen-type classification. These values are calculated with the following equations:

$$Q = \frac{SiO_2}{3} - \left(K_2O + Na_2O + \frac{2}{3}(CaO)\right)$$

$$P = K_2O - (Na_2O + CaO)$$

The P values have been plotted against the Q values in Fig. 5.8., allowing classification of the samples, based on the elemental analysis. The Archean sample, PC5A, plots in the Adamellite field, while the remaining samples plot in the Granite field. Also plotted in Fig. 5.8. are the P vs. Q values from Table 5.1, of the samples previously studied in this region. This allows a comparison, showing that the six samples studied plot in an expected range and are therefore consistent with the previously accumulated data set.

5.2.2. Normative Calculations

The results of calculating the CIPW Norm are shown in Table 5.4. The most significant numbers are the values for Normative Corundum and Normative Diopside. In cases such as sample 2 (PC6), where the Nd ppm is considered to be high (Table 5.2), the rock in question may be a young anorogenic granite pluton. Amounts of normative diopside > 3% and high levels of Nd are indicators that a pluton consists of "reworked" crustal material, rather than new mantle derived material.

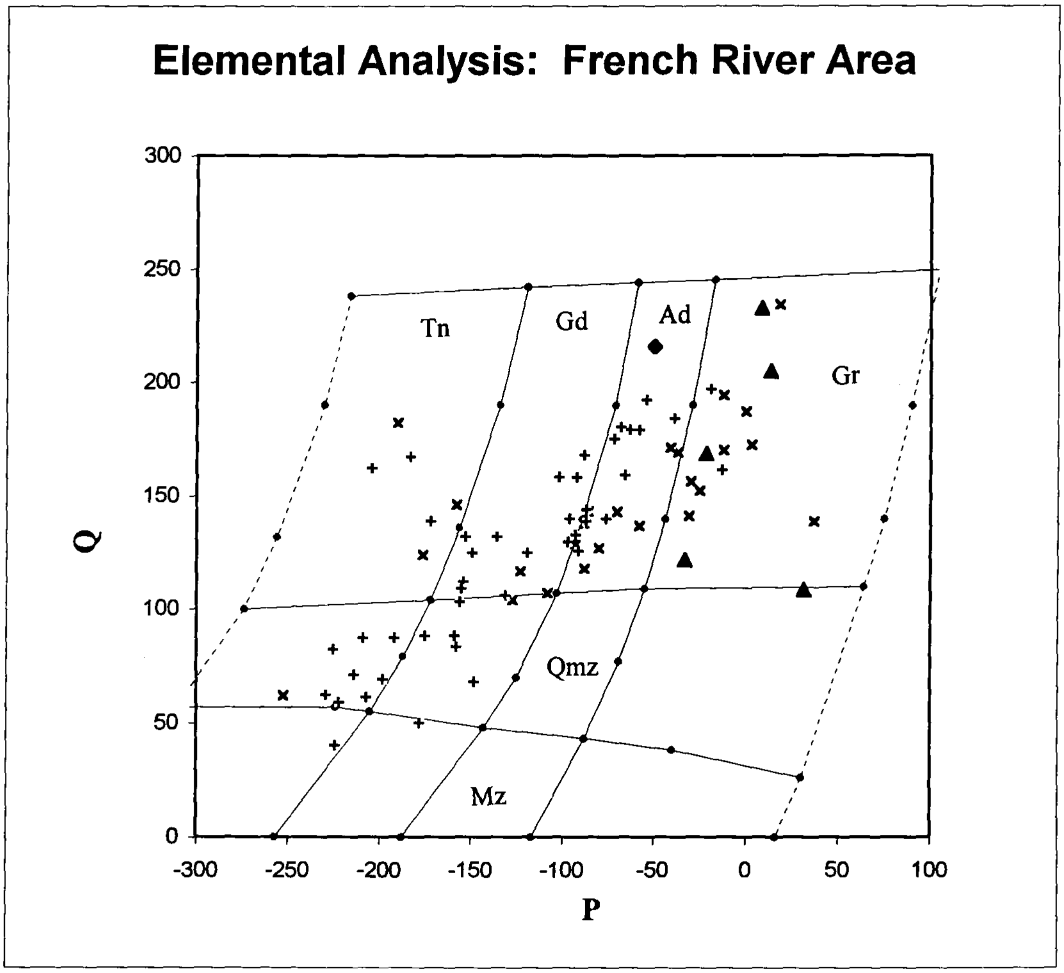


Fig. 5.8. Plot of Q vs. P for the French River area.

| | | | |
|---|---|---|---|
| + | represents Archean & "reworked Archean" $T_{DM}$ ages[1] | Tn | = tonalite |
| x | represents early Proterozoic $T_{DM}$ ages[1] | Gd | = granodiorite |
| ◆ | represents Archean & "reworked Archean" $T_{DM}$ ages[2] | Ad | = adamellite |
| ▲ | represents early Proterozoic $T_{DM}$ ages[2] | Gr | = Granite |
| | | Qmz | = Quartz-monzonite |
| | | Mz | = Monzonite |

1. From Dickin (1998)
2. From this study.

## Geophysical Mapping:

### 5.3.0. Introduction

During the sample collecting, several questions arose about the geology in the field area. The sampling began near the western edge of the area mapped by Corrigan et. al. (1994) (Fig. 5.5), and continued westward, as previously described. Existing maps have suggested a possible fold in the lithologic beds with a northwest-southeast trending axis. Localized field observations appear to support the existence of the inferred fold (Fig. 5.5), but suggest that the exact form of the fold is loosely constrained. It was decided that this required further investigation. Gabbro-anorthosites (Fig. 5.4, 5,5) which have high magnetic mineral content, are usually expected to produce a stronger magnetic signature than the surrounding granites and gneisses. It was also hypothesized that the rock types on either side of the suture could have significantly different magnetic signatures, allowing it to be traced out into Georgian Bay where there is no outcrop. Therefore, the questions to be answered by this study are:

1) Is the fold inferred by the mapped geology correct, or is there a more complex geologic structure here?

2) Would the gabbro-anorthosite produce a detectable magnetic high, which could be used to map the trends of the local lithologies?

3) Is there a difference in the magnetic signature of the rocks on either side of the known Nd model age discontinuity, which would allow further mapping of this boundary?

These questions can be addressed through a process of image integration to match and compare the geologic features observed in the magnetic data with the isotopic information and the mapped geology, the magnetic data is to be overlain on a processed Landsat TM image of the region.

### 5.3.1. Data Processing

The processing of the magnetic data and the Landsat TM images was conducted at the McMaster Applied Geophysics Laboratory. The approach involved processing the magnetic data to produce a map of magnetic property variations, as they relate to the geologic structures. The magnetic map allows identification of primary lithologies and secondary alterations associated with localized addition or removal of magnetic minerals, (i.e. faults, intrusive boundaries). This map overlaps areas of previously mapped geology with areas where geologic mapping was obscured by the presence of Georgian Bay.

The next step was to use a Landsat TM image of the French River Area to produce accurate maps, trace in the mapped geology and allow comparison and improved interpretation of the geology in the field area. Landsat TM optical bands 1, 2 and 3 are used, therefore the geology is mapped on the basis of colour zonation associated with rock types and topographic features which reflect different rates of weathering. Fracture-induced friability tends to increase weathering, thus faults and fractures are recognizable in the satellite image. Once the two data sets had been georectified to NAD27/UTM17, the magnetic map was imported to ERMapper, where the geologic information could be overlain on both data sets. The procedures used to process the magnetic data and the Landsat TM images are outlined below:

*Processing of the Magnetic Data*

1. Acquire Data: Sections were cut out of 2 sub-sets of the OGS provincial data set and merged to form a data-set covering the same area as the Ontario Topographic Map 41 H/15.

2. Import data into Geosoft Oasis

3. Convert Lat./Long. to UTM coordinates

4. Determine Line-Spacing: The grid cell size of the survey is approximately 200 $m^2$.

5. Remove Tie-line Interference: The Minty Method (Minty, 1991) was used to for this. A High-pass filter of 3 fiducials, was followed by a Low-pass filter of 5 fiducials.

6. Reduce-to-Pole: The following values were used - Mag. Dec. = -8.5
   - Mag. Inc. = 64.0

7. Upward Continue: 3 Grids were produced at intervals of 400 m, 800 m, and 1200 m. The 400 m & 800 m grids were selected for continued processing.

8. Grid Subtraction: Both the 400 m & 800 m upward continued grids were subtracted from the reduce-to-pole grid. The final grid selected was the result of the subtraction of the 800 m upward continue from the reduce-to-pole grid.

*Processing of the Landsat TM Images*

1. Acquire Data: The Landsat TM scene was imported into ERMapper.

2. Select Field Area: The French River Area was cut out of a larger Landsat TM scene. The area cut was selected to match the extent of the magnetic data set.

3. Image Setup: The data for the region has been collected in 7 different energy bands. Band 5 was imported to an intensity layer, Band 3 to the red pseudocolour layer, Band 2 to the green pseudocolor layer and Band 1 to the blue pseudocolour layer.

4. Image Filtering: Each of the afore-mentioned layers must be individually filtered to adjust the overall appearance of the image. This is done to reduce cloud interference and enhance features of interest.

5. Importing Magnetic Data: Once it is imported, the magnetic grid is displayed as an intensity layer in ERMapper.

6. Image Annotation: There were several layers were created to annotate different things. The important ones include
    A. The UTM Grid
    B. Mapped Geology
    C. Faults interpreted from the magnetics
    D. Geology interpreted from the magnetics
    E. Location of sample points
    F. Location of the suture

7. Comparison and Interpretation

5.3.2. Results

The following pages contain a series of colour images produced from processing the magnetic and remote sensing images. Fig. 5.9. shows the filtered satellite image, displaying the north shore of Georgian Bay. Nothing can be seen where the water absorbs the energy, but on the land, many lineations are visible. In this image, the lineations represent lithologic boundaries and faults. A large fold structure is evident in the center portion above Key Harbour, which matches the fold geometry shown in the existing geologic maps. In the Eastern portion of the image, there is some thin cloud interference, which could not be completely filtered out. However, this only alters the colouration of the image.

The next image, Fig. 5.10., shows the same scene as the previous image. The mapped lithologies have been shown in red and a possible location for the suture has been annotated on this image, using the edge of the Pickerel Complex (Culshaw, et. al., 2000). Mapped faults have been highlighted in light blue, the dotted lines marking major faults, which are now occupied by rivers. The sampling locations for the Nd model age mapping have also been shown in this image. The annotation was done by starting with the known geology from The Georgian Bay Transect (Culshaw, et. al., 2000) and improving on this by interpreting additional information evident in the satellite image. It is important to note in the center of the image, the inferred fold as described earlier.

The next image, Fig. 5.11., is the final colour-shaded grid produced from processing the magnetic data. Features of note in this scene have been numbered for easy reference. (1) is a strong magnetic high, edged by a magnetic low. This is the southeastern edge of the Grenville Front Tectonic Zone. The magnetic high is associated with a massive formation of pink-grey hornblende-biotite quartz monzonite (Davidson & Bethune, 1988). (2a) is a prominent magnetic high, which runs from the upper part of the image towards the southwestern corner. The magnetic high corresponds with the orthogneiss-migmatite complex of the Fox Bay gneiss association. The magnetic lows between the edge of the Pickerel Complex and the GFTZ are caused by migmatic gneisses, which may have supracrustal components (Davidson & Bethune, 1988). (2b) is the Pickerel Complex, which produces a magnetic low. Initially it was suspected that the gabbro-anorthosite would produce a magnetic high relative to the surrounding hornblende

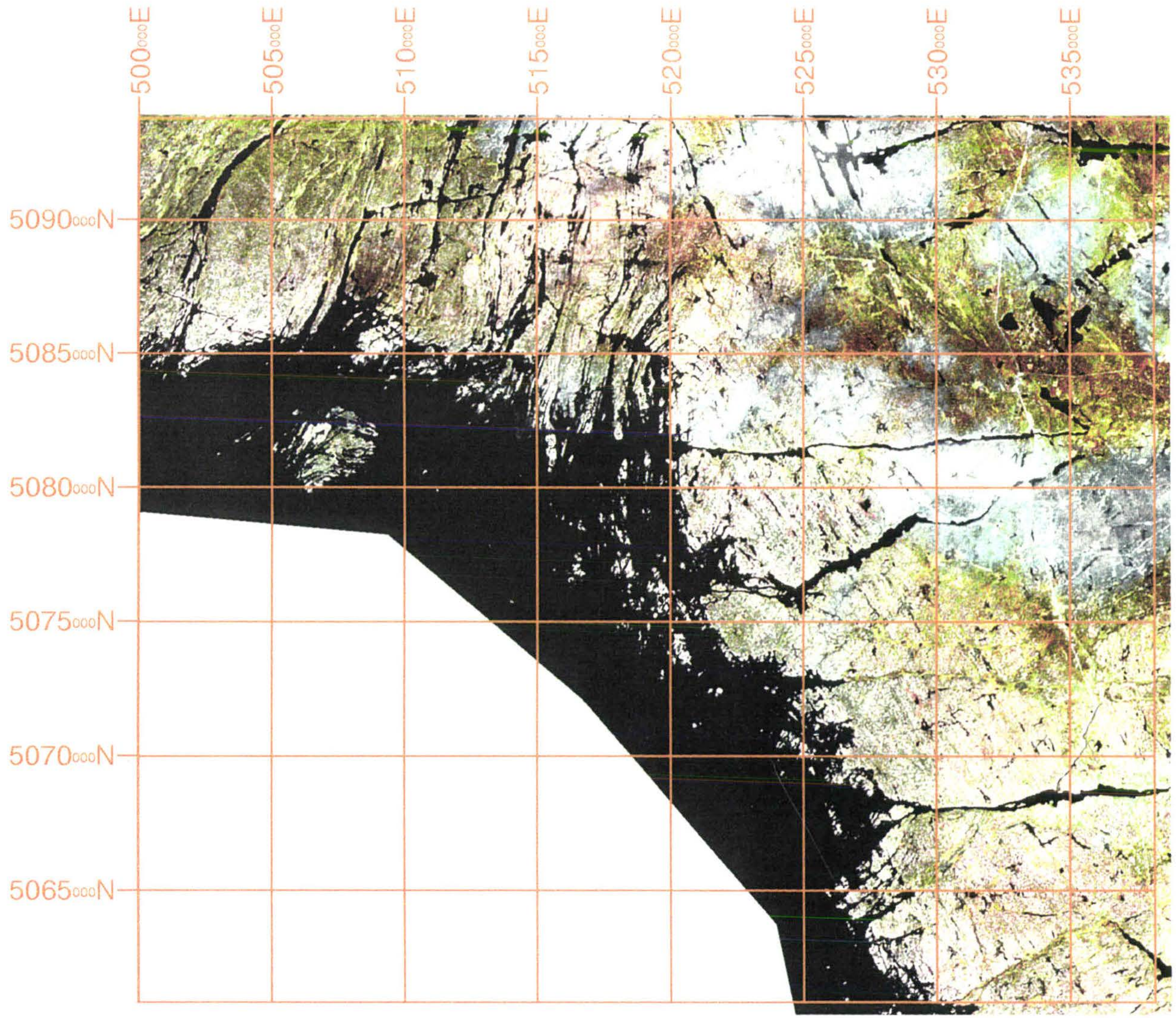


Fig. 5.9. Landsat TM Image of the Key Harbour Area.

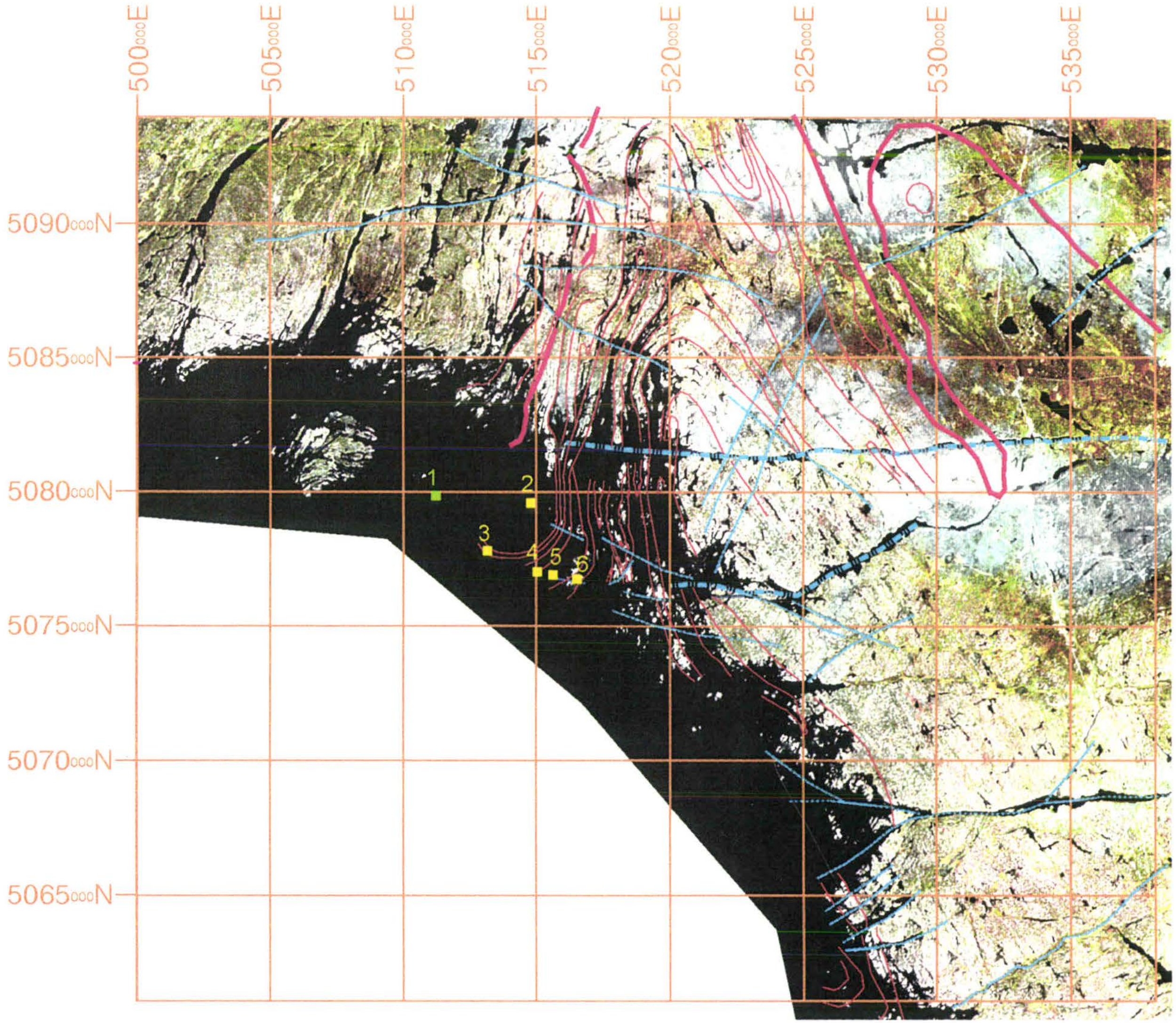


Fig. 5.10. Landsat TM of the Key Harbour area, with lithologies and faults annotated (Culshaw, et. al., 2000). Nd sample locations are shown, with Archean results in green and Paleoproterozoic in yellow.

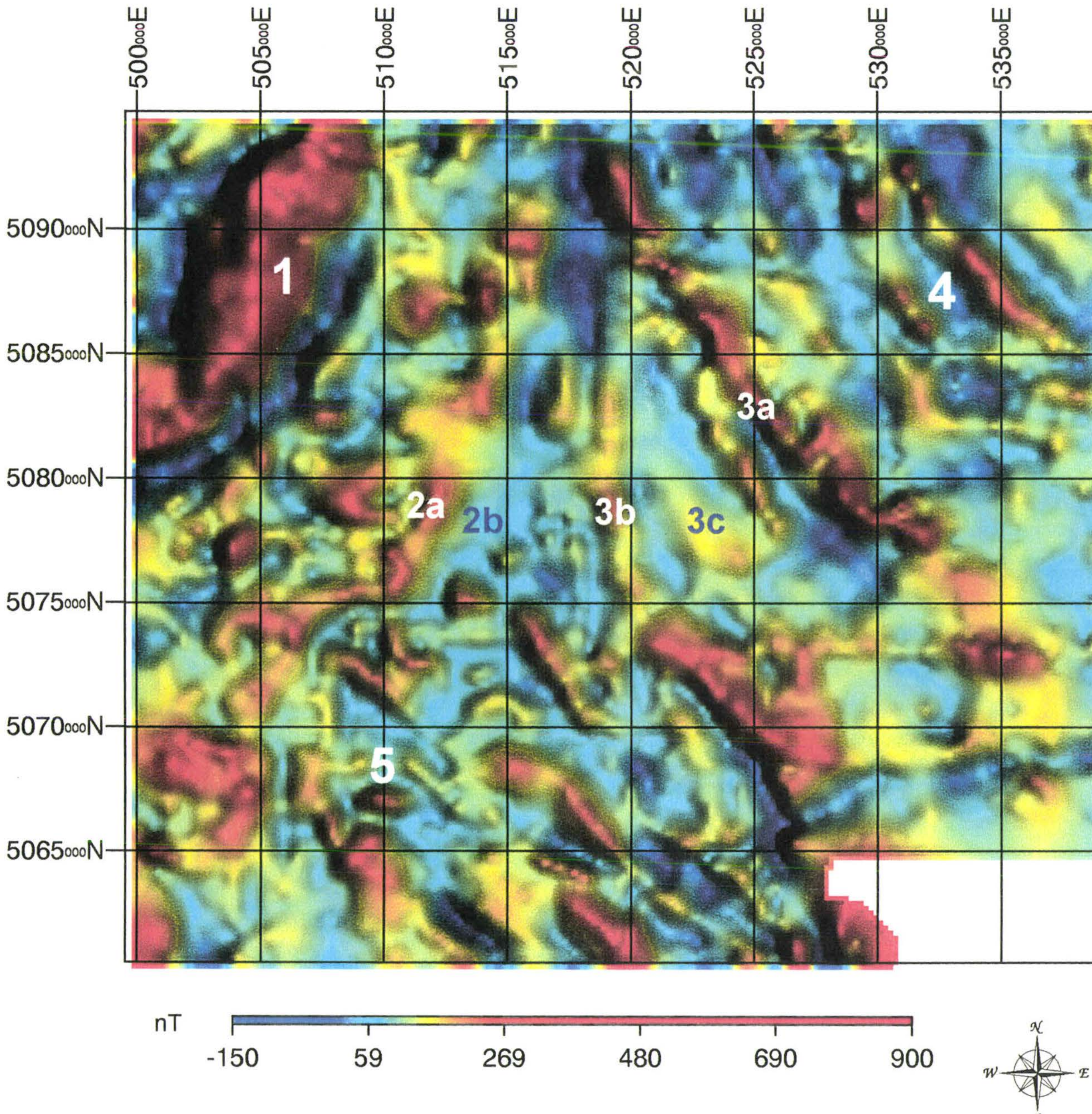


Fig. 5.11. Colour-shaded magnetic map of the Key Harbour Arrea.

granite, due to a high magnetite content. This is not the case. The whole Pickerel Complex is marked by a magnetic low, suggesting that the gabbro-anorthosite's signal is characterized by predominantly remanent magnetizations with a reversed polarity direction. The division between (2a) and (2b) marks the boundary between the Pickerel Complex and the Fox Bay orthogneisses (Davidson and Bethune, 1988). The rocks on either side of this boundary have a visibly different fabric, which means that this is a tectonic boundary. It is evident from the magnetic data that this boundary is broken into steps by various faults as it continues southwest into Georgian Bay. (3a) is a northwest-southeast trending magnetic high. This corresponds with the Key Harbour Leucogranite and (3b) corresponds with the Mann Island granodiorite (Corrigan et. al., 1994). The magnetic lows between these plutons correspond to Key Harbour gneiss association. In between these two magnetic highs lies (3c), a less prominent magnetic high with a northwest-southeast trend, which lies within the fold structure visible in the previous images. This magnetic high is the result of the Britt Pluton (Corrigan et. al., 1994), which is a quartz monzonite orthogneiss. (4) is a folded magnetic high, which is likely produced by similar rock to the Mann Island Pluton. (5) is a large fold structure, easily visible in the magnetic scene. Layers of non-magnetic gneisses and magnetic plutons can be seen within this structure.

The fourth scene, Fig. 5.12., shows the magnetics in a greyscale image. Overlain on this image is the mapped geology, as derived from the Landsat TM (Fig. 5.10.). Additional constraints provided by the magnetics define a large number of faults and some continuation of the lithologies. In this image, previously mapped faults and faults interpreted from the Landsat TM image are shown in light blue, while faults interpreted from the magnetic map are shown in dark blue. The previously mapped lithologic contacts are shown in red, and lithologies interpreted from the magnetics are shown in pink. There are two heavy red lines in this image, marking the margin of the Grenville Front Tectonic Zone and the tectonic boundary described in the previous paragraph. Also of significance in this image is the new interpretation of the geology in the center of the scene, where the samples were collected. This was originally thought to be a primarily folded structure, but the magnetic data has revealed that faulting also plays an important role here. The observed orientation of the gabbro-anorthosite unit in the field is now

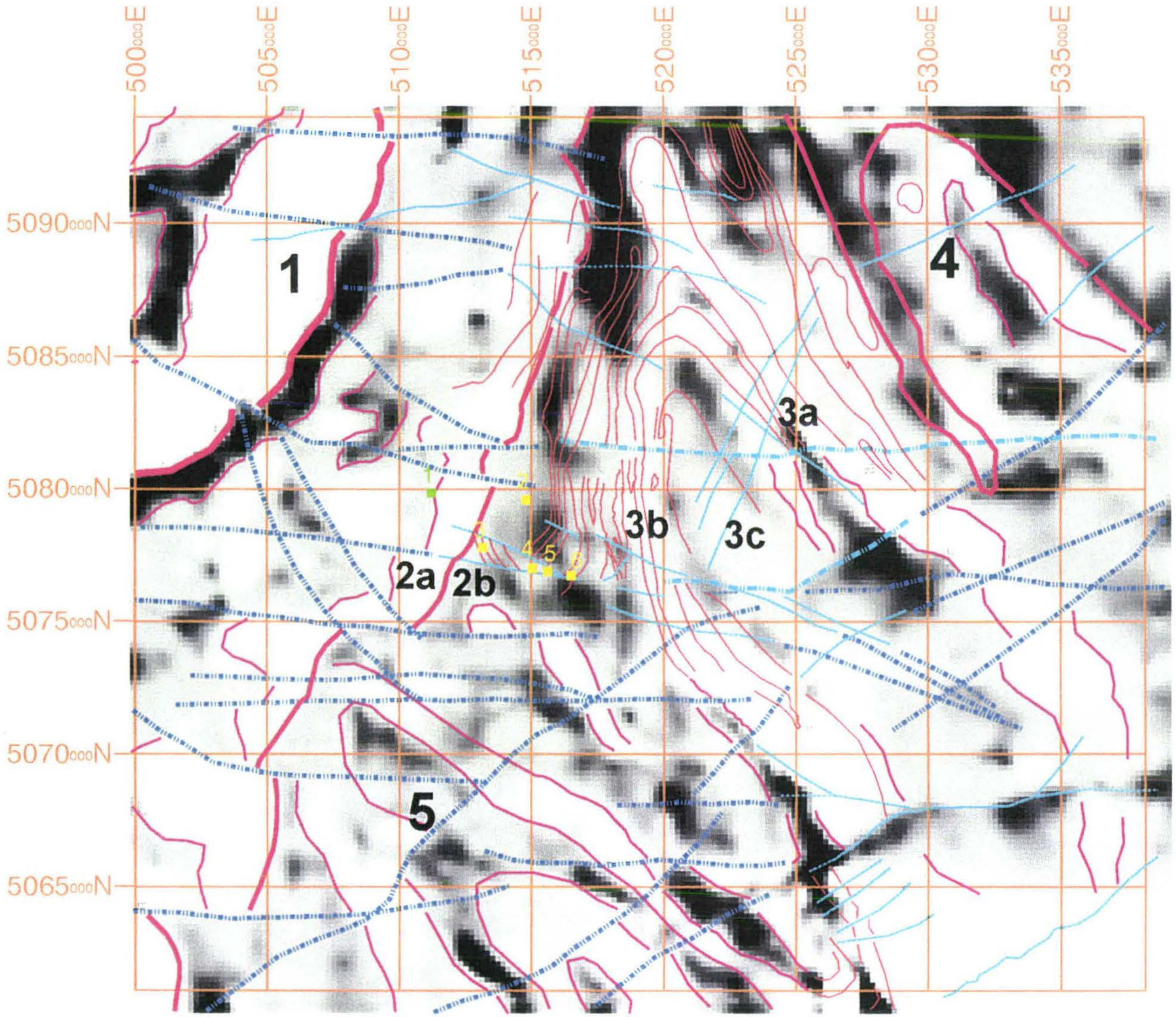


Fig. 5.12. Greyscale magnetic image of the Key Harbour region. Previously mapped lithologies and faults (Culshaw, et. al., 2000) are shown in red & light blue. Lithologies and faults interpreted from the magnetics are shown in pink and dark blue. The feautres described in Fig. 5.11. have been numbered in this image as well.

interpreted as a faulted slice, in which the lithologic beds have been twisted into their current orientation.

### 5.3.3. Extended Field Area

The next stage of the project was to determine if the Penokean Suture could be traced further out into Georgian Bay. A new magnetic scene was selected from the OGS Provincial data set. This scene was processed with the following procedure:

1. Acquire Data: A section was cut out of the OGS Georgian Bay data set. This section was chosen so that the northeastern corner would overlap the southwestern corner of the previous scene.
2. Import into Geosoft Oasis
3. Convert Lat./Long. to UTM coordinates
4. Determine Line-Spacing: The grid cell size of the survey is the same as in the previous scene, ~ 200 $m^2$.
5. Microlevelling: PGW's microlevelling toolkit for Geosoft Oasis was used to do the microlevelling.
6. Reduce-to-Pole: The following values were used - Mag. Dec. = -8.5
   - Mag. Inc. = 64.0
7. Upward Continue: 3 Grids were produced at intervals of 250 m, 500 m, and 750 m. The 500 m grid was selected for continued processing.
8. Grid Subtraction: The 500 m upward continued grid was subtracted from the reduce-to-pole grid to produce the final grid.

The resulting image, Fig. 5.13., is the colour-shaded grid resulting from this process. This scene is dominated by a sharp magnetic contrast, which runs from the northeastern corner to the southwestern corner. This magnetic contrast marks the tectonic boundary dividing the Pickerel Complex and the orthogneiss/supracrustal units identified in Fox Bay and on the Bustard Islands. The Nd model age results suggest that this boundary represents the westernmost location for the Penokean Suture in this region.

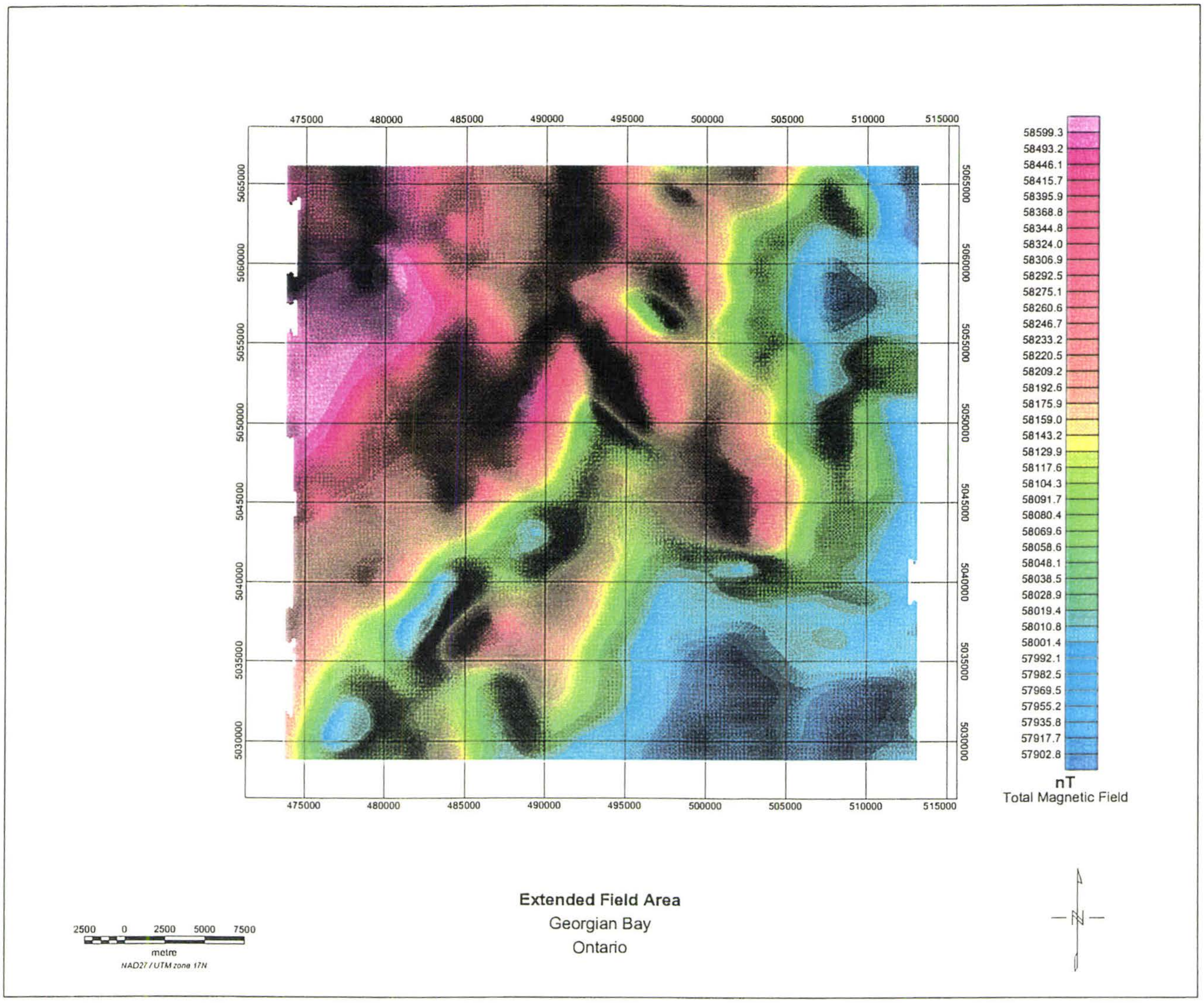


Fig. 5.13. Colour-shaded image of the extended field area to the southwest of the previous scenes..

In the middle of the scene, there is a magnetic high, likely a granitic or granodioritic pluton, which lies in very near proximity to the boundary in question. The prominence of the magnetic contrast in this scene suggests that processing and interpreting further scenes to map this boundary is worthwhile.

5.3.4. Discussion

There were three questions asked at the beginning of this study. The first question was regarding the fold structure in the gneissic sheets west of Key Harbour. As shown in Fig. 5.10., there appears to be more than just a simple folded structure here. Faulting activity has cut and twisted a slice of the basement rock, altering the structure of the fold in the visible outcrop. To truly determine what has occurred here requires a more detailed magnetic survey, since a majority of the outcrop lies beneath the waters of Georgian Bay.

The second question involved using the gabbro-anorthosite unit within the Pickerel Complex to map the regional foliation of the lithologies. Anorthosites have a high magnetite content, which means that they usually produce a high on magnetic maps. The gabbro-anorthosite layer did not produce a strong positive signal, rather it has a large negative magnetic signal. This means that the dominant magnetic signal is thermoremanent magnetization, and that the gabbro-anorthosite cooled during a period in which the Earth's magnetic polarity was reversed. McWilliams and Dunlop (1978) reported reversed polarities in Grenville Front anorthosites and Grenvillian dykes in the French River area. This made it relatively less important in the interpretation of the magnetic map, as several of the other lithologies present exhibited stronger magnetic signatures.

The final question was about the existence of the suture. The Nd model mapping shows that there is a step in the model ages, which defines a boundary. The number of samples collected and studied limits the precision of locating this boundary. Collecting further samples to precisely locate this boundary is problematic because of the Pickerel Complex. This pluton has intruded the area where the boundary should be found. The role that the Pickerel Complex plays in this system is not entirely understood. Dickin

(1998) suggests that it is a stitching pluton relative to the suture and tentatively locates the suture within the Pickerel Complex.

The samples collected and dated extend the proposed location of the Penokean Suture out into Georgian Bay. The Landsat TM images are also very important tools, as they allow the scene to be viewed on a broad scale. One problem with the satellite image is that the lineaments become less clear or even undetectable in some regions. The significance of a lineament visible in the satellite image can only be defined when additional information is applied. Looking at these images, it is clear that there is a change in the geologic fabric. The kilometer-scale fold structures evident in the eastern half of the image, do not exist west of the Pickerel Complex (Fig. 5.10.). Beyond this, the detail in the satellite image is insufficient to describe the boundary.

Looking at the magnetic maps (Fig. 5.11. & Fig. 5.12.), several important features can be observed. Where the Landsat TM images were limited to surficial data, the magnetic data will define structures beneath the surface. The boundary between the Pickerel Complex and the Fox Bay gneiss association truncates the isoclinal folds in the rocks east of it (Fig. 5.14). The rocks of the Fox Bay gneiss association exhibit a totally different fabric, as mentioned above. Therefore, this is probably a Grenvillian thrust boundary. The suture appears to be coincident with this thrust on the western margin of Pickerel Complex. The coarse magnetic survey (flight line spacing of 1 km) does not permit resolution of any detail in the Pickerel Complex. To acquire the required resolution would mean conducting more detailed magnetic surveys (20 m line spacing) as has been done in Lake Simcoe, studying the structures of the Central Metasedimentary Belt Shear Zone (i.e. Pozza, Boyce and Morris, 2001).

With the boundary defined as a Grenvillian tectonic boundary, it follows that the Penokean Suture can not be traced further to the west. There are two possible interpretations of the existence of this tectonic boundary. The first is this boundary marks the eastern margin of the Grenville Front tectonic zone, rather than the shear zone which passes through the French River main outlet. The alternate interpretation is that the rocks of the Fox Bay gneiss association represent a thrust slice (Fig. 15.14.) between the Grenville Front tectonic zone and the Britt Domain. Conducting magnetic surveys with increased sampling density would reveal greater detail about the geology between in this region. Combining the Landsat TM image with known geology maps, isotopic information and magnetic surveys will produce more accurate maps of the geologic structures and tectonic boundaries, enabling a more complete study of the Grenville Province.

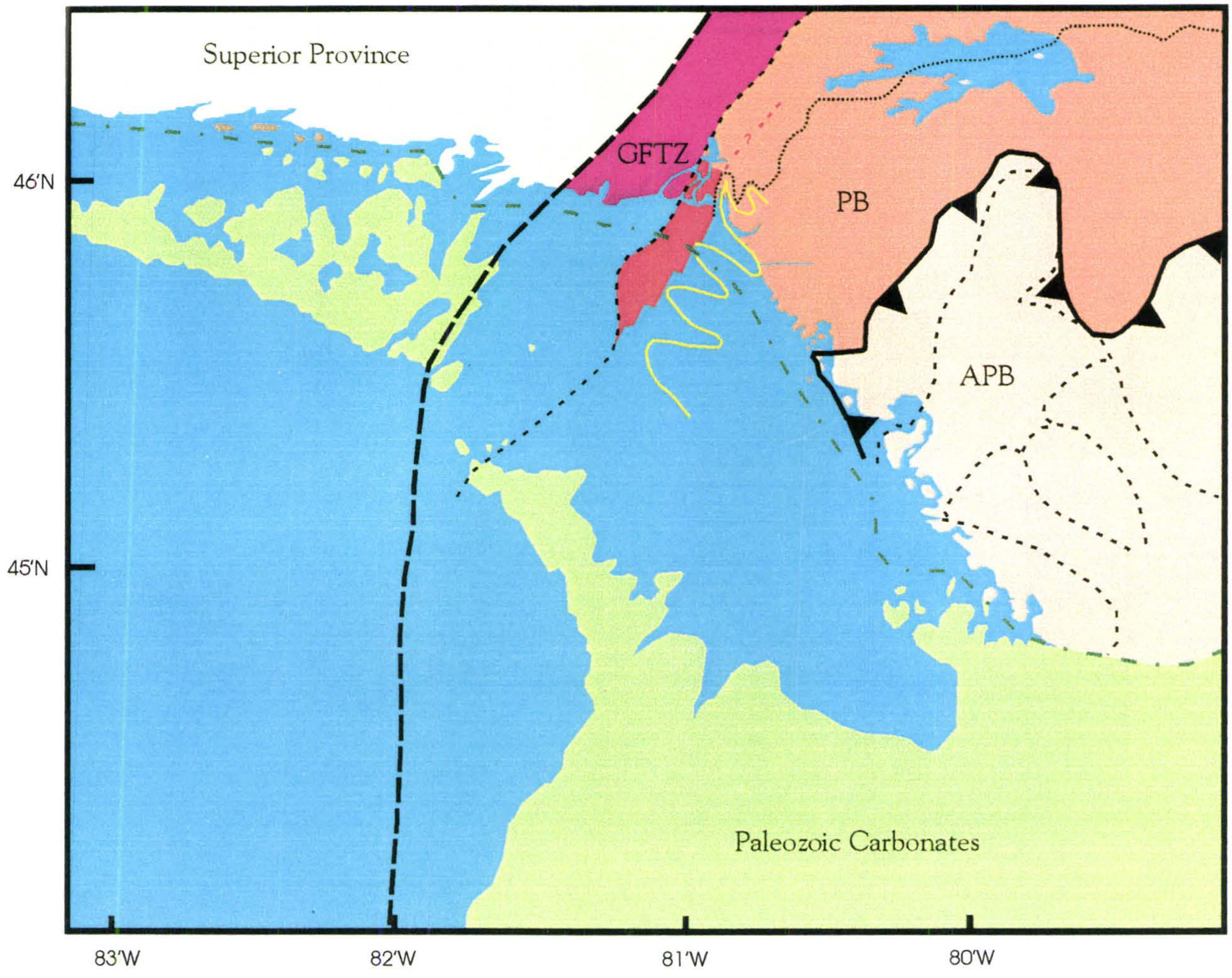


Fig. 5.14. Summary map, modified from White et al. (1994). The major tectonic boundaries of the Central Gneiss Belt are shown, along with the observations from the regional magnetic data, revealing a thrust slice between the parautochthonous belt and the Grenville Front tectonic zone.

# References


Arndt, N.T. & Goldstein, S.L. (1987) Use and abuse of crust-formation ages. Geology, **15**: 893-895.

Bennett, V.C. & DePaolo, D.J. (1987) Proterozoic crustal history of the western United States as determined by neodymium isotopic mapping. Geological Society of America Bullettin, **99**: 674-685.

Bethune, K.M. (1993) Evolution of the Grenville Front in the Tyson Lake area, southwest of Sudbury, Ontario, with emphasis on the tectonic significance of the Sudbury diabase dykes. Ph. D. thesis, Queen's University, Kingston, Ont.

Bethune, K.M. (1997) The Sudbury dyke swarm and its bearing on the tectonic development of the Grenville Front, Ontario, Canada. Precambrian Research, **85**: 117-146.

Bethune, K.M. & Davidson, A. (1997) Grenvillian metamorphism of the Sudbury diabase dyke-swarm: from Protolith to pyroxene-garnet coronite. The Canadian Mineralogist, **35**: 1191-1220.

Chen, Y.D., Krogh, T.E. & Lumbers, S.B. (1995) Neoarchean trondhjemitic and tonalitic orthogneisses identified within the northern Grenville Province in Ontario by precise U-Pb dating and petrologic studies. Precambrian Research, **72**: 263-281.

Condie, K.C., Bobrow, D.J. & Card, K.C. (1987) Geochemistry of Precambrian mafic dykes from the southern Superior Province of the Canadian Shield. *In* Mafic dyke swarms. *Edited by* H.C. Halls & W.F. Fahrig. Geological Association of Canada, Special Paper 34, 95-108.

Corrigan, D., Culshaw, N.G. & Mortensen, J.K. (1994) Pre-Grenvillian evolution and Grenvillian overprinting of the Parautochthonous Belt in Key Harbour, Ontario: U-Pb and field constraints. Canadian Journal of Earth Sciences, **31**: 583-596.

Culshaw, N.G., Davidson, A. & Nadeau, L. (1983) Structural subdivisions of the Grenville Province in the Parry Sound – Algonquin region, Ontario: Current Research, Part B, Geological Survey of Canada, Paper 83-1B, 243-252.

Culshaw, N.G., Corrigan, D., Drage J. & Wallace, P. (1988) Georgian Bay geological Synthesis: Key Harbour to Dillon, Grenville Province of Ontario: Current Research, Part C, Geological Survey of Canada, Paper 88-1C, 129-133.

Culshaw, N.G., Check, G., Corrigan, D., Drage, J., Gower, R., Haggart, M.J., Wallace, P., & Wodicka, N. (1989) Georgian Bay geological Synthesis: Dillon to Twelve Mile Bay, Grenville Province of Ontario: Current Research, Part C, Geological Survey of Canada, Paper 89-1C, 157-163.

Culshaw, N.G., Jamieson, R., Ketchum, J., Reynolds, P.H., Wodicka, N., Heaman, L. & Krogh, T. (1990) History of the Central Gneiss Belt, Grenville Province, along Georgian Bay, Ontario. Lithoprobe Abitibi-Grenville Project, Workshop Report 3. 73-76.

Culshaw, N. & Dostal, J. (1997) Sand Bay gneiss association, Grenville Province, Ontario: a Grenvillian rift- (and –drift) assemblage stranded in the Central Gneiss Belt?: Precambrian Research **85**, 97-113.

Culshaw, N., Ketchum, J.W.F., Wodicka, N. & Wallace, P. (1994) Deep crustal ductile extension following thrusting in the southwestern Grenville Province, Ontario: Canadian Journal of Earth Sciences **31**, 160-175.

Culshaw, N., Jamieson, R.A., Ketchum, J.W.F., Wodicka, N., Corrigan, D. & Reynolds, P.H. (1994) Transect across the northwest Grenville orogen, Georgian Bay, Ontario: polystage convergence and extension in the lower orogenic crust. Tectonics **16**, 966-982.

Culshaw, N.G., et. al. (2000) The Georgian Bay Transect, unpublished??

Davidson, A., Culshaw, N.G. & Nadeau, L. (1982) A tectono-metamorphic framework for part of the Grenville Province: implications for geochronology. Contributions to Mineralogy and Petrology, **100**: 291-299.

Davidson, A. & Grant, S.M. (1986) Reconnaissance geology of western and central Algonquin Park and detailed study of coronitic olivine metagabbro, Central Gneiss Belt, Grenville Province of Ontario. *In* Current research, part B. Geological Survey of Canada, Paper 86-1B, 837-848.

Davidson, A. & Bethune, K.M. (1988) Geology of the north shore of Georgian Bay, Grenville Province, Ontario. *In* Current research, part B. Geological Survey of Canada, Paper 88-1C, 135-144.

Davidson, A. (1995) A review of the Grenville orogen in its North American type area. Australian Geological Survey Organization, Journal of Australian Geology and Geophysics, **16**: 3-24.

Davidson, A. (1996) Geology of Grenville Province. Geological Survey of Canada, Open File 3346, scale 1:2,000,000.

Debon, F. & LeFort, P. (1983) A chemical-mineralogical classification of common plutonic rocks and associations. Trans. Roy. Soc. Edinburgh: Earth Sciences **73**, 135-149.

DePaolo, D.J. (1981) Neodymium isotopes in the Colorado Front Range and crust-mantle evolution in the Proterozoic: Nature **291**, 193-196.

DePaolo, D.J. (1988) Neodymium Isotope Geochemistry: an Introduction, Springer-Verlag, Germany, 187.

Dickin, A.P. (1998) Nd isotope mapping of a cryptic continental suture, Grenville Province of Ontario: Precambrian Research, **91**: 433-444.

Dickin, A.P. & McNutt, R.H. (1989) Nd model age mapping of the southeast margin of the Archean foreland in the Grenville province of Ontario: Geology **17**, 299-302.

Dickin, A.P. & McNutt, R.H. (1990) Nd model age mapping of Grenville lithotectonic domains: mid-Proterozoic crustal evolution in Ontario. *In* Mid-Proterozoic Laurentia-Baltica. *Edited by* C.F. Gower, T. Rivers and B. Ryan. Geological Association of Canada, Special Paper 38, 79-94.

Dickin, A.P., McNutt, R.H. & Clifford, P.M. (1990) A neodymium isotope study of plutons near the Grenville Front in Ontario, Canada: Chemical Geology **83**, 315-324.

Dickin, A.P. (2000) Crustal formation in the Grenville Province – Nd isotope evidence. Canadian Journal of Earth Sciences, **37**: 165-181.

Dickin, A.P. & Guo, A. (2001) The location of the Allochthon Boundary Thrust and the Archean-Proterozoic suture in the Mattawa area of the Grenville Province: Nd isotope evidence. Precambrian Research, in press.

Dudas, F.Ö, Davidson, A. & Bethune, K.M. (1994) Age of Sudbury diabase dykes and their metamorphism in the Grenville Province. *In* Radiogenic age and isotopic studies: Report 8. Geological Survey of Canada, Current Research 1994-F, 97-106.

Easton, R.M. (1986) Geochronology of the Grenville Province in Moore, J.M., Davidson, A. & Baer, A.J. eds., The Grenville Province: Geological Association of Canada Special Paper #31, 127-173.

Easton, R.M. (1988) Regional mapping and stratigraphic studies, Grenville Province with some notes on mineralization. *In* Field work and other activities 1988. Ontario Geological Survey, Misc. Paper 141, 300-308.

Fahrig, W.F., Gaucher, E.H. & Larochelle, A. (1965) Paleomagnetism of diabase dykes of the Canadian Shield. Canadian Journal of Earth Sciences, **2**: 278-298.

Farmer, G.L. & DePaolo, D.J. (1983) Origin of the Mesozoic and Tertiary granite in the western U.S. and implications for pre-Mesozoic crustal structure. I. Nd and Sr isotopic studies in the geocline of the northern Great Basin. Journal of Geophysical Research, **88**: 3379-3401.

Green, A.G., Milkereit, B., Davidson, A., Spencer, C. Hutchinson, D.R., Cannon, W.F., Lee, M.W., Agena, W.F., Behrendt, J.C. & Hinze, W.J. (1988) Crustal structure of the Grenville front end and adjacent terranes. Geology, **16**: 788-792.

Grossman, L. & Larimer, J.W. (1974) Early chemical history of the solar system. Rev. Geophys. Space Phys., **12**: 71-101.

Guo, A. & Dickin, A.P. (1996) The southern limit of Archean crust and significance of rocks with PaleoProterozoic model ages: Nd model age mapping in the Grenville Province of western Quebec. Precambrian Research **77**: 231–241.

Hoffman, P.F. (1989) Speculations on Laurentia's first gigayear (2.0 to 1.0 Ga). Geology, **17**: 135-138.

Holmden, C. & Dickin, A.P. (1995) PaleoProterozoic crustal history of the southwestern Grenville Province: evidence from Nd isotopic mapping. Canadian Journal of Earth Sciences, **32**: 472-485.

Indares, A. & Dunning, G. (1997) Coronitic metagabbro and eclogite from the Grenville Province of western Quebec: interpretation of U-Pb geochronology and metamorphism. Canadian Journal of Earth Sciences, **34**: 891-901.

Jamieson, R.A., Culshaw, N.G., Wodicka, N., Corrigan, D. & Ketchum, J.W.F. (1992) Timing and tectonic setting of Grenvillian metamorphism – constraints from a transect along Georgian Bay, Ontario. Journal of Metamorphic Geology, **10**: 321-332.

Kellet, R.L., Barnes, A.E. & Rive, M. (1994) The deep structure of the Grenville Front: a new perspective from western Quebec. Canadian Journal of Earth Sciences, **31**: 282-292.

Ketchum, J.W.F. (1994) Extensional shear zones and lithotectonic domains in the southwest Grenville orogen: structure, metamorphism, and U-Pb geochronology of the Central Gneiss Belt near Pointe-au-Baril, Ontario. Ph.D. thesis, Dalhousie University, Halifax, N.S.

Ketchum, J.W.F., Culshaw, N.G. & Jamieson, R.A. (1994) Extensional reactivation of the Allochthon Boundary Thrust, southwest Grenville orogen: Geological Association of Canada, program with abstracts, **19**: A56.

Ketchum, J.W.F., Heaman, L.M., Krogh, T.E., Culshaw, N.G. & Jamieson, R.A. (1998) Timing and thermal influence of late orogenic extension in the lower crust: a U-Pb geochronological study from the southwest Grenville orogen, Canada. Precambrian Research, **89**: 25-45.

Ketchum, J.W.F. (1998) U-Pb ages in the Pointe Au Baril Region, pers. com.

Ketchum, J.W.F. & Davidson, A. (2000) Crustal architecture and tectonic assembly of the Central Gneiss Belt, southwestern Grenville Province, Canada: a new interpretation. Canadian Journal of Earth Sciences, **37**: 217-234.

Krogh, T.E., Culshaw, N. & Ketchum, J. (1993) Multiple ages of metamorphism and deformation in the Parry Sound – Pointe au Baril area. Lithoprobe (Abitibi-Grenville Workshop IV) Rept. 33, 39.

Krogh, T.E., Corfu, F., Davis, D.W., Dunning, G.R., Heaman, L.M., Kamo, S.L., Machado, N., Greenhough, J.D. & Nakamura, N. (1987) Precise U-Pb isotopic ages of diabase dykes and mafic to ultramafic rocks using trace amounts of baddeleyite and zircon. *In* Mafic duke swarms. *Edited by* H.C. Halls and W.F. Fahrig. Geological Association of Canada, Special Paper 34, 147-152.

Lumbers, S.B. (1975) Geology of the Burwash area, District of Nipissing, Sudbury and Parry Sound. Ontario Division of Mines, Report 116.

Martin, C. (1992) Mid-proterozoic evolution of the Grenville Belt: evidence from neodymium isotopic mapping, Bancroft, Ontario: unpublished thesis, McMaster University.

Martignole, J. & Calvert, A.J. (1996) Crustal-scale shortening and extension across the Grenville Province of western Quebec. Tectonics, **15**: 376-386.

McCulloch, M.T. & Wasserburg, G.J. (1978) Sm-Nd and Rb-Sr chronology of the continental crust formation. Science, **200**: 1003-1011.

McWilliams, M.O. & Dunlop, D.J. (1978) Grenville paleomagnetism and tectonics. Canadian Journal of Earth Sciences, **15**: 687-695.

Milkerit, B., Forsyth, D.A., Green, A.G., Davidson, A., Hutchinson, D.R., Hinze, W.J., & Mereu, R.F. (1992) Seismic images of a Grenvillian terrane boudnary. Geology **20**, 1027-1030.

Minty, B.R.S. (1991) Simple micro-levelling for aeromagnetic data. Exploration Geophysics, **22**: 591-592.

Needham, T.W. (1992) The metamorphic evolution of the Frederick Inlet metagabbros, southwestern Grenville Province, Ontario, Canada. M.Sc. thesis, Queen's Univeristy, Kingston, Ont.

Nelson, B.K. & DePaolo, D.J. (1985) Rapid production of continental crust 1.7-1.9 b.y. ago: Nd isotope evidence from the basement of the North American mid-continent. Geological Society of America Bulletin, **96**: 746-754.

Patchett, P.J. & Bridgewater, D. (1984) Origin of the continental crust 1.9-1.7 Ga age defined by Nd isotopes of the Ketilidian terrane of South Greenland. Contributions to Mineralogy and Petrology, **87**: 311-318.

Pozza, M., Boyce, J. & Morris, W.A.M. (2000) Mapping terrane boundaries using high resolution lake-based magnetic surveys and satellite imagery. CRESTech Sept., 2000.

Rivers, T., Martignole, J., Gower, C.F. & Davidson, A. (1989) New tectonic divisions of the Grenville Province, southeast Canadian Shield: Tectonics **8**, 63-84.

Schulz, K.J. (1987) An early Proterozoic ophiolite in the Penokean orogeny [abstract]. Geological Association of Canada, program with abstracts, **12**: 87.

Schwerdtner, W.M. (1987) Interplay between folding and ductile shearing in the Proterozoic crust of the Muskoka – Parry Sound region, central Ontario. Canadian Journal of Earth Sciences, **24**: 1507-1525.

Sims, P.K. & Peterman, Z.E. (1983) Evolution of the Penokean foldbelt, Lake Superior region, and its tectonic environment, in Medaris, L.G., Jr. ed, Early Proterozoic geology of the Great Lakes region. Geological Society of America Memoir, **160**: 3-14.

Thirlwall, M.F. (1982) A triple filament method for rapid and precise analysis of rare-earth elements by isotope dilution. Chemical Geology, **35**: 155-166.

van Breeman, O., Davidson, A., Loveridge, W.D. & Sullivan, R.W. (1986) U/Pb zircon Geochronology of Grenville tectonites, granulites and igneous precursors, Parry Sound, Ontario in Moore, J.M., Davidson, A. & Baer, A.J., eds., The Grenville Province: Geological Association of Canada Special Paper #31, 191-207.

van Schmus, W.R. (1980) Chronology of igneous rocks associated with the Penokean orogeny in Wisconsin. Geological Society of America Special Paper 182, 159-168.

van Schums, W.R. & Bickford, M.E. (1981) Proterozoic chronology and evolution of the midcontinent region, North America. *In* Precambrian Plate Tectonics *Edited by* Kroner, A.: Elsevier Scientific Publishing Company, Amsterdam, 261-296.

White, D.J., Easton, R.M., Culshaw, N.G. Milkereit, B., Forsyth, D.A., Carr, S., Green, A.G. & Davidson, A. (1994) Seismic images of the Grenville Orogen in Ontario: Canadian Journal of Earth Sciences **31**, 293-307.

Wodicka, N., Parrish, R.R. & Jamieson, R.A. (1996) The Parry Sound domain: a far-travelled allochthon? New evidence from the U-Pb zircon geochronology. Canadian Journal of Earth Sciences, **33**: 1087-1104.

Zolnai, A.I., Price, R.A. & Helmsteadt, H. (1984) Regional cross section of the Southern Province adjacent to Lake Huron, Ontario: Implications for the tectonic significance of the Murray fault zone. Canadian Journal of Earth Sciences, **21**: 447-456.

# Appendix A:

## Analytical Methods:

### A1.0. Introduction

The analytical procedures for Sm/Nd geochronology are divided into 3 majour components. The first is sample collecting and crushing, the second is dissolution and column chromatography, and the last is mass spectrometry. The dissolution and column chromatography can be broken up into several stages: weighing and dissolution, splitting and spiking, cation exchange chromatography, and REE chromatography. Each of these procedures will be described below.

### A1.1. Rock Sampling & Crushing

The samples collected in the field would range between 5 to 10 kg of rock. In Field Areas 1 and 2, the sampling was done primarily by boat. Most of the samples were taken near to the shoreline, as a combination of wave action and higher water levels in previous years have protected the rocks from chemical weathering. Several samples in Field Area 1 and all the samples in Field Area 3 were collected from roadside outcrop. The outer surface of a sample is removed and then care is taken to prevent contamination with organic materials and local soil. The locations of the samples were pinpointed as accurately as possible on the 1:50000 Ontario Topographic Maps. The locations are reported as UTM Grid References in the Sm/Nd data tables and are accurate to ± 100 m.

In the rock-crushing lab, a sledgehammer is used to break the samples down to 1 or 2 kg pieces. These are then broken down further (~ 5 cm x 5 cm pieces) with a hydraulic splitter. A mechanical chipmunk jaw crusher is used to crush these pieces to < 1 cm sized gravel. After thorough cleaning of the jaw crusher, pre-contamination with some of the sample is standard to avoid contamination from the previous sample. The gravel is then split and homogenized by passing it through a tabletop sample divider several times. Once splitting is complete, 100 to 200 ml of the gravel is loaded into a tungsten carbide disc mill, which is then placed in a shatterbox. This is run for 2 to 5 minutes to produce a fine sand. Half of the sand is discarded, while the other half is pulverized further. This procedure ensures that the final powder will be representative of a large sample of crushed rock.

The sample is pulverized in the shatterbox for 5 to 10 minutes, producing a powder of approximately 300-mesh size. This results in 80 to 100 ml of fine powder, which is poured into a clean 125-ml glass container, then labeled and stored until the dissolution process begins.

Between each sample preparation, all the equipment and surfaces in the rock-crushing lab are cleaned meticulously with a vacuum, disposable paper towels and kimwipes. Prior to vacuuming and wiping, the jaw crusher is dismantled and its surfaces are scrubbed with a steel brush. The tabletop sample divider is blown clean with an air hose, ensuring that no dust remains in the chutes. In the case that the disc mill can not be completely cleaned, then 30 to 40 ml of pure quartz sand is added to the disc mill and it is run for several minutes, until the remaining sample grit is ground off. Throughout the procedure, latex gloves are worn to prevent dust-attracting skin oils from being deposited on any of the equipment. An air filtration system is used to minimize the amount of air-borne particles in the rock-crushing lab.

### A1.2. Weighing & Dissolution

When the sample powders are taken into the "Clean Lab", they undergo a series of processes to remove the unwanted elements, leaving only the Sm and Nd. Teflon bombs are selected and labeled with the appropriate sample numbers. The bombs are de-ionized to remove static charge, then weighed. They are weighed a second time, and subjected to further de-ionization if the weight results differ by more than 0.0002 g. Once the static is sufficiently removed, the balanced is tared at the bomb's mass. Then sample powder is carefully placed in the Teflon bomb and weighed. The objective is to have between 70 and 150 mg of sample powder. After this, 10 ml of concentrated HF acid (48%) is added to each bomb. The bombs are tightly sealed, placed in Teflon safety jackets and left in an oven at 140°C for 3 days.

After 3 days in the oven, the bombs are removed. They Teflon jackets are loosened and left to cool for several hours. The bombs are then opened and placed on a hot plate, in a laminar fumehood, allowing the HF acid to slowly evaporate. Once they are dry, 5 ml of concentrated $HNO_3$ (16M) was added to the bombs and evaporated off on the hot plates. When this was complete, 5 ml of 6M HCl is added to the bombs. They are once again placed within the Teflon safety jackets and returned to the oven overnight. The following day, the samples are removed from the oven and left to cool. Once cool, they are diluted with approximately 5 ml of milli-Q water. If no undissolved residue can be detected, the samples are ready for splitting and spiking.

A1.3. Splitting & Spiking

The mass of each bomb must be measured and recorded to begin this stage of the sample preparation. The solutions are divided in two, with approximately half being poured into an appropriately labeled 15 ml Teflon container and the bombs are reweighed. Approximately 5 drops of a REE spike enriched in $^{149}Sm$ and $^{150}Nd$ are added to the solution in the 15-ml containers. The weight of the spike added to each sample is determined by taring the balance with the spike solution on it prior to adding the 5 drops. This procedure is concluded by evaporating the samples in both the bombs and the beakers, then rediluting them in 2 ml of 2.5M HCl acid. A pre-determined mixture of and quantity of Sm and Nd isotopes are added to the unknown mixture of Sm and Nd. This is known as Isotope Dilution.

A1.4. Cation Exchange Chromatography

Prior to loading the samples in the cation columns, they are transferred to test-tubes and centrifuged for 10 minutes. From the test tubes, 1 ml of the 2.5M HCl sample is loaded into the cation column, while the remaining sample is saved in the case that a test tube repeat is necessary. The cation columns are 0.5 cm in diameter and each one contains approximately 18 cm of Dowex Bio-Rad Ag 50W (200 – 400 mesh) resin. Through a series of washes and elutions, 46 ml of 2.5M HCl passes through the polystyrene sulphionic acid resin. This is followed by eluting a total of 30 ml of 2M $HNO_3$ through the column. This procedure removes major elements such as Na, K, Ca and Ba before the REE's are collected in 14 ml of 7.5M $HNO_3$ acid. The cation columns must be cleaned before they are used. This requires eluting them with 10 ml of milli-Q water to neutralize the acid used to collect the REE. This is followed by 60 ml of HCl, which removes any substance left behind by the previous sample. Finally, 30 ml of 2.5M HCl acid is eluted through the columns, to condition them for the next sample introduction. While the columns are being cleaned, the bulk REE separates are placed under the heat lamps, evaporating off the nitric acid. They are redissolved in 1 ml of 0.2M HCl acid to await the REE chromatography procedure.

## A1.5. REE Chromatography

The "Reverse Phase Method" separates the Rare Earth Elements by running them through quartz columns containing a hexyl di-ethyl hydrogen phosphate resin, which is coated on small Teflon beads. The light REE (Nd) is collected prior to the heavier REE (Sm) when employing this method. Three different solutions are collected during this process. The unspiked Nd solution is used for the Nd isotope ratio determination. The other two solutions are derived from the spiked sample. Both the spiked Nd solution and the spiked Sm solution are used for isotope dilution.

The samples are loaded in a 1-ml mix of 0.2M HCl. Several elutions of 0.2M HCl are used to remove the unwanted REE. For the isotope ratio (IR) determination, there are 2 elutions prior to collecting the sample. The isotope dilution (ID) follows the same procedure. The Nd ID is collected at the same point as the Nd IR, then an elution of 0.5M HCl is applied. Following this, the Sm ID is collected in 0.5M HCl. All three solutions are then evaporated down and 2 drops of 3M $HNO_3$ with 1.3% $H_3PO_4$ is added. The samples are partially evaporated after this, leaving them in just a minute amount of phosphoric acid.

The REE columns are clean with 60 ml of 6M HCl. After that, between 25 and 30 ml of 0.2M HCl acid is eluted through to prepare the resin for the isotope solutions.

## A1.6. Mass Spectrometry

The samples are loaded onto glass beads with a Tantalum side-filament and a Rhenium center-filament. Prior to loading the samples the filaments are welded on to the filaments posts, then the beads and filaments are outgassed under a vacuum. A complete account of this procedure can be found in Thirlwall (1982). When the beads are ready, the samples are dissolved in approximately 0.3 μl of 0.3M $H_3PO_4$ acid. The acid-sample solution is loaded on the tantalum filaments, then heated with 2.0 – 2.5 amps to dry the sample on the filament.

The Sm-Nd isotope ratios are then measured using a VG 354 thermal ionization, solid source mass spectrometer. A 4-collector peak-switching program was employed. Before any analysis can be run, the mass spectrometer source must be pumped down to a pressure less than $2x10^{-7}$ millibars. The Nd isotope ratios are normalized against the $^{146}Nd/^{144}Nd$ ratio of 0.7219. During the year that these samples were measured, 29 runs of the La Jolla standard produced an average value of 0.511863 ± 0.000019 (2σ, population), which is within error of the recommended value of 0.511850. Average within-run precision (standard error) of samples was ± 0.012 (1σ). Sm and Nd amounts and $^{147}Sm/^{144}Nd$ ratios were determined by isotope dilution analysis in the single collector mode. On the basis of duplicate analyses of dissolutions, model ages are reproducible on average to ± 20 Ma (2σ).

**Table A1.1 La Jolla Standard Analyses ($^{143}Nd/^{144}Nd$, March – December, 1999)**

| | $^{143}Nd/^{144}Nd$ | Standard Error (/mil. 1) | | $^{143}Nd/^{144}Nd$ | Standard Error (/mil. 1) |
|---|---|---|---|---|---|
| 1. | 0.511844* | 0.009 | 16. | 0.511878* | 0.014 |
| 2. | 0.511856* | 0.011 | 17. | 0.511844* | 0.012 |
| 3. | 0.511851* | 0.011 | 18. | 0.511886* | 0.012 |
| 4. | 0.511835* | 0.011 | 19. | 0.511848 | 0.012 |
| 5. | 0.511863 | 0.011 | 20. | 0.511841 | 0.011 |
| 6. | 0.511874 | 0.009 | 21. | 0.511873 | 0.011 |
| 7. | 0.511855 | 0.010 | 22. | 0.511862* | 0.027 |
| 8. | 0.511866 | 0.010 | 23. | 0.511874* | 0.013 |
| 9. | 0.511861 | 0.009 | 24. | 0.511865 | 0.014 |
| 10. | 0.511867 | 0.011 | 25. | 0.511869* | 0.013 |
| 11. | 0.511864 | 0.014 | 26. | 0.511890 | 0.012 |
| 12. | 0.511885* | 0.011 | 27. | 0.511858 | 0.009 |
| 13. | 0.511864* | 0.010 | 28. | 0.511868 | 0.009 |
| 14. | 0.511894 | 0.011 | 29. | 0.511870 | 0.011 |
| 15. | 0.511828* | 0.011 | | | |

Average value of all 29 $^{143}Nd/^{144}Nd$ ratios: 0.511863 ± 0.000019 (2σ, population).
*Average value of all 13 $^{143}Nd/^{144}Nd$ ratios from this study: 0.511860 ± 0.000019 (2σ, population).

Table B1. Major Element Analysis for Britt Domain Samples in Chapter 3.

| SAMPLE | PB1 | PB2 | PB5 | SH2 | SH4 | SH6 | SH9A | SH11 | SH12 |
|---|---|---|---|---|---|---|---|---|---|
| $SiO_2$% | 66.20 | 65.54 | 66.79 | 55.59 | 65.13 | 63.46 | 73.06 | 75.71 | 71.86 |
| $Al_2O_3$% | 16.01 | 15.73 | 15.78 | 15.47 | 15.62 | 15.94 | 14.34 | 13.05 | 14.07 |
| $Fe_2O_3$% | 3.43 | 4.62 | 3.92 | 9.75 | 4.04 | 4.60 | 1.56 | 1.14 | 2.64 |
| MnO% | 0.073 | 0.095 | 0.091 | 0.195 | 0.079 | 0.096 | 0.038 | 0.065 | 0.076 |
| MgO% | 1.60 | 1.64 | 1.54 | 3.42 | 1.69 | 2.37 | 0.43 | 0.19 | 0.82 |
| CaO% | 3.97 | 3.17 | 3.25 | 5.94 | 3.55 | 4.30 | 1.79 | 0.62 | 1.87 |
| $Na_2O$% | 3.92 | 3.48 | 4.07 | 3.72 | 3.30 | 3.17 | 3.35 | 2.99 | 3.35 |
| $K_2O$% | 2.94 | 3.92 | 3.02 | 2.20 | 4.07 | 3.62 | 4.98 | 6.16 | 4.79 |
| $TiO_2$% | 0.408 | 0.593 | 0.506 | 1.369 | 0.479 | 0.497 | 0.340 | 0.202 | 0.414 |
| Total: | 98.55 | 98.79 | 98.97 | 97.65 | 97.96 | 98.05 | 99.89 | 100.13 | 99.89 |
| $Na_2O/K_2O$ | 2.0 | 1.3 | 2.0 | 2.6 | 1.2 | 1.3 | 1.0 | 0.7 | 1.1 |
| Q | 132 | 131 | 137 | 71 | 127 | 122 | 171 | 186 | 167 |
| P | -135 | -85 | -125 | -179 | -83 | -102 | -34 | 24 | -40 |

| SAMPLE | SH14 | SH21/R | SH24 | SH35 | SH43 | SH46 | SH47 | SH48 | SI5 |
|---|---|---|---|---|---|---|---|---|---|
| $SiO_2$% | 63.52 | 52.29 | 78.06 | 70.79 | 61.51 | 56.04 | 75.46 | 65.40 | 65.92 |
| $Al_2O_3$% | 19.00 | 17.81 | 11.87 | 15.08 | 16.76 | 17.46 | 13.04 | 15.75 | 15.91 |
| $Fe_2O_3$% | 2.92 | 10.97 | 0.85 | 2.19 | 7.12 | 9.11 | 1.83 | 4.11 | 5.36 |
| MnO% | 0.080 | 0.177 | 0.041 | 0.119 | 0.106 | 0.269 | 0.012 | 0.107 | 0.082 |
| MgO% | 1.54 | 4.06 | 0.11 | 0.53 | 2.02 | 2.48 | 0.25 | 1.59 | 1.54 |
| CaO% | 5.36 | 7.35 | 0.42 | 1.59 | 3.39 | 4.76 | 0.13 | 2.97 | 3.85 |
| $Na_2O$% | 4.93 | 3.20 | 2.50 | 2.74 | 4.69 | 5.16 | 2.68 | 4.51 | 3.48 |
| $K_2O$% | 2.35 | 1.90 | 6.16 | 6.51 | 2.99 | 2.89 | 6.47 | 3.85 | 2.88 |
| $TiO_2$% | 0.235 | 1.342 | 0.165 | 0.513 | 1.148 | 1.410 | 0.330 | 0.528 | 0.629 |
| Total: | 99.94 | 99.10 | 100.18 | 100.06 | 99.73 | 99.58 | 100.20 | 98.82 | 99.65 |
| $Na_2O/K_2O$ | 3.2 | 2.6 | 0.6 | 0.6 | 2.4 | 2.7 | 0.6 | 1.8 | 1.8 |
| Q | 80 | 59 | 217 | 147 | 86 | 27 | 194 | 101 | 147 |
| P | -205 | -194 | 43 | 22 | -148 | -190 | 49 | -117 | -120 |

Table B2. Major Element Analysis for Shawanaga Domain Samples in Chapter 3.

| SAMPLE | DI1 | DI2 | DI3 | FI1 | FI4 | FI7 | FI8 | OB1 | OB3 | SH8 | SH10 |
|---|---|---|---|---|---|---|---|---|---|---|---|
| $SiO_2$% | 55.55 | 68.40 | 68.38 | 65.29 | 63.14 | 58.58 | 59.65 | 69.47 | 70.27 | 59.32 | 47.86 |
| $Al_2O_3$% | 16.56 | 15.79 | 15.68 | 15.93 | 17.77 | 19.91 | 17.10 | 14.35 | 14.67 | 17.44 | 27.89 |
| $Fe_2O_3$% | 9.61 | 3.50 | 3.39 | 3.94 | 3.92 | 4.94 | 6.40 | 3.19 | 2.69 | 5.80 | 3.89 |
| MnO% | 0.244 | 0.065 | 0.046 | 0.061 | 0.063 | 0.073 | 0.111 | 0.065 | 0.049 | 0.102 | 0.058 |
| MgO% | 5.46 | 1.46 | 1.57 | 1.70 | 1.03 | 2.35 | 2.49 | 1.84 | 1.00 | 3.67 | 2.30 |
| CaO% | 1.65 | 3.06 | 2.97 | 2.91 | 3.89 | 7.98 | 4.98 | 1.96 | 1.83 | 6.62 | 10.51 |
| $Na_2O$% | 4.95 | 3.95 | 4.71 | 4.05 | 3.96 | 4.84 | 4.02 | 4.55 | 4.02 | 3.89 | 2.78 |
| $K_2O$% | 3.32 | 3.12 | 2.32 | 3.65 | 4.36 | 0.78 | 3.51 | 2.80 | 4.12 | 1.47 | 2.54 |
| $TiO_2$% | 1.163 | 0.516 | 0.523 | 0.541 | 0.532 | 0.436 | 0.836 | 0.532 | 0.442 | 0.408 | 0.309 |
| Total: | 98.51 | 99.86 | 99.59 | 98.07 | 98.67 | 99.89 | 99.10 | 98.76 | 99.09 | 98.72 | 98.14 |
| $Na_20/K_2O$ | 2.3 | 1.9 | 3.1 | 1.7 | 1.4 | 9.4 | 1.7 | 2.5 | 1.5 | 4.0 | 1.7 |
| Q | 59 | 150 | 143 | 120 | 84 | 58 | 68 | 156 | 151 | 94 | -3 |
| P | -119 | -116 | -156 | -105 | -104 | -282 | -144 | -122 | -75 | -212 | -223 |

| SAMPLE | SH18 | SH20 | SH34 | SH40 | SH44 | SH45 | SI2 | SI3 | SI7 | SI8 | SI9 |
|---|---|---|---|---|---|---|---|---|---|---|---|
| $SiO_2$% | 65.41 | 73.92 | 70.28 | 60.19 | 64.78 | 52.01 | 57.54 | 56.19 | 65.77 | 64.78 | 70.65 |
| $Al_2O_3$% | 16.14 | 14.10 | 13.53 | 20.60 | 16.45 | 16.90 | 17.69 | 18.30 | 16.68 | 15.56 | 14.71 |
| $Fe_2O_3$% | 4.14 | 1.73 | 4.48 | 3.80 | 4.38 | 10.68 | 6.11 | 6.74 | 3.95 | 4.23 | 2.82 |
| MnO% | 0.065 | 0.033 | 0.076 | 0.058 | 0.104 | 0.158 | 0.117 | 0.118 | 0.058 | 0.066 | 0.050 |
| MgO% | 1.91 | 0.33 | 0.84 | 1.58 | 1.06 | 3.75 | 2.77 | 2.57 | 1.05 | 1.96 | 0.83 |
| CaO% | 3.76 | 1.16 | 1.92 | 7.20 | 2.78 | 6.81 | 5.67 | 5.78 | 3.38 | 3.29 | 1.92 |
| $Na_2O$% | 4.40 | 3.47 | 2.83 | 5.33 | 4.52 | 3.96 | 4.29 | 4.10 | 3.55 | 3.97 | 3.61 |
| $K_2O$% | 3.11 | 5.31 | 5.38 | 0.75 | 4.11 | 2.13 | 2.90 | 3.07 | 4.55 | 4.19 | 4.92 |
| $TiO_2$% | 0.570 | 0.230 | 0.616 | 0.354 | 0.547 | 1.647 | 0.912 | 1.039 | 0.481 | 0.557 | 0.422 |
| Total: | 99.51 | 100.28 | 99.95 | 99.86 | 98.73 | 98.05 | 98.00 | 97.91 | 99.47 | 98.60 | 99.93 |
| $Na_20/K_2O$ | 2.1 | 1.0 | 0.8 | 10.8 | 1.7 | 2.8 | 2.2 | 2.0 | 1.2 | 1.4 | 1.1 |
| Q | 111 | 172 | 162 | 61 | 94 | 35 | 52 | 46 | 114 | 104 | 149 |
| P | -143 | -20 | -11 | -285 | -108 | -204 | -178 | -170 | -78 | -98 | -46 |

Table B3. Major Element Analysis for Plutonic Samples & Samples with mixed model ages in Chapter 3

| SAMPLE | GI2 | GF117 | GF118.5 | SH1 | SH3 | SH5* | SH7 | SH9B | SH13 | SH19 |
|---|---|---|---|---|---|---|---|---|---|---|
| $SiO_2$% | 68.83 | 62.34 | 60.77 | 65.45 | 61.92 | 70.70 | 63.30 | 62.49 | 61.23 | 64.98 |
| $Al_2O_3$% | 14.14 | 17.60 | 18.31 | 13.72 | 13.81 | 17.42 | 14.57 | 14.49 | 14.34 | 17.15 |
| $Fe_2O_3$% | 3.61 | 4.48 | 5.57 | 7.45 | 8.37 | 0.90 | 6.76 | 7.76 | 9.41 | 3.58 |
| MnO% | 0.078 | 0.063 | 0.093 | 0.130 | 0.157 | 0.016 | 0.123 | 0.147 | 0.173 | 0.072 |
| MgO% | 0.79 | 2.66 | 1.52 | 1.00 | 1.60 | 0.47 | 1.27 | 1.98 | 1.90 | 0.94 |
| CaO% | 2.33 | 4.00 | 4.75 | 3.07 | 3.78 | 3.39 | 3.60 | 3.11 | 4.06 | 3.51 |
| $Na_2O$% | 2.58 | 4.19 | 4.18 | 3.13 | 3.03 | 5.53 | 3.52 | 3.00 | 3.03 | 3.55 |
| $K_2O$% | 5.70 | 2.76 | 3.49 | 4.34 | 4.08 | 1.57 | 4.42 | 4.04 | 3.34 | 4.53 |
| $TiO_2$% | 0.715 | 0.793 | 0.623 | 1.013 | 1.372 | 0.107 | 1.168 | 1.417 | 1.610 | 0.491 |
| Total: | 98.77 | 98.89 | 99.31 | 99.30 | 98.12 | 100.10 | 98.73 | 98.43 | 99.09 | 98.80 |
| $Na_20/K_2O$ | 0.7 | 2.3 | 1.8 | 1.1 | 1.1 | 5.3 | 1.2 | 1.1 | 1.4 | 1.2 |
| Q | 150 | 105 | 72 | 134 | 114 | 141 | 101 | 127 | 123 | 108 |
| P | -4 | -148 | -145 | -63 | -78 | -206 | -84 | -66 | -99 | -81 |

| SAMPLE | SH22 | SH23 | SH30 | SH31 | SH32 | SH49* | SI4 /R | SI6 |
|---|---|---|---|---|---|---|---|---|
| $SiO_2$% | 69.56 | 74.20 | 67.16 | 66.28 | 59.07 | 68.89 | 75.01 | 66.15 |
| $Al_2O_3$% | 14.48 | 13.28 | 15.37 | 13.65 | 17.92 | 15.29 | 12.74 | 13.88 |
| $Fe_2O_3$% | 4.37 | 1.81 | 4.74 | 7.39 | 7.09 | 3.49 | 1.85 | 6.93 |
| MnO% | 0.069 | 0.048 | 0.127 | 0.125 | 0.119 | 0.054 | 0.022 | 0.131 |
| MgO% | 1.32 | 0.40 | 1.52 | 0.96 | 1.95 | 1.67 | 0.42 | 0.98 |
| CaO% | 2.20 | 1.22 | 3.18 | 2.97 | 4.24 | 3.44 | 1.23 | 2.93 |
| $Na_2O$% | 3.42 | 2.42 | 2.39 | 3.04 | 3.75 | 3.84 | 2.62 | 3.05 |
| $K_2O$% | 3.59 | 6.13 | 3.85 | 4.44 | 3.53 | 2.57 | 5.74 | 4.82 |
| $TiO_2$% | 0.649 | 0.310 | 0.690 | 1.008 | 0.812 | 0.373 | 0.247 | 0.956 |
| Total: | 99.66 | 99.82 | 99.03 | 99.86 | 98.48 | 99.62 | 99.88 | 99.83 |
| $Na_20/K_2O$ | 1.4 | 0.6 | 0.9 | 1.0 | 1.6 | 2.3 | 0.7 | 1.0 |
| Q | 174 | 189 | 176 | 140 | 82 | 163 | 195 | 132 |
| P | -73 | 31 | -52 | -57 | -122 | -131 | 16 | -48 |

* Intermediate or mixed age gneiss sample

Table B4. Major Element Analysis for samples in Chapter 4.

| SAMPLE | SH26 | SH27 | SH28 | R3 | PO5 | PO6 | AH5 | AH8 | AH10 |
|---|---|---|---|---|---|---|---|---|---|
| $SiO_2$% | 50.24 | 49.42 | 47.47 | 74.52 | 61.82 | 55.15 | 49.59 | 47.49 | 74.98 |
| $Al_2O_3$% | 14.00 | 14.87 | 13.58 | 13.55 | 16.13 | 14.65 | 15.74 | 17.69 | 13.19 |
| $Fe_2O_3$% | 14.30 | 12.37 | 16.07 | 1.78 | 5.78 | 11.62 | 12.16 | 12.83 | 1.51 |
| MnO% | 0.206 | 0.183 | 0.345 | 0.058 | 0.149 | 0.188 | 0.203 | 0.174 | 0.029 |
| MgO% | 5.35 | 6.59 | 5.22 | 0.50 | 1.64 | 2.80 | 5.97 | 4.91 | 0.52 |
| CaO% | 7.45 | 8.42 | 8.32 | 1.48 | 3.65 | 5.82 | 8.09 | 8.80 | 0.93 |
| $Na_2O$% | 2.91 | 3.09 | 3.23 | 3.68 | 3.82 | 3.13 | 2.84 | 3.79 | 3.19 |
| $K_2O$% | 1.88 | 2.17 | 1.61 | 4.06 | 4.46 | 3.69 | 2.31 | 0.99 | 5.61 |
| $TiO_2$% | 1.843 | 1.436 | 2.050 | 0.273 | 0.913 | 1.943 | 1.315 | 1.624 | 0.186 |
| Total: | 98.18 | 98.55 | 97.90 | 99.90 | 98.36 | 98.99 | 98.22 | 98.30 | 100.15 |
| $Na_2O/K_2O$ | 2.3 | 2.2 | 3.0 | 1.4 | 1.3 | 1.3 | 1.9 | 5.8 | 0.9 |
| Q | 57 | 28 | 26 | 191 | 82 | 58 | 38 | 16 | 183 |
| P | -187 | -204 | -219 | -59 | -94 | -126 | -187 | -258 | 0 |



| SAMPLE | PO1 | PO2 | PO7 | PO8 | PO9 | PO11 | PO12 | PO14 |
|---|---|---|---|---|---|---|---|---|
| $SiO_2$% | 70.20 | 64.73 | 63.76 | 59.16 | 46.56 | 67.44 | 53.22 | 71.74 |
| $Al_2O_3$% | 13.85 | 15.96 | 16.08 | 16.04 | 18.55 | 15.22 | 18.37 | 15.10 |
| $Fe_2O_3$% | 2.84 | 5.90 | 5.74 | 7.03 | 12.94 | 3.98 | 7.39 | 2.51 |
| MnO% | 0.071 | 0.089 | 0.102 | 0.127 | 0.237 | 0.086 | 0.178 | 0.083 |
| MgO% | 1.30 | 1.83 | 0.80 | 2.79 | 5.28 | 1.31 | 4.07 | 0.93 |
| CaO% | 3.19 | 3.30 | 2.94 | 4.83 | 9.19 | 3.24 | 7.70 | 2.61 |
| $Na_2O$% | 4.13 | 3.05 | 4.54 | 4.94 | 3.52 | 3.42 | 5.11 | 3.88 |
| $K_2O$% | 2.90 | 3.76 | 4.30 | 2.36 | 1.15 | 3.68 | 1.18 | 2.98 |
| $TiO_2$% | 0.381 | 0.670 | 0.769 | 0.773 | 1.270 | 0.639 | 0.800 | 0.248 |
| Total: | 98.86 | 99.29 | 99.03 | 98.05 | 98.70 | 99.02 | 98.02 | 100.08 |
| $Na_2O/K_2O$ | 2.2 | 1.2 | 1.6 | 3.2 | 4.6 | 1.4 | 6.6 | 2.0 |
| Q | 157 | 142 | 81 | 62 | 11 | 147 | 14 | 179 |
| P | -128 | -77 | -107 | -195 | -253 | -90 | -277 | -108 |

Table B5. Normative Calculation Results for samples with Paleoproterozoic model ages in Chapter 3

| Sample | PB1 | PB2 | PB5 | Sh2 | Sh4 | SH9A | Sh11 | Sh12 | Sh14 |
|---|---|---|---|---|---|---|---|---|---|
| *Q* | 20.05 | 18.72 | 20.26 | 6.14 | 18.43 | 29.32 | 32.50 | 27.46 | 11.75 |
| *Or* | 17.35 | 23.14 | 17.83 | 12.99 | 24.02 | 29.39 | 36.36 | 28.27 | 13.87 |
| *Ab* | 33.13 | 29.41 | 34.40 | 31.44 | 27.89 | 28.31 | 25.27 | 28.31 | 41.67 |
| *An* | 17.38 | 14.34 | 15.06 | 18.99 | 15.76 | 8.48 | 2.88 | 8.61 | 22.74 |
| *C* | 0.00 | 0.50 | 0.29 | 0.00 | 0.00 | 0.33 | 0.41 | 0.21 | 0.00 |
| *Di* | 1.09 | 0.00 | 0.00 | 5.93 | 0.71 | 0.00 | 0.00 | 0.00 | 2.47 |
| *Hy* | 8.26 | 10.48 | 9.29 | 18.85 | 9.53 | 3.02 | 2.04 | 5.62 | 6.92 |
| *Ol* | 0.00 | 0.00 | 0.00 | 0.00 | 0.00 | 0.00 | 0.00 | 0.00 | 0.00 |
| *Mt* | 0.50 | 0.67 | 0.57 | 1.41 | 0.59 | 0.23 | 0.17 | 0.38 | 0.42 |
| *Il* | 0.78 | 1.13 | 0.96 | 2.60 | 0.91 | 0.65 | 0.38 | 0.79 | 0.45 |
| *Ap* | 0.33 | 0.46 | 0.35 | 1.14 | 0.33 | 0.13 | 0.07 | 0.22 | 0.28 |
| Total: | 98.86 | 98.85 | 99.00 | 99.49 | 98.17 | 99.85 | 100.06 | 99.88 | 100.57 |

| Sample | Sh21 | Sh24 | Sh35 | Sh43 | Sh46 | Sh47 | Sh48 | Sl5 |
|---|---|---|---|---|---|---|---|---|
| *Q* | 1.03 | 38.42 | 24.58 | 9.62 | - | 33.50 | 14.54 | 21.12 |
| *Or* | 11.21 | 36.36 | 38.42 | 17.65 | - | 38.19 | 22.72 | 17.00 |
| *Ab* | 27.05 | 21.13 | 23.16 | 39.64 | - | 22.65 | 38.12 | 29.41 |
| *An* | 28.59 | 1.95 | 7.62 | 13.54 | - | 0.38 | 11.34 | 18.10 |
| *C* | 0.00 | 0.37 | 0.73 | 0.84 | - | 1.48 | 0.00 | 0.43 |
| *Di* | 4.72 | 0.00 | 0.00 | 0.00 | - | 0.00 | 1.41 | 0.00 |
| *Hy* | 22.96 | 1.40 | 4.11 | 14.47 | - | 2.96 | 9.01 | 11.33 |
| *Ol* | 0.00 | 0.00 | 0.00 | 0.00 | - | 0.00 | 0.00 | 0.00 |
| *Mt* | 1.59 | 0.12 | 0.32 | 1.03 | - | 0.27 | 0.60 | 0.78 |
| *Il* | 2.55 | 0.31 | 0.98 | 2.18 | - | 0.63 | 1.00 | 1.20 |
| *Ap* | 0.74 | 0.04 | 0.09 | 1.09 | - | 0.09 | 0.57 | 0.33 |
| Total: | 100.44 | 100.11 | 100.00 | 100.06 | NA | 100.15 | 99.31 | 99.69 |

Table B6. Normative Calculation Results for samples with Mesoproterozoic model ages in Chapter 3.

| Sample | DI1 | DI2 | DI3 | FI1 | FI4 | FI7 | FI8 | OB1 | OB3 | Sh8 | Sh10 |
|---|---|---|---|---|---|---|---|---|---|---|---|
| *Q* | 0.00 | 23.07 | 21.87 | 17.02 | 11.73 | 7.60 | 7.21 | 23.84 | 24.50 | 10.55 | - |
| *Or* | 19.60 | 18.42 | 13.69 | 21.54 | 25.73 | 4.60 | 20.72 | 16.53 | 24.32 | 8.68 | - |
| *Ab* | 41.84 | 33.38 | 39.81 | 34.23 | 33.47 | 40.91 | 33.98 | 38.45 | 33.98 | 32.88 | - |
| *An* | 6.48 | 14.05 | 13.48 | 13.31 | 17.81 | 30.26 | 18.22 | 8.73 | 8.73 | 25.75 | - |
| *C* | 2.44 | 0.76 | 0.47 | 0.43 | 0.00 | 0.00 | 0.00 | 0.63 | 0.39 | 0.00 | - |
| *Di* | 0.00 | 0.00 | 0.00 | 0.00 | 0.47 | 6.71 | 3.94 | 0.00 | 0.00 | 4.97 | - |
| *Hy* | 15.48 | 8.37 | 8.43 | 9.60 | 7.68 | 9.64 | 13.05 | 8.79 | 6.05 | 15.26 | - |
| *Ol* | 8.59 | 0.00 | 0.00 | 0.00 | 0.00 | 0.00 | 0.00 | 0.00 | 0.00 | 0.00 | - |
| *Mt* | 1.39 | 0.51 | 0.49 | 0.57 | 0.57 | 0.72 | 0.93 | 0.46 | 0.39 | 0.84 | - |
| *Il* | 2.21 | 0.98 | 0.99 | 1.03 | 1.01 | 0.83 | 1.59 | 1.01 | 0.84 | 0.78 | - |
| *Ap* | 0.57 | 0.37 | 0.42 | 0.37 | 0.31 | 0.42 | 0.59 | 0.33 | 0.33 | 0.35 | - |
| Total: | 98.60 | 99.91 | 99.66 | 98.11 | 98.79 | 101.68 | 100.23 | 98.78 | 99.53 | 100.06 | NA |

| Sample | Sh18 | Sh20 | Sh34 | Sh40 | Sh44 | Sh45 | SI2 | SI3 | SI7 | SI8 | SI9 |
|---|---|---|---|---|---|---|---|---|---|---|---|
| *Q* | 16.15 | 29.49 | 25.59 | 8.49 | 13.00 | - | 4.76 | 2.94 | 16.82 | 14.78 | 24.07 |
| *Or* | 18.36 | 31.34 | 31.75 | 4.43 | 24.26 | - | 17.12 | 18.12 | 26.86 | 24.73 | 29.04 |
| *Ab* | 37.19 | 29.33 | 23.92 | 45.05 | 38.20 | - | 36.26 | 34.65 | 30.00 | 33.55 | 30.51 |
| *An* | 14.65 | 5.42 | 8.31 | 30.03 | 12.44 | - | 20.42 | 22.43 | 15.77 | 12.24 | 8.73 |
| *C* | 0.16 | 0.65 | 0.00 | 0.00 | 0.00 | - | 0.00 | 0.00 | 0.13 | 0.00 | 0.24 |
| *Di* | 0.00 | 0.00 | 0.25 | 3.96 | 0.36 | - | 4.99 | 3.35 | 0.00 | 2.57 | 0.00 |
| *Hy* | 10.41 | 3.21 | 8.09 | 7.40 | 8.59 | - | 12.68 | 13.76 | 8.11 | 9.42 | 5.86 |
| *Ol* | 0.00 | 0.00 | 0.00 | 0.00 | 0.00 | - | 0.00 | 0.00 | 0.00 | 0.00 | 0.00 |
| *Mt* | 0.60 | 0.25 | 0.65 | 0.55 | 0.64 | - | 0.89 | 0.98 | 0.57 | 0.61 | 0.41 |
| *Il* | 1.08 | 0.44 | 1.17 | 0.67 | 1.04 | - | 1.73 | 1.98 | 0.92 | 1.06 | 0.80 |
| *Ap* | 1.33 | 0.11 | 0.31 | 0.31 | 0.31 | - | 0.57 | 0.74 | 0.33 | 0.33 | 0.26 |
| Total: | 99.94 | 100.24 | 100.04 | 100.89 | 98.84 | NA | 99.41 | 98.95 | 99.50 | 99.30 | 99.93 |

Table B7. Normative Calculation Results for plutonic samples and samples with with mixed model ages in Chapter 3.

| Sample | Gl2 | GF117 | GF118.5 | Sh1 | Sh3 | Sh5* | Sh6 | Sh7 | Sh9B | Sh13 |
|---|---|---|---|---|---|---|---|---|---|---|
| *Q* | 24.34 | 13.04 | 8.23 | 19.92 | 16.03 | 24.10 | 16.63 | 15.26 | 16.75 | 15.59 |
| *Or* | 33.64 | 16.29 | 20.60 | 25.62 | 24.08 | 9.27 | 21.37 | 26.09 | 23.85 | 19.71 |
| *Ab* | 21.81 | 35.41 | 35.33 | 26.45 | 25.61 | 46.74 | 26.79 | 29.75 | 25.35 | 25.61 |
| *An* | 10.15 | 17.93 | 20.86 | 10.55 | 12.01 | 16.54 | 18.55 | 10.88 | 12.21 | 15.62 |
| *C* | 0.00 | 1.14 | 0.00 | 0.00 | 0.00 | 0.55 | 0.00 | 0.00 | 0.70 | 0.01 |
| *Di* | 0.02 | 0.00 | 1.16 | 2.11 | 2.63 | 0.00 | 1.70 | 3.22 | 0.00 | 0.00 |
| *Hy* | 6.56 | 12.42 | 11.04 | 11.63 | 13.75 | 2.43 | 11.60 | 10.38 | 15.00 | 17.13 |
| *Ol* | 0.00 | 0.00 | 0.00 | 0.00 | 0.00 | 0.00 | 0.00 | 0.00 | 0.00 | 0.00 |
| *Mt* | 0.52 | 0.65 | 0.81 | 1.08 | 1.21 | 0.13 | 0.67 | 0.98 | 1.13 | 1.36 |
| *Il* | 1.36 | 1.51 | 1.19 | 1.93 | 2.61 | 0.20 | 0.95 | 2.22 | 2.70 | 3.06 |
| *Ap* | 0.46 | 0.63 | 0.44 | 0.74 | 1.22 | 0.09 | 0.24 | 1.07 | 1.07 | 1.51 |
| Total: | 98.86 | 99.02 | 99.65 | 100.03 | 99.16 | 100.05 | 98.49 | 99.86 | 98.76 | 99.60 |

| Sample | Sh19 | Sh22 | Sh23 | Sh30 | Sh31 | Sh32 | Sh49* | Sl4/R | Sl6 |
|---|---|---|---|---|---|---|---|---|---|
| *Q* | 16.17 | 26.84 | 33.30 | 26.87 | 21.03 | 11.77 | 24.97 | 33.55 | 19.87 |
| *Or* | 26.74 | 21.19 | 36.18 | 22.72 | 26.21 | 20.84 | 15.17 | 33.88 | 28.45 |
| *Ab* | 30.00 | 28.90 | 20.45 | 20.20 | 25.69 | 31.69 | 32.45 | 22.14 | 25.78 |
| *An* | 16.61 | 10.25 | 5.78 | 14.84 | 10.47 | 10.47 | 16.20 | 5.70 | 9.93 |
| *C* | 0.31 | 1.21 | 0.54 | 1.82 | 0.00 | 4.09 | 0.25 | 0.12 | 0.00 |
| *Di* | 0.00 | 0.00 | 0.00 | 0.00 | 1.87 | 7.56 | 0.00 | 0.00 | 2.22 |
| *Hy* | 7.27 | 9.18 | 1.57 | 10.29 | 11.54 | 10.99 | 8.29 | 3.57 | 10.80 |
| *Ol* | 0.00 | 0.00 | 0.00 | 0.00 | 0.00 | 0.00 | 0.00 | 0.00 | 0.00 |
| *Mt* | 0.52 | 0.63 | 0.26 | 0.69 | 1.07 | 1.03 | 0.51 | 0.27 | 1.00 |
| *Il* | 0.93 | 1.23 | 2.70 | 1.31 | 1.92 | 1.54 | 0.71 | 0.47 | 1.82 |
| *Ap* | 0.26 | 0.22 | 0.09 | 0.31 | 0.70 | 0.55 | 0.28 | 0.13 | 0.68 |
| Total: | 98.81 | 99.66 | 100.87 | 99.06 | 100.50 | 100.52 | 98.83 | 99.85 | 100.56 |

* Intermediate or mixed age gneiss sample

Table B8. Normative Calculations for rocks west of the Powassan Batholith in Chapter 4

| SAMPLE | Sh26 | Sh27 | Sh28 | R3 | PO5 | PO6 | AH5 | AH8 | AH10 |
|---|---|---|---|---|---|---|---|---|---|
| *Q* | 0.00 | - | 0.00 | 32.77 | 10.15 | 5.18 | 0.00 | 0.00 | 31.72 |
| *Or* | 11.10 | - | 9.50 | 23.96 | 26.32 | 21.78 | 13.63 | 5.84 | 33.11 |
| *Ab* | 24.59 | - | 27.30 | 31.10 | 32.29 | 26.45 | 24.00 | 32.03 | 26.96 |
| *An* | 19.56 | - | 17.78 | 6.81 | 13.67 | 15.00 | 23.35 | 28.30 | 3.89 |
| *C* | 0.00 | - | 0.00 | 0.60 | 0.00 | 0.00 | 0.00 | 0.00 | 0.44 |
| *Di* | 12.16 | - | 18.30 | 0.00 | 3.74 | 7.28 | 12.70 | 10.70 | 0.00 |
| *Hy* | 22.44 | - | 11.46 | 3.68 | 10.90 | 18.61 | 15.74 | 1.98 | 2.99 |
| *Ol* | 5.08 | - | 12.95 | 0.00 | 0.00 | 0.00 | 7.43 | 16.31 | 0.00 |
| *Mt* | 2.07 | - | 2.33 | 0.26 | 0.84 | 1.68 | 1.76 | 1.86 | 0.22 |
| *Il* | 0.82 | - | 0.82 | 0.52 | 1.74 | 3.70 | 2.50 | 3.09 | 0.82 |
| *Ap* | 0.98 | - | 0.61 | 0.17 | 0.72 | 1.77 | 0.50 | 0.85 | 0.24 |
| Total: | 98.81 | NA | 101.05 | 99.89 | 100.37 | 101.45 | 101.62 | 100.97 | 100.40 |

| SAMPLE | PO1 | PO2 | PO7 | PO8 | PO9 | PO11 | PO12 | PO14 |
|---|---|---|---|---|---|---|---|---|
| *Q* | 26.73 | 19.58 | 11.44 | 6.38 | - | 22.67 | 0.00 | 29.40 |
| *Or* | 17.12 | 22.19 | 25.38 | 13.93 | - | 21.72 | 6.96 | 17.59 |
| *Ab* | 34.91 | 25.78 | 38.37 | 41.75 | - | 28.90 | 43.19 | 32.79 |
| *An* | 10.67 | 15.05 | 10.78 | 14.60 | - | 14.82 | 23.67 | 12.28 |
| *C* | 0.00 | 1.35 | 0.00 | 0.00 | - | 0.17 | 0.00 | 0.98 |
| *Di* | 3.69 | 0.00 | 2.09 | 6.90 | - | 0.00 | 10.66 | 0.00 |
| *Hy* | 5.34 | 12.84 | 8.81 | 13.43 | - | 8.57 | 7.28 | 5.98 |
| *Ol* | 0.00 | 0.00 | 0.00 | 0.00 | - | 0.00 | 6.00 | 0.00 |
| *Mt* | 0.41 | 0.86 | 0.83 | 1.02 | - | 0.58 | 1.07 | 0.36 |
| *Il* | 0.72 | 1.27 | 1.46 | 1.47 | - | 1.22 | 1.52 | 0.47 |
| *Ap* | 0.24 | 0.44 | 0.46 | 0.37 | - | 0.42 | 0.55 | 0.22 |
| Total: | 99.82 | 99.35 | 99.62 | 99.85 | NA | 99.07 | 100.90 | 100.08 |